Final Report

High Accuracy Methods For Numerical Flow Analysis Using Adaptive Non-Linear Wavelets

AFOSR/AOARD Reference Number: AOARD-Grant-104001

AFOSR/AOARD Program Manager: Dr. Kenneth C. Caster

Period of Performance: May 2010 – May 2012

Submission Date: Aug. 1, 2012

PI: Dohyung Lee, Hanyang University

Report Documentation Page

Form Approved
OMB No. 0704-0188

1. REPORT DATE	2. REPORT TYPE	3. DATES COVERED
05 OCT 2012	**Final**	**06-05-2010 to 05-05-2012**

4. TITLE AND SUBTITLE
High-Accuracy Methods for Numerical Flow Analysis Using Adaptive Non-Linear Wavelets.

5a. CONTRACT NUMBER
5b. GRANT NUMBER
5c. PROGRAM ELEMENT NUMBER

6. AUTHOR(S)
Dohyung Lee

5d. PROJECT NUMBER
5e. TASK NUMBER
5f. WORK UNIT NUMBER

7. PERFORMING ORGANIZATION NAME(S) AND ADDRESS(ES)
Hanyang University,1271 Sa 3 Dong, SangRok-Gu,Ansan, GyungKi-Do 425-791,Korea,NA,NA

8. PERFORMING ORGANIZATION REPORT NUMBER
N/A

9. SPONSORING/MONITORING AGENCY NAME(S) AND ADDRESS(ES)
AOARD, UNIT 45002, APO, AP, 96338-5002

10. SPONSOR/MONITOR'S ACRONYM(S)
AOARD

11. SPONSOR/MONITOR'S REPORT NUMBER(S)
AOARD-104001

12. DISTRIBUTION/AVAILABILITY STATEMENT
Approved for public release; distribution unlimited

13. SUPPLEMENTARY NOTES

14. ABSTRACT
Nonlinear adaptive wavelets are developed for compact data representation and efficient flow solution algorithms. To flow solution algorithms, proposed new adaptive wavelets enhance the computational efficiency as well as preserve the numerical accuracy in steady and unsteady flow computations. These advantageous features of the wavelet are confirmed by the numerical tests of two-dimensional airfoil problem and unsteady shock-vortex interaction problem. An adaptive wavelet method with higher order of accuracy is also proposed to allow more accurate flow computation. For the high order accuracy of a solution, higher order of interpolating polynomial is utilized in wavelet decomposition process. This high order adaptive wavelet method was successfully applied to one-dimensional shock-sine interaction, two-dimensional shock-vortex interaction, isentropic vortex, and viscous shock tube problems. Through these applications, computational efficiency is substantially enhanced while higher order numerical accuracy of a CFD solver is successfully preserved.

15. SUBJECT TERMS

16. SECURITY CLASSIFICATION OF:			17. LIMITATION OF ABSTRACT	18. NUMBER OF PAGES	19a. NAME OF RESPONSIBLE PERSON
a. REPORT	b. ABSTRACT	c. THIS PAGE			
unclassified	**unclassified**	**unclassified**	**Same as Report (SAR)**	**44**	

Table of Contents

Final Report for AOARD Grant 104001

"High-Accuracy Methods for Numerical Flow Analysis Using Adaptive Non-Linear Wavelets"

Aug. 1, 2012

PI and Co-PI information: Dohyung Lee; dohyung@hanyang.ac.kr; Hanyang University; Department of Mechanical Engineering; Hanynag University, 1271 Sa 1 Dong, Ansan 425-791, KyungKi-Do, Republic of Korea; +82-10-2606-5289.

Period of Performance: 5/6/2010 – 5/5/2012

Abstract: Nonlinear adaptive wavelets are developed for compact data representation and efficient flow solution algorithms. To flow solution algorithms, proposed new adaptive wavelets enhance the computational efficiency as well as preserve the numerical accuracy in steady and unsteady flow computations. Theses advantageous features of the wavelet are confirmed by the numerical tests of two-dimensional airfoil problem and unsteady shock-vortex interaction problem. An adaptive wavelet method with higher order of accuracy is also proposed to allow more accurate flow computation. For the high order accuracy of a solution, higher order of interpolating polynomial is utilized in wavelet decomposition process. This high order adaptive wavelet method was successfully applied to one-dimensional shock-sine interaction problem, two-dimensional shock-vortex interaction problem, isentropic vortex problem, and viscous shock tube problem. Through these applications, the computational efficiency is substantially enhanced while higher order numerical accuracy of a CFD solver is successfully preserved.

Introduction: In various aerospace transportation and exploration systems, the prediction capability of flow including supersonic/hypersonic phenomena is highly important in the design of aerospace vehicles. For the improvement of the capability, high fidelity simulation of Computational Fluid Dynamics (CFD) is required that entails the development of high order method of discretized equations and large number of grid point clustering. However, current level of technologies often falls short of the need to meet both accuracy and efficiency at the same time. Accuracy order increment and dense grid system, as an effort to unveil complex physical flow phenomena, eventually pay back with substantial increase of computation time. Hence, it is important to accurately compute the flow phenomena and at the same time it should efficiently alleviate the computational workload.

For the efficient and accurate computations of the flow phenomena, there have been many attempts for the advancement of CFD algorithms: one of the representative examples is the higher order spatial interpolation scheme with the limiting process. The main purpose of higher order scheme is the reduction of the number of grid points without the loss of the accuracy of CFD calculations. However, high order computations always involve the unnecessary numerical oscillations near a discontinuity whenever shock waves are present. Because these numerical oscillations deteriorate the stability and convergence properties of the CFD computations, there is an additional treatment of limiting algorithms for oscillation removal [1-3]. However, computational cost of high order accurate flux evaluation is generally expensive, which decreases the computational efficiency.

The adaptability of CFD data can allow the possibility to overcome this defect; generally in the CFD solution, the major parts of computational domain contain smooth flow pattern which

can be simply and accurately interpolated by using the values in neighboring cells. A dense grid is only needed in the rapidly changing regions such as shock waves, vortex and boundary layer, etc. For that reason several types of adaptive methods, especially, the adaptive wavelet methods have been studied as a way of improving the computational efficiency [4-6].

There are two ways to apply wavelets in performing the flow analysis. According to the classification by Vasilyev and Kevlahan [8], wavelet-based numerical methods for solution algorithm can be classified as adaptive wavelet Galerkin methods (AWGM) [9-12] and adaptive wavelet collocation methods (AWCM) [4-8]. The major difference between these two approaches is as follows. According to the research by Bacry, Mallat and Papanicolaou [10] or Holmström and Walden [11], AWGM solves PDE problems in a wavelet coefficient space. It is mentioned that nonlinear operators, such as multiplication, are too computationally expensive when done directly in a wavelet basis. To resolve this problem, Beylkin and Keiser [12] alternate the computing space between the physical and the wavelet domain in order to compute the operators. In other words, multiplication is performed in physical space and differentiation is performed in wavelet space.

On the other hand, dealing with nonlinearity and general boundary conditions is not complicated in AWCM because all computations are performed on the physical space. One can directly link every wavelet coefficients with the collocation points on the physical domain. In AWCM studies, Harten presents an adaptive multi-resolution scheme for computing the discontinuous solutions of hyperbolic PDEs. [4] Holmström makes the algorithm for organizing an adaptive dataset with an interpolating wavelet transformation [5]. Sjögreen uses a multi-resolution scheme to solve compressible Euler equations and also utilizes an interpolating wavelet transformation to construct the adaptive dataset [6]. He concludes that the multi-resolution method can yield considerable gains in efficiency by using computationally expensive method with a large number of grids.

However, the accuracy and efficiency of an interpolating wavelet transformation are very sensitive to threshold values during multi-resolution process. In this research, numerical errors of which the extent reaches a magnitude equal to that of the threshold value inevitably occur at the excluded cells of an adaptive dataset and they eventually prevent the solutions from converging. They are transferred to the entire computational domain through a time integration process, disturb the stable organization of an adaptive dataset, decrease the compression ratio and finally deteriorate the computational efficiency.

The objective of the study is the improvement of computational efficiency of CFD computation with preserving the spatial and temporal accuracies of conventional CFD solvers. In order to meet these objectives, improved adaptive wavelet method includes the modified threshold method, residual interpolation, and restriction technique as follows.

First, the modified threshold method consists of the modified threshold value and the stabilization process. The modified threshold value considers grid spacing and time step for retaining the original spatial and temporal accuracy of conventional solvers by automatically adjusting the threshold value. And stabilization process is involved in stable construction of an adaptive dataset by obstructing the additional $O(\varepsilon)$ error due to threshold is transferred to the adjacent computational domain during the time integration process. Therefore, it can contribute the enhancement of the compression ratio of the current method.

Secondly, general adaptive wavelet procedure is modified by adopting residual interpolation at the n time step, not the $n+1$ time step. A residual based interpolation concept was introduced by Chiavassa and Donat for point value setting [13]. In this paper, this method is modified for cell value setting and time integration is performed on the entire domain, i.e., residual values at excluded cells in an adaptive dataset are interpolated by using the calculated residual values at

included cells in an adaptive dataset. Because the interpolation is performed at the n time step, there is no need to add several adjacent cells to an adaptive dataset. In addition, this approach can be applied to implicit time integration methods because all residual values are computed.

Thirdly, restriction technique is applied after the time integration on the entire domain. In this method, if the flow variations in time are small enough at the excluded cells in an adaptive dataset when compared with the order of the threshold value, these variations are discarded and restricted by multiplying the weighting factor. This process can especially contribute the convergence acceleration of steady state flow simulations.

Throughout these processes, spatial and temporal accuracies of a conventional solver are preserved with a substantial reduction in computing time. Various steady and unsteady flow simulations are conducted to verify the enhancement of both efficiency and accuracy of the proposed method.

This report is organized in the following order. After the introduction, development of nonlinear wavelet is described as a preliminary background in section 1 of **Experiment**. In section 2 and 3 of **Experiment**, we describe the implementation of the new adaptive wavelet method for a reference CFD solver and development of adaptive wavelet method based high order scheme. In section 1, 2, and 3 of **Results and Discussion**, several numerical simulations using adaptive wavelet methods are performed and a conclusion is drawn.

Experiment:

1. Development of nonlinear wavelets

The phenomena of general interest in CFD, consist of several flow features such as Shock, Vortex, Boundary layer, Expansion fan, etc. and those flow features are depicted as follows.

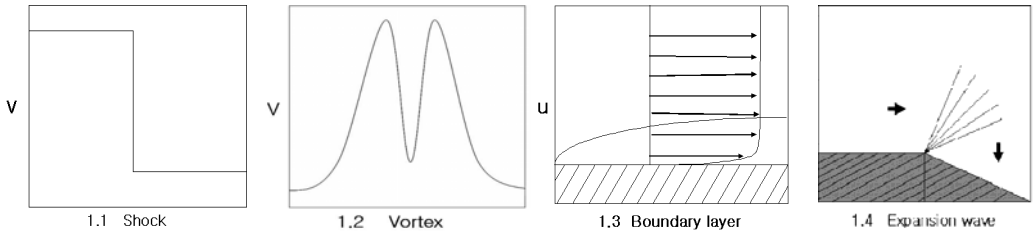

Fig. 1-1 Schematic of principal flow conditions

In the analysis and representation of these data, the wavelets have attractive features as locality and compactness. Through these features, the wavelets perform properly the role of filtering that classifies primary into a region of rapidly changing such as shock, vortex, boundary layers, etc. and a smooth region of mild changing in flow properties.

Let us assume a dyadic grid set as shown in Eq. (1-1).

$$V_l = \{x_{l,k} \in R : x_{l,k} = 2^{-l}k, k \in Z\},\ l \in Z\ . \tag{1-1}$$

The key idea of the adaptive wavelet method is that smoothness of flow pattern can be easily determined by the magnitude of difference value between original function value and approximated value based on neighboring cells. That is, the original value can be accurately

approximated by the values at neighboring cells in the smooth region but not vice versa in rapidly changing region. Here, interpolating polynomial is used at the odd numbered cells for the approximation of original function values and then the dyadic dataset is decomposed as Eq. (1-2).

$$\begin{cases} \tilde{f}_{l+1,2k} = f_{l,k} \\ \tilde{f}_{l+1,2k+1} = P_{l+1,2k+1}(f_{l,k-\frac{p}{2}+1}, \cdots, f_{l,k}, f_{l,k+1}, \cdots, f_{l,k+\frac{p}{2}}) \end{cases}, \tag{1-2}$$

where $P_{l,k}$ is the order of interpolating polynomial; the 4th order of interpolating polynomial is shown in Eq. (1-3).

$$\tilde{f}_{l+1,2k+1} = -\frac{1}{16} f_{l,k-1} + \frac{9}{16} f_{l,k} + \frac{9}{16} f_{l,k+1} - \frac{1}{16} f_{l,k+2} . \tag{1-3}$$

After the approximation, the difference can be computed as Eq. (1-4).

$$d_{l,k} = f_{l+1,2k+1} - \tilde{f}_{l+1,2k+1}, \forall k \in Z . \tag{1-4}$$

In smooth region, the order of difference value is very small and the corresponding cell can be partially rejected in the whole dataset; an adaptive dataset is acquired according to the local features of solution. And the maximum error is bounded within the order of threshold value as Eq. (1-5).

$$\left| d_{l,k} \right|_\infty = \left| f_{l,k} - \tilde{f}_{l,k} \right|_\infty < O(\varepsilon) . \tag{1-5}$$

2. Flow solution algorithm using adaptive wavelets for CFD solution algorithm

The two-dimensional Euler equations are used as the governing equations of the flow problems. The two-dimensional Euler equations are written as Eq. (2-1).

$$\frac{\partial Q}{\partial t} + \frac{\partial E}{\partial x} + \frac{\partial F}{\partial y} = 0 , \tag{2-1}$$

where $$Q = \begin{bmatrix} \rho \\ \rho u \\ \rho v \\ \rho e_t \end{bmatrix}, \; E = \begin{bmatrix} \rho u \\ \rho u^2 + p \\ \rho uv \\ (\rho \rho_t + p)u \end{bmatrix}, \; F = \begin{bmatrix} \rho v \\ \rho uv \\ \rho v^2 + p \\ (\rho \rho_t + p)v \end{bmatrix},$$

and $e_t = \frac{a^2}{\gamma(\gamma - 1)} + \frac{1}{2}(u^2 + v^2)$.

All the properties and governing equations are non-dimensionalized.

By the generalized coordinate transformation, Eq. (2-1) is rewritten as Eq. (2-2).

$$\frac{\partial \overline{Q}}{\partial \tau} = -[\frac{\partial \overline{E}}{\partial \xi} + \frac{\partial \overline{F}}{\partial \eta}] = -\overline{R}_{i,j}^{n}, \tag{2-2}$$

where $\overline{Q} = \frac{Q}{J}$, $\overline{E} = \frac{1}{J}[\xi_t + \xi_x E, +\xi_y F]$, $\overline{F} = \frac{1}{J}[\eta_t + \eta_x E, +\eta_y F]$.

To improve the computational efficiency of steady/unsteady flow problems, the general adaptive wavelet procedure is changed by adopting residual interpolation at the n time step and time integration is performed on the entire domain. The procedure of selecting and adding additional cells to an adaptive dataset according to the wavelet resolution levels and positions is excluded. And modified threshold method is applied in order to maintain the spatial and temporal accuracies of reference schemes. Also, a stabilization method is applied again to unsteady problems to stably construct an adaptive dataset while the compressibility of the wavelet method is enhanced. Especially in steady state problems, the restriction technique is applied for the acceleration of the convergence. The flowchart in Fig. 2-1 shows the overall implementation of the new adaptive wavelet method in a reference solver. This implementation is comprised of the following sequential steps.

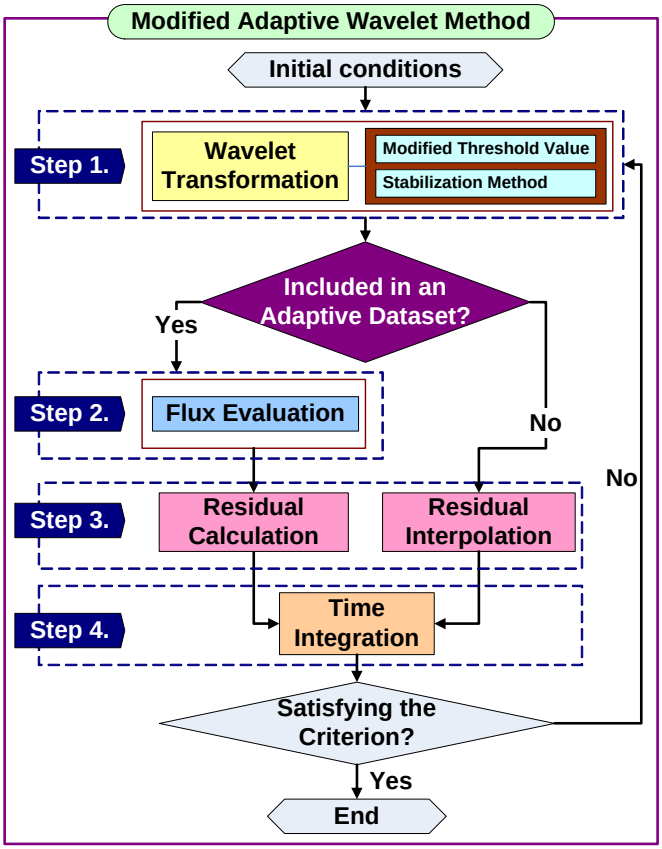

Fig. 2-1 Overall procedure of flow simulation with the new adaptive wavelet method

2-1. Construction of an adaptive dataset

The set of dyadic grids in two-dimensions can be presented as shown in Fig. 2-2 Positions of

the symbol ○ are even numbered grids and the other positions of symbols □, △, and X are odd numbered cells. The 4th order interpolating polynomials are shown in Eq. (2-3).

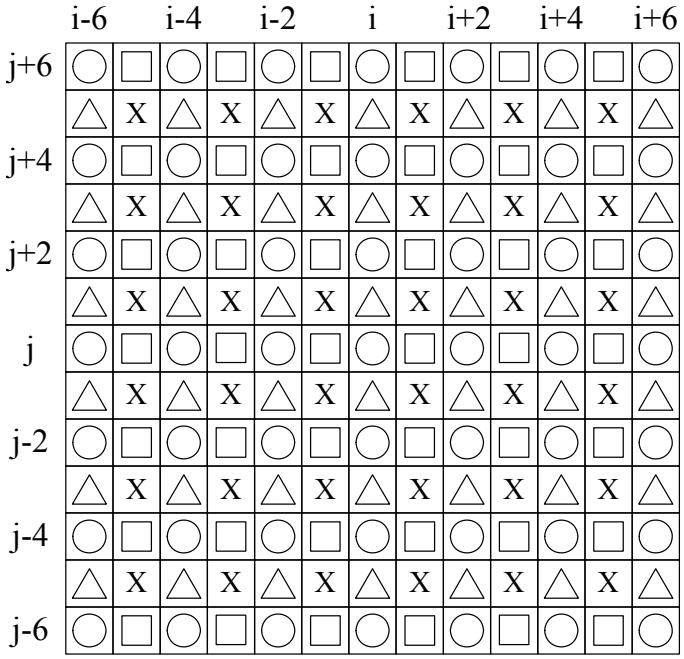

Fig. 2-2 Example of a two-dimensional dyadic grid set.

$$
\begin{aligned}
&\square: \ \widetilde{Q}^n_{i+1,j} = -\frac{1}{16}Q^n_{i-2,j} + \frac{9}{16}Q^n_{i,j} + \frac{9}{16}Q^n_{i+2,j} - \frac{1}{16}Q^n_{i+4,j}, \\
&\triangle: \ \widetilde{Q}^n_{i,j+1} = -\frac{1}{16}Q^n_{i,j-2} + \frac{9}{16}Q^n_{i,j} + \frac{9}{16}Q^n_{i,j+2} - \frac{1}{16}Q^n_{i,j+4}, \\
&\mathrm{X}: \ \widetilde{Q}^n_{i+1,j+1} = 0.5\times(-\frac{1}{16}Q^n_{i-2,j-2} + \frac{9}{16}Q^n_{i,j} + \frac{9}{16}Q^n_{i+2,j+2} - \frac{1}{16}Q^n_{i+4,j+4}) + \\
&\qquad\qquad 0.5\times(-\frac{1}{16}Q^n_{i-2,j+4} + \frac{9}{16}Q^n_{i,j+2} + \frac{9}{16}Q^n_{i+2,j} - \frac{1}{16}Q^n_{i+4,j-2})
\end{aligned}
\qquad (2\text{-}3)
$$

Especially in unsteady problems, a tiny change of flow may grow into a large change with time. Thus, even a tiny variation has to be considered. In this case, we used the 6th order of interpolating polynomial and present the two dimensional formulations as shown in Eq. (2-4).

$$
\begin{aligned}
&\square: \ \widetilde{Q}^n_{i+1,j} = \frac{3}{256}Q^n_{i-4,j} - \frac{25}{256}Q^n_{i-2,j} + \frac{75}{128}Q^n_{i,j} + \frac{75}{128}Q^n_{i+2,j} - \frac{25}{256}Q^n_{i+4,j} + \frac{3}{256}Q^n_{i+6,j} \\
&\triangle: \ \widetilde{Q}^n_{i,j+1} = \frac{3}{256}Q^n_{i,j-4} - \frac{25}{256}Q^n_{i,j-2} + \frac{75}{128}Q^n_{i,j} + \frac{75}{128}Q^n_{i,j+2} - \frac{25}{256}Q^n_{i,j+4} + \frac{3}{256}Q^n_{i,j+6}.
\end{aligned}
\qquad (2\text{-}4)
$$

$$\widetilde{Q}^n_{i+1,j+1} = \frac{1}{512}\times(3Q^n_{i,j-4} + 3Q^n_{i+2,j-4} + 2Q^n_{i-2,j-2} - 27Q^n_{i,j-2} - 27Q^n_{i+2,j-2} + 2Q^n_{i+4,j-2}$$

X : $$+ 3Q^n_{i-4,j} - 27Q^n_{i-2,j} + 174Q^n_{i,j} + 174Q^n_{i+2,j} - 27Q^n_{i+4,j} + 3Q^n_{i+6,j}$$

$$+ 3Q^n_{i-4,j+2} - 27Q^n_{i-2,j+2} + 174Q^n_{i,j+2} + 174Q^n_{i+2,j+2} - 27Q^n_{i+4,j+2} + 3Q^n_{i+6,j+2}$$

$$+ 2Q^n_{i-2,j+4} - 27Q^n_{i,j+4} - 27Q^n_{i+2,j+4} + 2Q^n_{i+4,j+4} + 3Q^n_{i,j+6} + 3Q^n_{i+2,j+6})$$

Here, the formulation at the X position in Eq. (2-3), (2-4) uses 24 cells for the 6th order interpolating polynomial and is very complicated. Instead of this equation, we formulated Eq. (2-5) using 12 cells as follows.

$$\begin{aligned}\widetilde{Q}^n_{i+1,j+1} = \frac{1}{512}\times(&3Q^n_{i-4,j-4} - 25Q^n_{i-2,j-2} + 150Q^n_{i,j} + 150Q^n_{i+2,j+2}\\ &- 25Q^n_{i+4,j+4} + 3Q^n_{i+6,j+6}) + \frac{1}{512}\times(3Q^n_{i-4,j+6} - 25Q^n_{i-2,j+4}\\ &+ 150Q^n_{i,j+2} + 150Q^n_{i+2,j} - 25Q^n_{i+4,j-2} + 3Q^n_{i+6,j-4})\end{aligned} \quad \text{(2-5)}$$

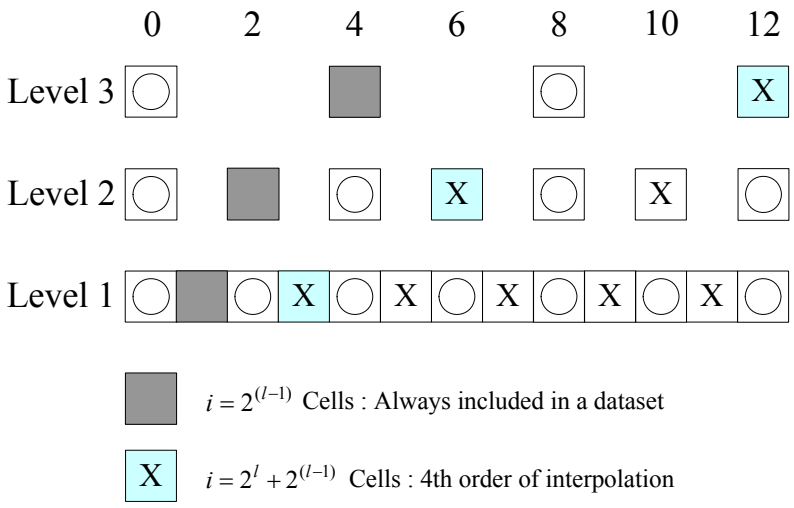

Fig. 2-3 Boundary treatment in wavelet decomposition

Based on many numerical simulations, Eq. (4-5) has much better efficiency than the accurate formulation with little lose of accuracy. Note that some indices of $Q_{i,j}$ are located outside of the computation domain near its boundaries. In order to avoid this situation, cells $i = 2^{(l-1)}$ ($l_{\text{Coarsest Level}} \le l < L_{\text{Finest Level}}$) are always included in the adaptive dataset. At the next odd numbered cells $i = 2^l + 2^{(l-1)}$, the 4th order interpolating polynomial is applied. The overall boundary treatment is presented in Fig. 2-3, and the same procedure can be applied to the other side of boundary, or the boundaries along the j-direction.
Then, the wavelet coefficients of each □, △, and X position are found as follows:

$$\square: \quad d^n_{i+1,j} = Q^n_{i+1,j} - \widetilde{Q}^n_{i+1,j}$$

$$\triangle: \quad d^n_{i,j+1} = Q^n_{i,j+1} - \widetilde{Q}^n_{i,j+1}. \tag{2-6}$$
$$\mathrm{X}: \quad d^n_{i+1,j+1} = Q^n_{i+1,j+1} - \widetilde{Q}^n_{i+1,j+1}$$

After the wavelet decomposition, the thresholding process is performed. The threshold method consists of the modification of a threshold value and the stabilization of an adaptive dataset. By this method, it is possible to maintain the spatial and temporal accuracies of reference method. Also, due to the stable construction of an adaptive dataset, it can enhance the compression ratio of wavelet method and improve computational efficiency.

In order to maintain the l^{th} order of spatial accuracy and m^{th} order of temporal accuracy of reference method, the modified threshold value is written as Eq. (2-7).

$$\varepsilon' = \min[\varepsilon, \max(\Delta x^l, CFL^m \cdot \Delta x^m)], \tag{2-7}$$

where Δx is determined at the finest resolution level.

Based on this modified threshold value, ε', We can control the flag values of the cells and threshold a dataset. If $d^n_{i,j}$ is larger than ε', the flag value of cell (i,j) is determined as 1 and the cell is included in a $I(\varepsilon')^n$ dataset; if not, the flag value is set as 0 and the cell is excluded from the $I(\varepsilon')^n$ dataset. Then, the dataset is adapted to the flow features while maintaining the numerical accuracy of reference schemes.

Also, we prevent the flag value's switching between 0 and 1 due to additional errors to originate from the organization of an adaptive dataset and realize the stable construction of an adaptive dataset that leads to the enhancement of the compression ratio.

2-2. Modified thresholding method

Because $\left|d^n_{i,j}\right|_\infty$ is bounded within $O(\varepsilon)$, $O(\varepsilon)$ errors are added to the solutions by the wavelet transformation. Then, each primitive variable or flux value has $O(\varepsilon)$ errors as Eq. (2-8).

$$\begin{aligned}
&\widetilde{\rho}^n_{i,j} = \rho^n_{i,j} + O(\varepsilon), \quad \widetilde{u}^n_{i,j} = u^n_{i,j} + O(\varepsilon) \quad , \\
&\widetilde{v}^n_{i,j} = v^n_{i,j} + O(\varepsilon), \quad \widetilde{p}^n_{i,j} = p^n_{i,j} + O(\varepsilon) \quad , \\
&\widetilde{E}^n_{1/2} = E^n_{1/2} + O(\varepsilon), \quad \widetilde{F}^n_{1/2} = F^n_{1/2} + O(\varepsilon) \quad .
\end{aligned} \tag{2-8}$$

Also, if the flux values are discretized with l^{th} order of spatial accuracy, each primitive variable or flux value has l^{th} order of truncation error term as Eq. (2-9).

$$\begin{aligned}
&\rho^n_{i,j} = \rho^n_{i,j,real} + O(\Delta x^l), \quad u^n_{i,j} = u^n_{i,j,real} + O(\Delta x^l) \quad , \\
&v^n_{i,j} = v^n_{i,j,real} + O(\Delta x^l), \quad p^n_{i,j} = p^n_{i,j,real} + O(\Delta x^l) \quad , \\
&E^n_{1/2} = E^n_{1/2,real} + O(\Delta x^l), \quad F^n_{1/2} = F^n_{1/2,real} + O(\Delta x^l) \quad .
\end{aligned} \tag{2-9}$$

From the combination of Eqs. (2-8) and (2-9), the fluxes come to have the following order of errors due to spatial discretization and thresholding, as shown in Eq. (2-10).

$$\widetilde{E}^n_{1/2} = E^n_{1/2,real} + O(\Delta x^l) + O(\varepsilon), \quad \widetilde{F}^n_{1/2} = F^n_{1/2,real} + O(\Delta x^l) + O(\varepsilon). \tag{2-10}$$

By m^{th} order of time integration, all terms of numerical errors are derived as Eq. (2-11).

$$\begin{aligned}\widetilde{Q}_{i,j}^{n+1} = \widetilde{Q}_{i,j}^{n} - \frac{\Delta t}{\Delta x}(E_{1/2,real}^{n} - E_{-1/2,real}^{n} + F_{1/2,real}^{n} - F_{-1/2,real}^{n}) \\ + O(\Delta x^{l} \cdot \Delta t) + O(\Delta t^{m+1}) + O(\varepsilon \cdot \Delta t)\end{aligned} . \quad (2\text{-}11)$$

Therefore, $O(\varepsilon)$ have to be smaller than $O(\Delta x^{l})$ and $O(\Delta t^{m})$ in order not to damage the l^{th} order of spatial accuracy and m^{th} order of temporal accuracy of the conventional method. For the satisfaction of this purpose, modified threshold value is developed as Eq. (2-12) [14, 15].

$$\varepsilon' = \min[\varepsilon, \max(\Delta x^{l}, CFL^{m} \cdot \Delta x^{m})] . \quad (2\text{-}12)$$

Because our target is 3rd order accuracy, 3rd order of spatial and temporal accuracy of the numerical schemes are used. Then, the modified threshold value in this research is proposed as Eq. (2-13). where *CFL* means the constant of CFL conditions.

$$\varepsilon' = \min[\varepsilon, \max(\Delta x^{3}, CFL^{3} \cdot \Delta x^{3})] . \quad (2\text{-}13)$$

Based on this modified threshold value, the odd numbered cells are included in the dataset if $d_{i,j}^{n}$ is larger than ε'; if not, the cells are excluded from the dataset. Then, the dataset is constructed to follow the local features of the solution with the conservation of the numerical accuracy of the conventional CFD schemes.

2-3. Flux evaluation at included cells in an adaptive dataset

After constructing the $I(\varepsilon')^{n}$ dataset, the flag values of the dataset determine whether the flux values are to be evaluated or not. If the flag value is 1, the flux value is calculated by reference schemes such as AUSMPW+ or Roe's FDS method. In this research, we use the Finite Volume Method (FVM); i.e. the numerical fluxes $\overline{E}$, $\overline{F}$ are defined at these interfaces. Thus, if the flag value of cell (i, j) is 1, flux evaluations are performed on all sides of the cell, and residual values at cell (i, j) are calculated. If the flag value is 0, flux evaluation is not performed, so the total computation time is decreased.

2-4. Stabilization of an adaptive dataset

If the solution changes after the time integration step, the adaptive dataset, $I(\varepsilon')^{n}$ also changes in order to be adapted to the latest solution. Independent of a solver, ε' order errors are suddenly imposed due to changes of the adaptive dataset and are transferred to the surroundings throughout the time integration step. Thus, both the surroundings and wavelet coefficients at the surroundings have the ε' order errors. The ε' order errors in the wavelet coefficients obstruct the construction of an adaptive dataset adapted to the solution. Consequently, the compression ratio becomes reduced and the computational efficiency of the overall adaptive wavelet method decreases. For the efficient construction of an adaptive dataset, the alteration of flag values due to ε order errors should be restricted.

We use algorithm 1 (defined below) for keeping $I(\varepsilon')^{n}$ from being switched regardless of the

solution's properties. First, I compare $I(\varepsilon')^n$ with $I(\varepsilon')^{n-1}$, in the case where the point was already included in $I(\varepsilon')^{n-1}$, the point can be excluded from $I(\varepsilon')^n$ only if the wavelet coefficient at that point is smaller than $\alpha\varepsilon'$ ($\alpha<1$), not smaller than ε'. On the other hand, in the case where the point was already excluded from $I(\varepsilon')^{n-1}$, then the point can be included in $I(\varepsilon')^n$ if the wavelet coefficient is larger than $\beta\varepsilon'$ ($\beta>1$) but not ε'.

2-5. Switching of residual calculation method

Generally, flow properties are interpolated after time integration in previous wavelet methods. That is, flow properties are reconstructed at the $n+1$ time step based on the $I(\varepsilon')^n$. This discrepancy of time step causes the following numerical problem: if the flow changes rapidly, e.g., the shock or vortex propagation, etc., the neighboring cells of the cell that is included in $I(\varepsilon')^n$ become important as well as the cell in $I(\varepsilon')^n$ itself. If they are not included in $I(\varepsilon')^n$, the interpolation at these neighboring cells cannot guarantee the solution accuracy and may deteriorate it at the $n+1$ time step.

For resolving this problem residual interpolation process is introduced in this study. Residual values at excluded cells in an adaptive dataset are calculated by interpolation polynomials which uses the values at even numbered positions (O positions) in Fig. 2-2. The 4th order equations for residual interpolation are as follows:

$$
\begin{aligned}
&\square:\ \widetilde{R}^n_{i+1,j} = -\frac{1}{16}R^n_{i-2,j} + \frac{9}{16}R^n_{i,j} + \frac{9}{16}R^n_{i+2,j} - \frac{1}{16}R^n_{i+4,j}\,,\\
&\triangle:\ \widetilde{R}^n_{i,j+1} = -\frac{1}{16}R^n_{i,j-2} + \frac{9}{16}R^n_{i,j} + \frac{9}{16}R^n_{i,j+2} - \frac{1}{16}R^n_{i,j+4}\,,\\
&\text{X:}\ \widetilde{R}^n_{i+1,j+1} = 0.5\times(-\frac{1}{16}R^n_{i-2,j-2} + \frac{9}{16}R^n_{i,j} + \frac{9}{16}R^n_{i+2,j+2} - \frac{1}{16}R^n_{i+4,j+4}) + \\
&\qquad\qquad 0.5\times(-\frac{1}{16}R^n_{i-2,j+4} + \frac{9}{16}R^n_{i,j+2} + \frac{9}{16}R^n_{i+2,j} - \frac{1}{16}R^n_{i+4,j-2})\,.
\end{aligned}
\tag{2-14}
$$

Especially in unsteady problems, for representing the tiny variations of flow properties, the 6th order interpolating polynomial is used as shown in Eq. (15).

$$
\begin{aligned}
&\square:\ \widetilde{R}^n_{i+1,j} = \frac{3}{256}R^n_{i-4,j} - \frac{25}{256}R^n_{i-2,j} + \frac{75}{128}R^n_{i,j} + \frac{75}{128}R^n_{i+2,j} - \frac{25}{256}R^n_{i+4,j} + \frac{3}{256}R^n_{i+6,j}\\
&\triangle:\ \widetilde{R}^n_{i,j+1} = \frac{3}{256}R^n_{i,j-4} - \frac{25}{256}R^n_{i,j-2} + \frac{75}{128}R^n_{i,j} + \frac{75}{128}R^n_{i,j+2} - \frac{25}{256}R^n_{i,j+4} + \frac{3}{256}R^n_{i,j+6}\,.\\
&\text{X:}\ \widetilde{R}^n_{i+1,j+1} = \frac{1}{512}\times(3R^n_{i-4,j-2} - 25R^n_{i-2,j-2} + 150R^n_{i,j} + 150R^n_{i+2,j+2} - 25R^n_{i+4,j+4} + 3R^n_{i+6,j+6}) + \\
&\qquad\qquad \frac{1}{512}\times(3R^n_{i-4,j+6} - 25R^n_{i-2,j+4} + 150R^n_{i,j+2} + 150R^n_{i+2,j} - 25R^n_{i+4,j-2} + 3R^n_{i+6,j-4})
\end{aligned}
\tag{2-15}
$$

After the construction of residual values in the whole computational domain, time integration is performed by using conventional schemes.

3. Development of adaptive wavelet based high order scheme

3-1. High order spatial interpolation schemes for CFD

High-accuracy numerical methods are required to obtain converged solution as well as to capture correct flow physics. High-fidelity simulation calls for high-accuracy algorithm and/or dense grid system, leading to substantial computation workload. Thereby, it is very important to develop an efficient numerical scheme that achieves high order of accuracy at the same time captures correct unsteady flow phenomena. There are various high order numerical methods developed to date, such as TVD (Total Variation Diminishing) scheme [16-18], ENO/WENO (Essentially Non-Oscillatory / Weighted Essentially Non-Oscillatory) scheme [19, 20], MLP (Multi-dimensional Limiting Process) scheme [2], e-MLP (enhanced Multi-dimensional Limiting Process) scheme [3], Galerkin method, Spectral and Spectral volume methods.

Table 3-1. Higher order schemes for CFD

	TVD	ENO	MLP	e-MLP
Discontinuity in one dimension	**O**	**O**	**O**	**O**
Discontinuity in multi-dimension	**X**	**X**	**O**	**O**
Local extrema	**X**	**O**	**X**	**O**

Those offer some advantageous features but none of them is universally better than the others. In TVD, incorrect results such as clipping phenomena appears at local extrema, and generally not easy to extend to multi-dimensions since it was developed in 1D based equations. The usage of ENO scheme can avoid clipping phenomena, but undershoot/overshoot may appear in multi-dimensional analysis. In addition, the use of unstructured mesh gives some difficulty in the construction of an appropriate stencil, leading to excessive memory load. MLP shows a monotonic and stable calculation of the shock wave in multi-dimensional problems. However, MLP damps out the flow and is unsuitable for local extrema in a continuous region as with other limiting functions, which decreases the accuracy of the solutions. e-MLP has distinguishing step. Through this step, the computational domain is divided into continuous, linear discontinuous and nonlinear discontinuous regions. Appropriate limiting criteria are then applied to each region. This increases the accuracy of the solution and makes it robust against shock instability. For the development of adaptive wavelet method based high order scheme, we adopt TVD and e-MLP scheme respectively.

3-2. High order accurate wavelet decomposition

If an initial two-dimensional dyadic grid set with level l is use, as shown in Fig. 5-1, then ○ cells are even numbered and the others are odd numbered cells.

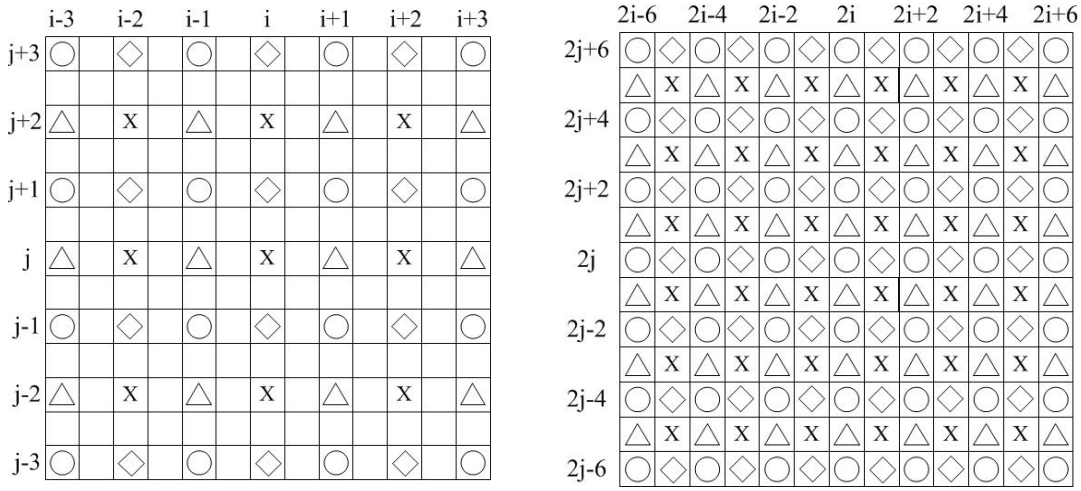

(a) Level l (b) Level l+1

Fig. 3-1 Example of a two-dimensional dyadic grid set.

$$
\begin{cases}
Q_{l+1,2i,2j} = Q_{l,i,j} \\
\widetilde{Q}_{l+1,2i+1,2j} = \mathrm{P}_{l+1,2i+1,2j}(Q_{l,i-\frac{p}{2}+1,j},\cdots,Q_{l,i,j},Q_{l,i+1,j},\cdots,Q_{l,i+\frac{p}{2},j}) \\
\widetilde{Q}_{l+1,2i,2j+1} = \mathrm{P}_{l+1,2i,2j+1}(Q_{l,i,j-\frac{p}{2}+1},\cdots,Q_{l,i,j},Q_{l,i,j+1},\cdots,Q_{l,i,j+\frac{p}{2}}) \\
\widetilde{Q}_{l+1,2i,+12j+1} = \mathrm{P}_{l+1,2i+1,2j+1}\begin{pmatrix}
Q_{l,i-\frac{p}{2}+1,j-\frac{p}{2}+1},\cdots,Q_{l,i-\frac{p}{2}+1,j},Q_{l,i-\frac{p}{2}+1,j+1},\cdots,Q_{l,i-\frac{p}{2}+1,j+\frac{p}{2}} \\
\vdots \\
Q_{l,i,j-\frac{p}{2}+1},\cdots,Q_{l,i,j},Q_{l,i,j+1},\cdots,Q_{l,i,j+\frac{p}{2}} \\
Q_{l,i+1,j-\frac{p}{2}+1},\cdots,Q_{l,i+1,j},Q_{l,i+1,j+1},\cdots,Q_{l,i+1,j+\frac{p}{2}} \\
\vdots \\
Q_{l,i+\frac{p}{2},j-\frac{p}{2}+1},\cdots,Q_{l,i+\frac{p}{2},j},Q_{l,i+\frac{p}{2},j+1},\cdots,Q_{l,i+\frac{p}{2},j+\frac{p}{2}}
\end{pmatrix}, \ \forall k \in Z
\end{cases}
\tag{3-1}
$$

The values at even numbered cells are saved to cells in the coarser level grid. In the other odd numbered cells, an interpolating polynomial is applied to approximate the values using the values at the even numbered cells, as in Eq. (3-1). Where $\mathrm{P}_{l,i,j}$ is the interpolating polynomial, and p is an even number.

Wavelet coefficients at odd numbered cells are then calculated as the difference between the solution values and the approximated values. In order to maintain the original numerical accuracy of the conventional CFD method, higher order accurate wavelet transformation is needed. For the selection of the order of interpolation in the wavelet decomposition, let us consider the spatial discretization method with 3rd order accuracy. The residual values in this case have the 4th order of the spatial error term as given by Eq. (3-2).

$$
\begin{aligned}
\widetilde{R}^n_{i,j} &= \left(\Delta y_{i+\frac{1}{2},j}\widetilde{E}^n_{i+\frac{1}{2}} - \Delta y_{i-\frac{1}{2},j}\widetilde{E}^n_{i-\frac{1}{2}}\right) + \left(\Delta x_{i,j+\frac{1}{2}}\widetilde{F}^n_{j+\frac{1}{2}} - \Delta x_{i,j-\frac{1}{2}}\widetilde{F}^n_{j-\frac{1}{2}}\right) \\
&\approx \Delta y\left(E^n_{i+\frac{1}{2}} - E^n_{i-\frac{1}{2}} + O(\Delta x^3)\right) + \Delta x\left(F^n_{j+\frac{1}{2}} - F^n_{j-\frac{1}{2}} + O(\Delta y^3)\right) \\
&= R^n_{i,j} + O(\Delta x^3 \Delta y) + O(\Delta y^3 \Delta x) \\
&\approx R^n_{i,j} + O(\Delta x^4)
\end{aligned}
\tag{3-2}
$$

From Eq. (3-2), the 5th order of the interpolating polynomial is sufficiently accurate and is recommended for the accurate reconstruction of residuals in the excluded cells in the adaptive dataset. Especially in unsteady flow computations, an at least 6th order interpolating polynomial is needed for more precise calculation of the local flow features in an unsteady problem [8]. For consistent accuracy, the same order of interpolating polynomials is necessary not only for the residual interpolation, but also for interpolation in wavelet decomposition. Therefore, the 6th order interpolating polynomial is used for the wavelet decomposition process as well as for the residual interpolation process. Eq. (3-3) shows the details of the sixth-order wavelet decomposition process.

$$
\begin{aligned}
\diamond:\ & \widetilde{Q}^n_{i+1,j} = \frac{1}{256}(3Q^n_{i-4,j} - 25Q^n_{i-2,j} + 150Q^n_{i,j} + 150Q^n_{i+2,j} - 25Q^n_{i+4,j} + 3Q^n_{i+6,j}) \\
\triangle:\ & \widetilde{Q}^n_{i+1,j} = \frac{1}{256}(3Q^n_{i,j-4} - 25Q^n_{i,j-2} + 150Q^n_{i,j} + 150Q^n_{i,j+2} - 25Q^n_{i,j+4} + 3Q^n_{i,j+6}) \\
& \widetilde{Q}^n_{i+1,j+1} = \frac{1}{512}\times(3Q^n_{i,j-4} + 3Q^n_{i+2,j-4} + 2Q^n_{i-2,j-2} - 27Q^n_{i,j-2} - 27Q^n_{i+2,j-2} + 2Q^n_{i+4,j-2} \\
\times:\ & \qquad + 3Q^n_{i-4,j} - 27Q^n_{i-2,j} + 174Q^n_{i,j} + 174Q^n_{i+2,j} - 27Q^n_{i+4,j} + 3Q^n_{i+6,j} \\
& \qquad + 3Q^n_{i-4,j+2} - 27Q^n_{i-2,j+2} + 174Q^n_{i,j+2} + 174Q^n_{i+2,j+2} - 27Q^n_{i+4,j+2} + 3Q^n_{i+6,j+2} \\
& \qquad + 2Q^n_{i-2,j+4} - 27Q^n_{i,j+4} - 27Q^n_{i+2,j+4} + 2Q^n_{i+4,j+4} + 3Q^n_{i,j+6} + 3Q^n_{i+2,j+6})
\end{aligned}
\tag{3-3}
$$

After interpolation of the solution data at the odd numbered cells, the difference values, $d^n_{i,j}$ of each $\diamond$, $\triangle$ and X position are calculated as in Eq. (2-4).

$$
\begin{aligned}
\diamond:\ & d^n_{i+1,j} = Q^n_{i+1,j} - \widetilde{Q}^n_{i+1,j} \\
\triangle:\ & d^n_{i,j+1} = Q^n_{i,j+1} - \widetilde{Q}^n_{i,j+1} \\
\times:\ & d^n_{i+1,j+1} = Q^n_{i+1,j+1} - \widetilde{Q}^n_{i+1,j+1}
\end{aligned}
\tag{3-4}
$$

The decomposition process is performed at the next coarseness level of grid set and all $d^n_{i,j}$ are calculated with multi-resolution.

3-3. Preservation of high order accuracy

Because $\left|d^n_{i,j}\right|_\infty$ is bounded within $O(\varepsilon)$, $O(\varepsilon)$ errors are added to the solutions by the wavelet transformation. Thus, each primitive variable or flux value has $O(\varepsilon)$ errors as in Eq. (3-5).

$$
\begin{aligned}
& \widetilde{\rho}^n_{i,j} = \rho^n_{i,j} + O(\varepsilon),\ \ \widetilde{u}^n_{i,j} = u^n_{i,j} + O(\varepsilon), \\
& \widetilde{v}^n_{i,j} = v^n_{i,j} + O(\varepsilon),\ \ \widetilde{p}^n_{i,j} = p^n_{i,j} + O(\varepsilon), \\
& \widetilde{E}^n_{1/2} = E^n_{1/2} + O(\varepsilon),\ \ \widetilde{F}^n_{1/2} = F^n_{1/2} + O(\varepsilon).
\end{aligned}
\tag{3-5}
$$

Also, if the flux values are discretized with the l^{th} order of spatial accuracy, each primitive variable or flux value has a l^{th} order truncation error term, as in Eq. (3-6).

$$\rho_{i,j}^n = \rho_{i,j,real}^n + O(\Delta x^l),\quad u_{i,j}^n = u_{i,j,real}^n + O(\Delta x^l),$$
$$v_{i,j}^n = v_{i,j,real}^n + O(\Delta x^l),\quad p_{i,j}^n = p_{i,j,real}^n + O(\Delta x^l), \tag{3-6}$$
$$E_{1/2}^n = E_{1/2,real}^n + O(\Delta x^l),\quad F_{1/2}^n = F_{1/2,real}^n + O(\Delta x^l).$$

Combining Eq. (3-5) and (3-6), the fluxes have the following order of errors due to spatial discretization and thresholding, as shown in Eq. (3-7).

$$\widetilde{E}_{1/2}^n = E_{1/2,real}^n + O(\Delta x^l) + O(\varepsilon),\quad \widetilde{F}_{1/2}^n = F_{1/2,real}^n + O(\Delta x^l) + O(\varepsilon) \tag{3-7}$$

Then, by the m^{th} order of time integration, all terms of the numerical errors are derived as Eq. (3-8).

$$\begin{aligned}\widetilde{Q}_{i,j}^{n+1} = \widetilde{Q}_{i,j}^n - \frac{\Delta t}{\Delta x}(E_{1/2,real}^n - E_{-1/2,real}^n + F_{1/2,real}^n - F_{-1/2,real}^n) \\ + O(\Delta x^l \cdot \Delta t) + O(\Delta t^{m+1}) + O(\varepsilon \cdot \Delta t)\end{aligned} \tag{3-8}$$

Therefore, $O(\varepsilon)$ has to be smaller than $O(\Delta x^l)$ and $O(\Delta t^m)$ in order to avoid damaging the l^{th} order of spatial accuracy and the m^{th} order of temporal accuracy of the conventional method. To this end, the modified threshold value is developed as in Eq. (3-9) by assuming a linear advection equation and introducing the CFL condition.

$$\varepsilon' = \min[\varepsilon, \max(\Delta x^l, CFL^m \cdot \Delta x^m)] \tag{3-9}$$

Because our target is third-order accuracy, the third-order spatial and temporal accuracies of the numerical schemes are used. The modified threshold value in this research is then proposed as Eq. (3-10).

$$\varepsilon' = \min[\varepsilon, \max(\Delta x^3, CFL^3 \cdot \Delta x^3)] \tag{3-10}$$

Based on this modified threshold value, ε', the odd numbered cells are included in the dataset only if $d_{i,j}^n$ is greater than ε'. The dataset is then constructed to follow the local features of the solution while preserving the numerical accuracy of the conventional CFD schemes.

3-4. Flux evaluation

In view of Godunov-type approach, the steps to construct a numerical flux at a cell-interface usually consist of interpolation stage and evaluation stage. It is known that interpolation stage is generally independent of evaluation stage where the local Riemann problem is solved at a cell interface. Thus, for higher order spatial accuracy, interpolation stage is modified without changing a Riemann solver. Referring that piecewise constant state generates first order spatial accuracy, a piecewise linear or quadratic distribution is applied for second or third spatial accuracy. From constructing the adaptive dataset, flux values are evaluated in the included cells in the adaptive dataset. This research uses the Finite Volume Method (FVM) to calculate the numerical fluxes $\overline{E}$, $\overline{F}$; flux values are then computed on all sides of the cell with third-order accuracy. For the development of adaptive wavelet method based high order scheme, we adopt

TVD and e-MLP scheme.

3-4-1. TVD (Total Variation Diminishing) limiting process

The cell interface values determined by third-order interpolation with the TVD limiting function are then derived as in Eq. (3-11).

$$\mathbf{\Phi}_L = \overline{\mathbf{\Phi}}_i + 0.5\max(0, \min(2\Delta\mathbf{\Phi}_{i+\frac{1}{2}}, 2\Delta\mathbf{\Phi}_{i-\frac{1}{2}}, \beta_L \Delta\mathbf{\Phi}_{i-\frac{1}{2}})), \tag{3-11a}$$

$$\mathbf{\Phi}_R = \overline{\mathbf{\Phi}}_{i+1} - 0.5\max(0, \min(2\Delta\mathbf{\Phi}_{i+\frac{1}{2}}, 2\Delta\mathbf{\Phi}_{i+\frac{3}{2}}, \beta_R \Delta\mathbf{\Phi}_{i+\frac{3}{2}})). \tag{3-11b}$$

where $\Delta\mathbf{\Phi}_{i-\frac{1}{2}} = \overline{\mathbf{\Phi}}_i - \overline{\mathbf{\Phi}}_{i-1,}$, $\Delta\mathbf{\Phi}_{i+\frac{1}{2}} = \overline{\mathbf{\Phi}}_{i+1} - \overline{\mathbf{\Phi}}_i$, $\Delta\mathbf{\Phi}_{i+\frac{3}{2}} = \overline{\mathbf{\Phi}}_{i+2} - \overline{\mathbf{\Phi}}_{i+1}$ and $\overline{\mathbf{\Phi}}$ represents a cell averaged value, and β_L and β_R are

$$\beta_L = \frac{1+2r_{L,i}}{3} \text{ where } r_{L,i} = \frac{\Delta\mathbf{\Phi}_{i+\frac{1}{2}}}{\Delta\mathbf{\Phi}_{i-\frac{1}{2}}}, \tag{3-12a}$$

$$\beta_R = \frac{1+2r_{R,i+1}}{3} \text{ where } r_{R,i+1} = \frac{\Delta\mathbf{\Phi}_{i+\frac{1}{2}}}{\Delta\mathbf{\Phi}_{i+\frac{3}{2}}}. \tag{3-12b}$$

Using these cell interface values, spatial discretization is performed with conventional schemes such as AUSMPW+ or Roe's FDS method.

3-4-2. e-MLP (enhanced Multi-dimensional Limiting Process)

The key ideas of e-MLP can be summarized into three points. First, an independent distinguishing step, which is separated from high order interpolation and spatial discretization schemes, is introduced to a solver. In this step, multi-dimensional discontinuities are carefully searched for by using Gibbs phenomena. Subsequently, the computational domain is divided into continuous, linear discontinuous and nonlinear discontinuous regions using a sophisticate method. Second, based on the regional information, appropriate limiting criteria are associated with each region in high order interpolation; in a continuous region, there is no limiting process. In a linear discontinuous region such as a region of contact discontinuity, the conventional TVD criterion is applied. In a nonlinear discontinuous region, e.g., a region associated with a shock discontinuity, MLP is used for the removal of numerical oscillation. Third, this elaborate information is fed into a spatial discretization scheme as well as a high order interpolation scheme. Based on this information, proper numerical dissipation is added to a nonlinear discontinuous region for robust calculation, as with the entropy fix in Roe's FDS.

Through these ideas, e-MLP can contribute to the improvement of the solver in terms of accuracy, robustness and efficiency. The brief summary of 3rd order accurate interpolation with e-MLP is shown in Eq. (3-13 ~ 3-16).

(a) 3rd order accuracy

$$\beta_L = \frac{1+2r_{L,i}}{3}, \quad \beta_R = \frac{1+2r_{R,i+1}}{3}, \tag{3-13}$$

where $r_{L,i} = \dfrac{\overline{\mathbf{\Phi}}_{i+1} - \overline{\mathbf{\Phi}}_i}{\overline{\mathbf{\Phi}}_i - \overline{\mathbf{\Phi}}_{i-1}}$ $r_{R,i+1} = \dfrac{\overline{\mathbf{\Phi}}_{i+1} - \overline{\mathbf{\Phi}}_i}{\overline{\mathbf{\Phi}}_{i+2} - \overline{\mathbf{\Phi}}_{i+1}}$.

(b) Continuous region: No limiting function

$$\mathbf{\Phi}_L = \overline{\mathbf{\Phi}}_i + 0.5\beta_L \Delta\mathbf{\Phi}_{i-\frac{1}{2}}, \tag{3-14a}$$

$$\mathbf{\Phi}_R = \overline{\mathbf{\Phi}}_{i+1} - 0.5\beta_R \Delta\mathbf{\Phi}_{i+\frac{3}{2}}. \tag{3-14b}$$

(c) Linear discontinuous region:

TVD criterion, $\phi(r) = \max(0, \min(2, 2r))$

$$\mathbf{\Phi}_L = \overline{\mathbf{\Phi}}_i + 0.5\max(0, \min(2\Delta_{i+\frac{1}{2}}, 2\Delta 2_{\,i-\frac{1}{2}}, \beta_L \Delta\Phi_{i-\frac{1}{2}})), \tag{3-15a}$$

$$\mathbf{\Phi}_R = \overline{\mathbf{\Phi}}_{i+1} - 0.5\max(0, \min(2\Delta_{i+\frac{1}{2}}, 2\Delta 2_{\,i+\frac{3}{2}}, \beta_R \Delta\Phi_{i+\frac{3}{2}})). \tag{3-15a}$$

(d) Nonlinear discontinuous region:

MLP limiter, $\phi(r) = \max(0, \min(\alpha, \alpha r))$

$$\mathbf{\Phi}_L = \overline{\mathbf{\Phi}}_i + 0.5\max(0, \min(\alpha_L \Delta_{i+\frac{1}{2}}, \alpha_L \Delta\Phi_{i-\frac{1}{2}}, \beta_L \Delta\Phi_{i-\frac{1}{2}})), \tag{3-16a}$$

$$\mathbf{\Phi}_R = \overline{\mathbf{\Phi}}_{i+1} + 0.5\max(0, \min(\alpha_R \Delta_{i+\frac{1}{2}}, \alpha_R \Delta\Phi_{i+\frac{3}{2}}, \beta_R \Delta\Phi_{i+\frac{3}{2}})), \tag{3-16b}$$

where $\alpha_{L,R}$ are MLP coefficients.

After the interpolation of primitive variables at the cell interface, AUSMPW+ or Roe's FDS scheme is applied for the spatial discretization.

3-5. Residual interpolation and time integration

In cells excluded from the adaptive dataset, residual interpolation is adopted before time integration. As explained in the previous section, the sixth-order interpolating polynomial is needed in the wavelet decomposition and residual interpolation process in order to maintain the third-order spatial accuracy of the conventional CFD schemes. Therefore, as in Equation (3-3) in the wavelet decomposition process, the sixth-order interpolating polynomial is proposed for residual interpolation, as shown in Equation (3-17).

$$\begin{aligned}
\diamond:\quad & \widetilde{R}^n_{i+1,j} = \frac{3}{256}R^n_{i-4,j} - \frac{25}{256}R^n_{i-2,j} + \frac{75}{128}R^n_{i,j} + \frac{75}{128}R^n_{i+2,j} - \frac{25}{256}R^n_{i+4,j} + \frac{3}{256}R^n_{i+6,j} \\
\triangle:\quad & \widetilde{R}^n_{i,j+1} = \frac{3}{256}R^n_{i,j-4} - \frac{25}{256}R^n_{i,j-2} + \frac{75}{128}R^n_{i,j} + \frac{75}{128}R^n_{i,j+2} - \frac{25}{256}R^n_{i,j+4} + \frac{3}{256}R^n_{i,j+6} \\
& \widetilde{R}^n_{i+1,j+1} = \frac{1}{512}\times(3R^n_{i,j-4} + 3R^n_{i+2,j-4} + 2R^n_{i-2,j-2} - 27R^n_{i,j-2} - 27R^n_{i+2,j-2} + 2R^n_{i+4,j-2} \\
\times:\quad & \qquad + 3R^n_{i-4,j} - 27R^n_{i-2,j} + 174R^n_{i,j} + 174R^n_{i+2,j} - 27R^n_{i+4,j} + 3R^n_{i+6,j} \\
& \qquad + 3R^n_{i-4,j+2} - 27R^n_{i-2,j+2} + 174R^n_{i,j+2} + 174R^n_{i+2,j+2} - 27R^n_{i+4,j+2} + 3R^n_{i+6,j+2} \\
& \qquad + 2R^n_{i-2,j+4} - 27R^n_{i,j+4} - 27R^n_{i+2,j+4} + 2R^n_{i+4,j+4} + 3R^n_{i,j+6} + 3R^n_{i+2,j+6})
\end{aligned} \tag{3-17}$$

After the calculation of residual values in the whole computational domain, time integration is performed using conventional schemes.

Results and Discussion:

1. Compact data representation using adaptive wavelet

To test distinguish of region using wavelets, the test function is selected as a superposition of a sine function and a Gaussian as Eq. (1-1).

$$f(x) = \sin(2\pi x) + e^{-a(x-0.5)^2} \text{ with } \quad a = 10{,}000 \tag{1-1}$$

That is, it is smooth in most of the domain with a small interval of sharp variation. The function has the 1,025 grid points with unit interval as shown in Fig. 1-1(a). After 5 resolution of the adaptive wavelet transformation, the remaining number of grid points is only 57. Also, as shown in Fig. 1-1(b), the dataset follows the local features of solution. That is, the remaining number of grid points is small in the smooth region but large in the rapidly changed region. This compressibility of data is great advantage of wavelets in terms of computational efficiency.

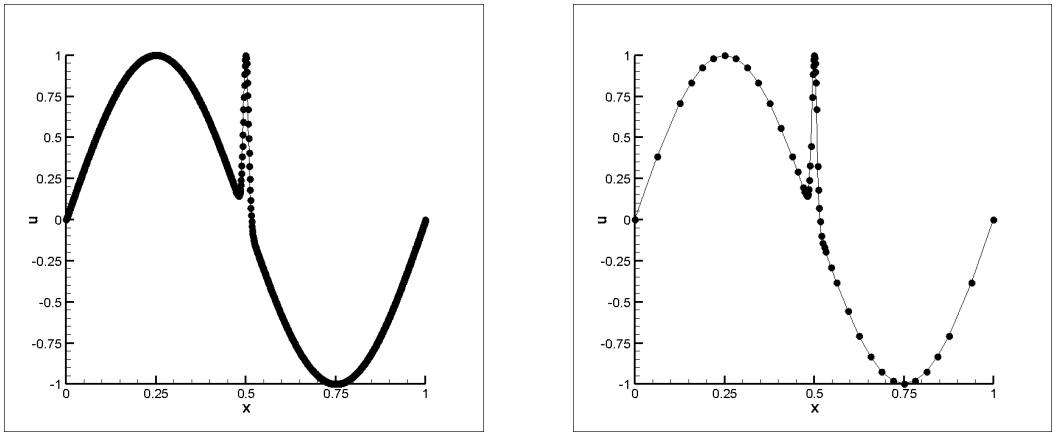

(a) Grid points in an original dataset (b) Grid points in an adaptive dataset

Fig. 1-1. Example of the adaptive wavelet transformation

Generally, wavelet transformation has procedure of abbreviation of wavelet coefficients that are smaller than some threshold value by user. Due to omitting the data, compressed data and original data is always different, and this becomes error of computation. Especially in CFD, each numerical scheme has different order of accuracy depending on truncation error, and if due to the compression of data error is bigger than truncation error, it deteriorate the numerical accuracy of the conventional schemes. Therefore, for efficient compression of data with maintaining the computational accuracy, it should needed to research for thresholding value.

If the wavelet filtering using the wavelet transformation performed to CFD data, computational domain is divided to primary and non-primary flow region. Through the appropriate flagging grid cells, remained primary cell is 1 and non-primary cell is 0 using tag after the wavelet transformation. Accordingly original grid system can be well reconstructed using the only tagged location as 1. To reconstruction of grid, simple concept of one dimensional grid system is shown in Fig. 1-2.

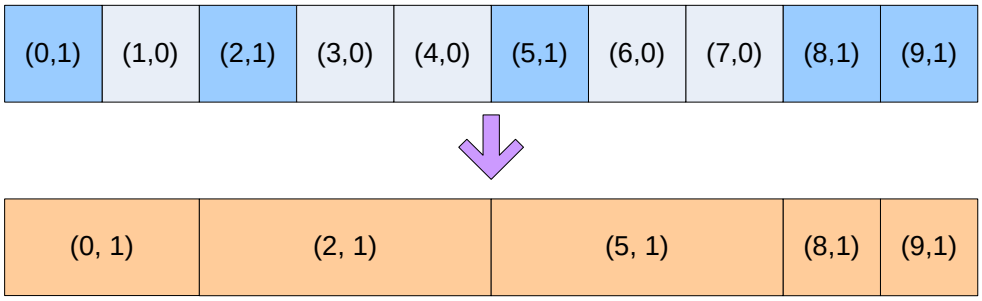

Fig. 1-2 Reconstruction of one dimensional grid system

Data representation of two dimensional grid system is as shown in Fig. 1-3. Original flow data is the NACA0012 airfoil at that Mach number is 0.8 and angle of attack is 5°. Fig. 1-3(a) is original flow data and Fig. 1-3(b) is represented data of original data through the flagging wavelet of 4th resolution. Fig. 1-3(c) is flagged region by tagging cells(1 or 0) and Fig. 1-3(d) is error between original and represented data. In this two dimensional data representation test, thresholding value is 1E-5 and compression ratio is 0.41(compressed data point / original data point). So if the threshoding value is small, error is small but compression ratio is big.

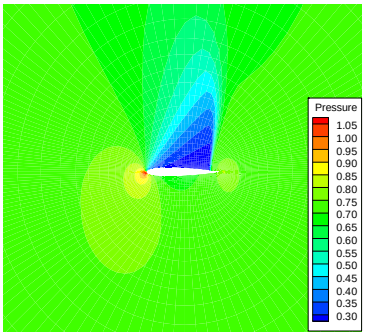

(a) Original pressure distribution

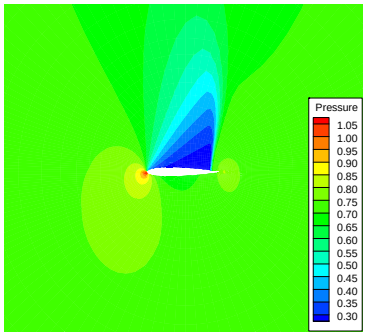

(b) Represented pressure distribution

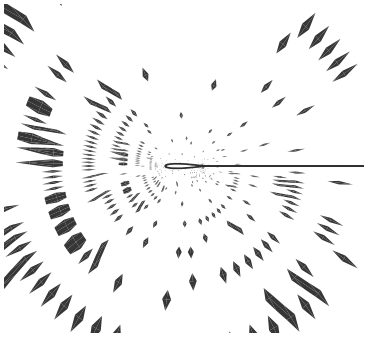

(c) Flagged region as 1

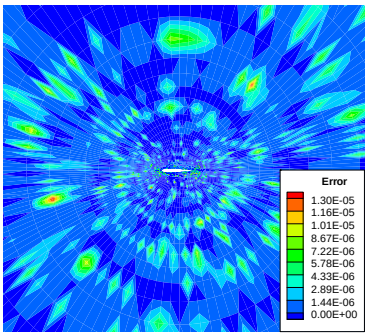

(d) Error of data

Fig. 1-3 Data representation using wavelet transformation

2. Numerical tests of adaptive wavelet method for CFD solution algorithm

2-1. Efficiency of adaptive wavelet in steady problem

Combining all of the introduced methods, i.e. the modified threshold value, the stabilization technique, residual interpolation and restriction technique, we checked the overall enhancement in computational efficiency of NACA0012 flow problems. Here, the AUSMPW+ scheme [21] is used for spatial discretization and the LU-SGS implicit methods [22] is for the time integration. The total iteration number, CPU time gain and difference in lift coefficient associated to each case are summarized in table 2-1. Figs. 2-1 show the pressure contours of the reference solver and adaptive wavelet method with a 2nd level resolution, respectively.

Table 2-1 Test cases and results for the flow at NACA0012 airfoil

NACA0012 Airfoil	Time Integration	Wavelet Decomposition Level	Iteration	CPU Time	Time Ratio	Lift Coefficient	Difference (%)
Subsonic (Ma=0.3, AOA=5)	Dense grid	Reference				0.5497	
	LU-SGS (201×97)	Reference	3698	213.19	1.00	0.5340	2.86
		Level 1	2046	113.84	1.87	0.5331	3.02
		Level 2	1995	101.77	2.09	0.5361	2.47
		Level 3	2015	103.45	2.06	0.5346	2.75

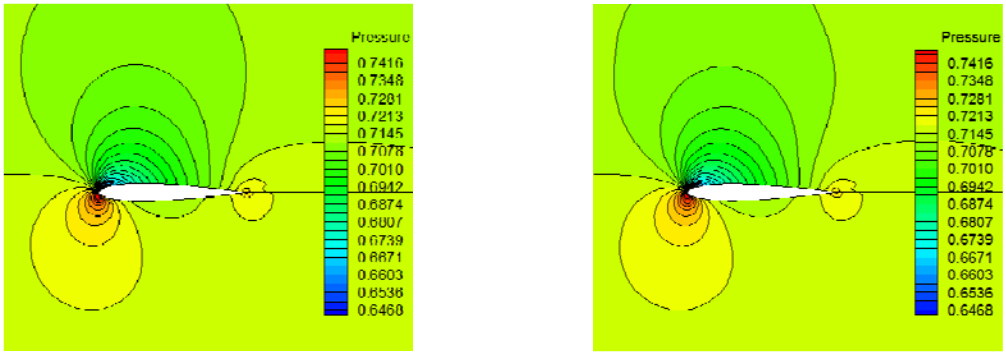

(a) Pressure contours of the reference solver (b) Pressure contours of adaptive wavelet method

Fig. 2-1. LU-SGS time integration for subsonic flow (Ma=0.3, AOA=5°)

From table 2-1, differences in lift coefficients have little relation to the resolution level and change within a 2nd order of accuracy. Concerning the time ratio, the adaptive wavelet method with a 2nd level resolution is better than a 1st level while the difference in the time ratio between the 2nd level and the 3rd level is slight. There exists the proper level according to the complexity of solution and the number of grid points in order to gain optimum efficiency. If the number of grid points is not enough to express the flow physics accurately, it is hard to expect improvements in computing efficiency simply by increasing the resolution level of an adaptive wavelet method. In this case, the appropriate level is the second.

2-2. Efficiency of adaptive wavelet in unsteady problem

Overall enhancement in computational efficiency of shock-vortex interaction problems [2, 23] is evaluated. Here, the AUSMPW+ scheme [21] is used for spatial discretization and 4th order Runge-Kutta explicit method [16] is for the time integration. Fig. 2-2 shows the adaptive datasets according to the wavelet resolution level at t=15 sec. Here, the dataset follows the change of flow features and many cells remains in $I(\varepsilon')$ near the vortex and shock regions. In the other regions, the changes of flow properties are negligible, and the remaining cells are sparsely distributed. The $I(\varepsilon')$ dataset is effectively adapted to solution's features. Also, in these figures, the adaptive datasets between level 3 and 4 are very similar. There is a proper level of wavelet resolution according to the solution complexity. In this case, the appropriate level is 4.

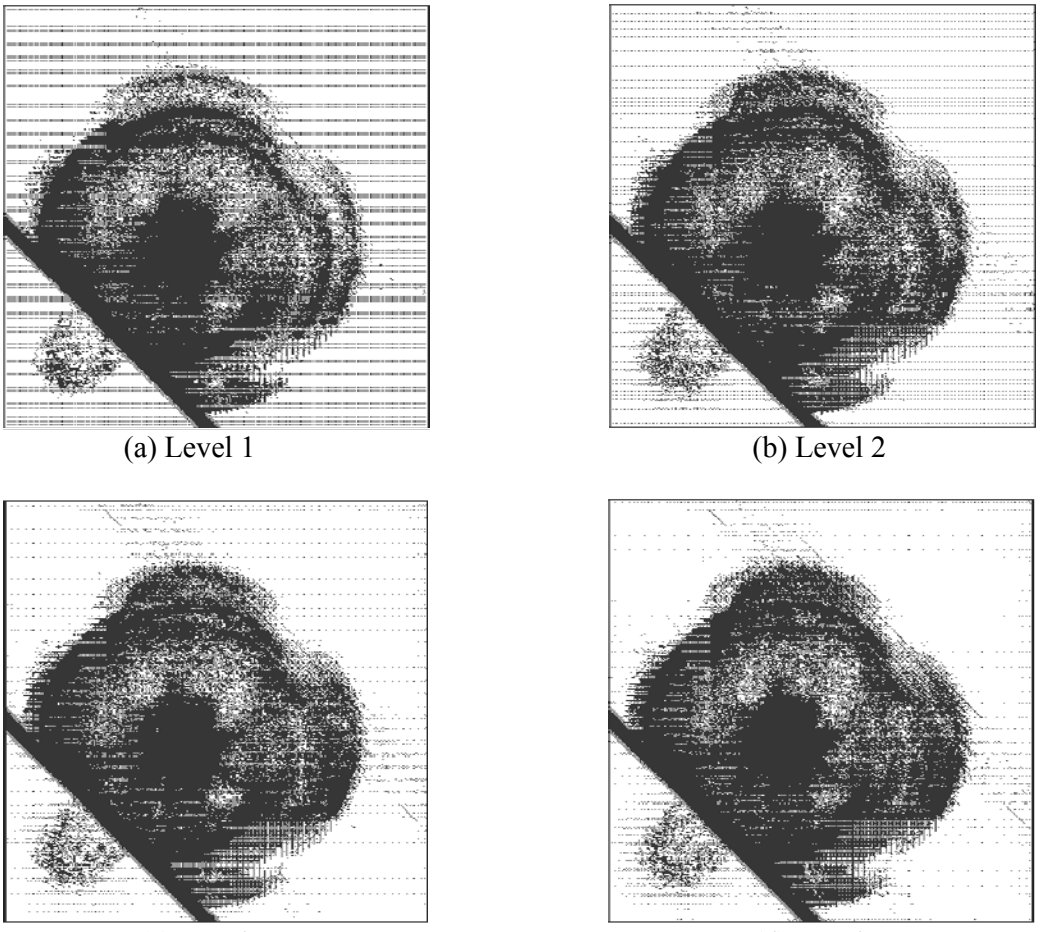

(a) Level 1 (b) Level 2

(a) Level 3 (d) Level 4

Fig. 2-2 Adaptive datasets of shock-vortex interaction problem according to wavelet decomposition level at t=15 sec

Fig. 2-3 and 2-4 show the change of density contours, variation of the compression ratio, and CPU time/iteration during the time integration, respectively. The CPU time/iteration of the reference method was constant 1.58 sec. At the beginning of the calculation, that of the new adaptive wavelet method was much smaller. However, as time went on, the moving vortex

penetrated into and interacted with the stationary normal shock, which complicated the flow features. Then, the CPU time/iteration of the new adaptive wavelet method increased gradually because more grid points were included in the dataset to adapt the dataset to the flow features. Therefore, the compression ratio decreased and accompanied the increase of the CPU time/iteration of the adaptive wavelet method.

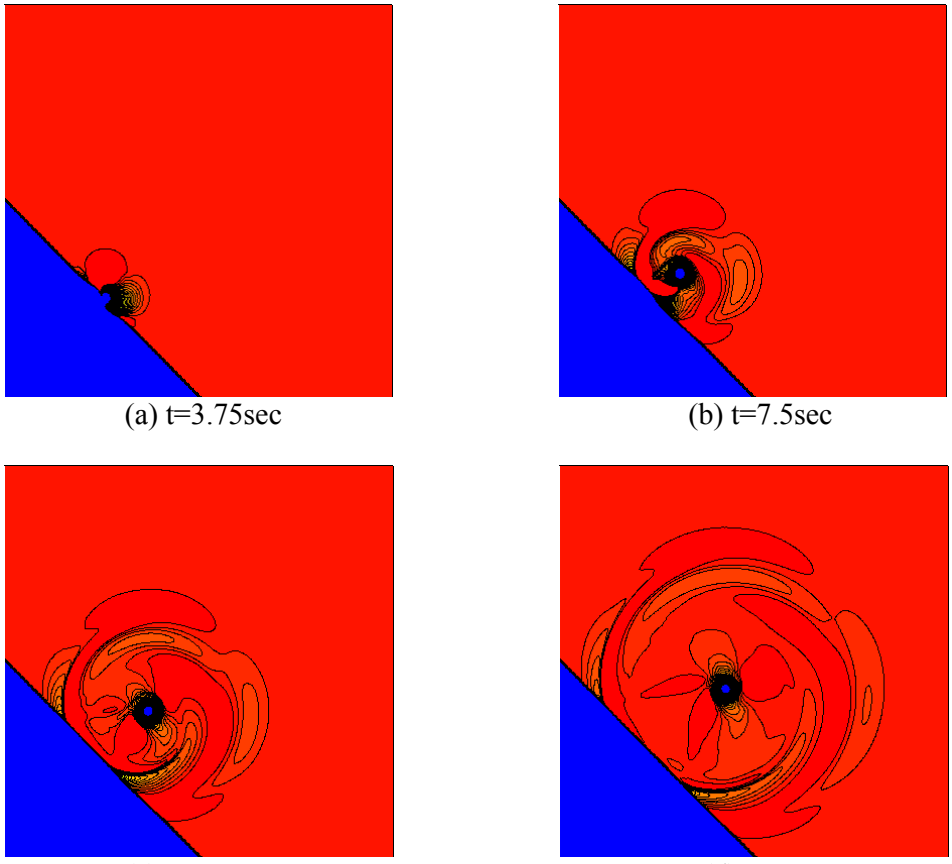

(a) t=3.75sec (b) t=7.5sec

(c) t=11.25sec (d) t=15sec

Fig. 2-3 Change of density contour of shock-vortex interaction problem according to time

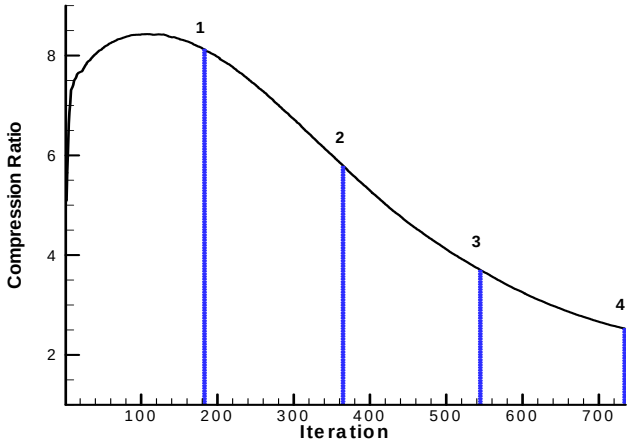

(a) Variation of compression ratio

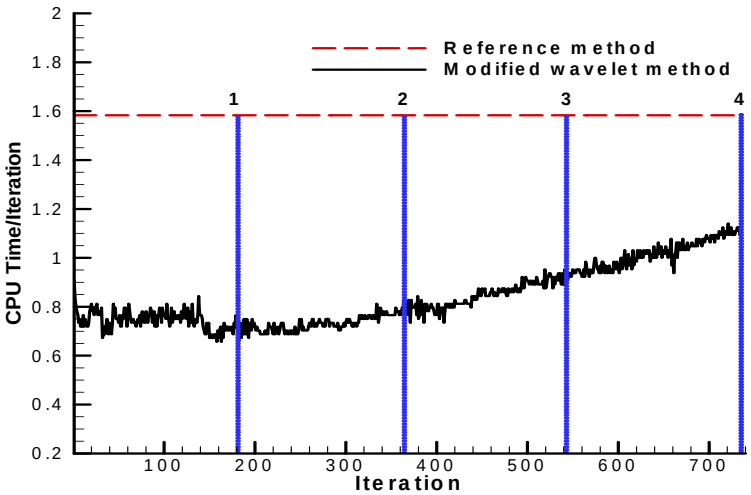

(b) Variation of CPU time/iteration

Fig. 2-4 Variation of compression ratio and CPU time/iteration of shock-vortex interaction problem according to time

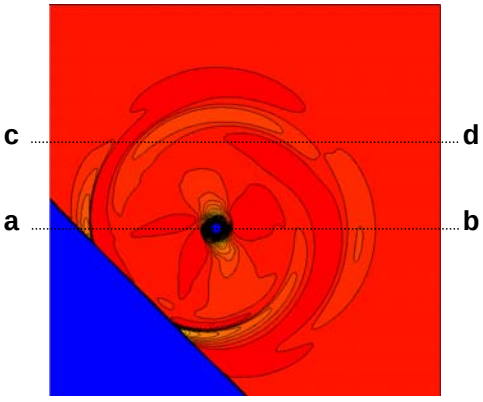

(a) Reference method

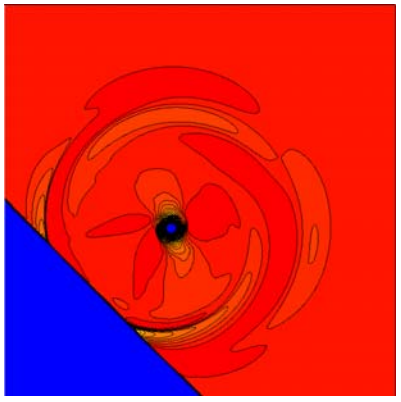

(b) New adaptive wavelet method

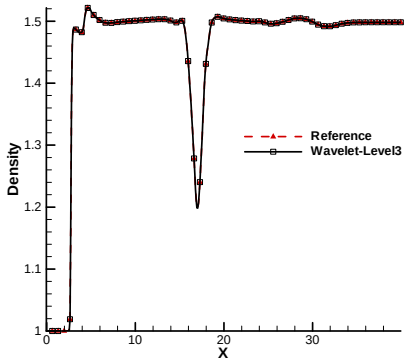

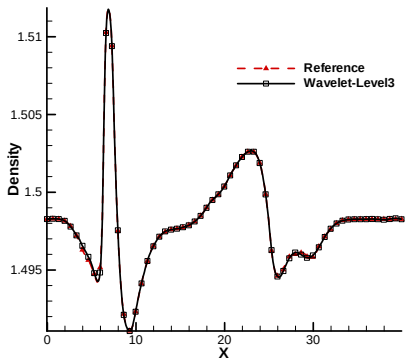

(c) Density contours at a-b line (y=17) (d) Density contours at c-d line (y=25)

Fig. 2-5 Density contours of shock-vortex interaction problem at t=15sec; the wavelet decomposition level is 3.

Overall, the computation time became about 2.0 times faster at maximum when the resolution level of wavelet was 4. The L2 norm between the solutions of the reference solver and the new adaptive wavelet method was 2.56×10^{-7}. The overall efficiency improvement and the L2 error according to wavelet decomposition level are summarized in Table 4. Generally, if the number of cells becomes large, higher computational efficiency can be obtained because the portion of the region where the flow properties change smoothly increases and the compression ratio of the wavelet method is enhanced. To confirm this result, I performed the same simulations except for resizing the number of grid points as 241×241 and summarize the results in Table 5. Although the order of L2 errors was very similar for all cases, the maximum improvement of computational efficiency was reduced from 2.0 times to 1.74 times. The present method can become more effective in flow problems that require a huge size of grid points.

Fig. 2-5 (a) and (b) show the density contours of the reference and the new adaptive wavelet method at t=15sec, respectively. The comparisons of density contours at y=17(a-b line) and y=25(c-d line) are presented in Fig. 2-5 (c) and (d), respectively. The density contours are very similar to each other. Also in Fig. 2-5 (c) and (d), the original features around the vortex core or the shock discontinuity region are exactly represented by the adaptive wavelet method.

3. Extensive applications of adaptive wavelet based high order scheme

3-1. High accurate adaptive wavelet with TVD

3-1-1. Shock Sine Wave Interaction Problem

First, the higher order accurate adaptive wavelet method was tested with the one-dimensional shock-sine wave interaction problem. The governing equation was the one-dimensional Euler equation and the initial conditions are shown in Eq. (3-1).

$$\begin{aligned}(\rho,U,p)&=(3.8571,2.6294,10.333) \quad \text{where} \quad 0\le x\le 1,\\ (\rho,U,p)&=(1+0.2\sin(5(x-5)),0,1) \quad \text{where} \quad 1\le x\le 10.\end{aligned} \tag{3-1}$$

Here, 3rd order interpolation with TVD limiting function was utilized for the evaluation of cell

interface values. Then, AUSMPW+ method was used for spatial discretization and 3rd order of Runge-Kutta method was for time integration, respectively [21, 24, 25]. And the number of grid points is set as $m \times 2^l + 1$ because of easy dyadic coarsening during the wavelet transformation. The value of ε was set as 10^{-5}.

In order to confirm that the adaptive wavelet method maintains the numerical accuracy of the conventional schemes, grid convergence tests are performed. Fig. 3-1 shows the results of the 3rd order accurate conventional method and the adaptive wavelet method. It is shown in Fig. 3 that the higher order accurate adaptive wavelet method maintains the 3rd order of accuracy of a conventional solver by setting the thresholding values.

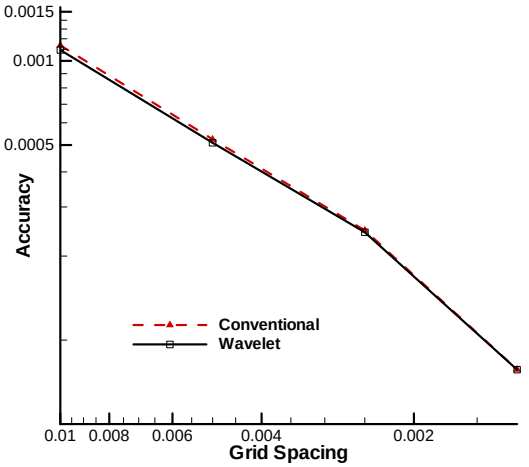

Fig. 3-1 Results of grid convergence test.

The CPU times of the higher order adaptive wavelet method are compared to those of a conventional 3rd order accurate CFD solver according to the wavelet decomposition level in Table 3-1. In the case of higher order accurate adaptive wavelet method with a 1st level resolution, the CPU time rather increases. This is because the increase in CPU time due to additional computations for the adaptive wavelet method exceeds the decrease in CPU time from the flux evaluation step. On the other hand, in the case of other resolutions, the decrease in CPU time for the evaluation of fluxes is dominant and the overall CPU time decreases. For example, in a 3rd level of wavelet decomposition with 8001 grid points, the computation of the wavelet method is 1.93 times faster than that of a conventional solver.

Table 3-1 Comparison of CPU times in shock-sine wave interaction problem

Level	Grid Number	CPU Time		Time Ratio
		Original	Wavelet	
1	1001	70.656	73.828	0.96
	2001	139.422	144.547	0.97
	4001	277.359	286.344	0.97
	8001	550.453	571.547	0.96
2	1001	70.656	50.531	1.40
	2001	139.422	97.000	1.44
	4001	277.359	189.594	1.46
	8001	550.453	377.844	1.46
3	1001	70.656	48.547	1.46

2001	139.422	84.891	1.64
4001	277.359	143.047	1.94
8001	550.453	285.641	1.93

Fig. 3-2 shows the solutions of a conventional solver and the higher order adaptive wavelet method at t=1 with 8001 grid points. The original solution of a conventional solver and that of the wavelet method are almost same. In order to verify it more precisely, the density contours of a conventional solver and the wavelet method with 3rd level resolution are enlarged at positions A and B in Fig. 3-3. In both rapidly changing region of A and the smooth region of B, the results of adaptive wavelet method show good agreement with those of a conventional solver.

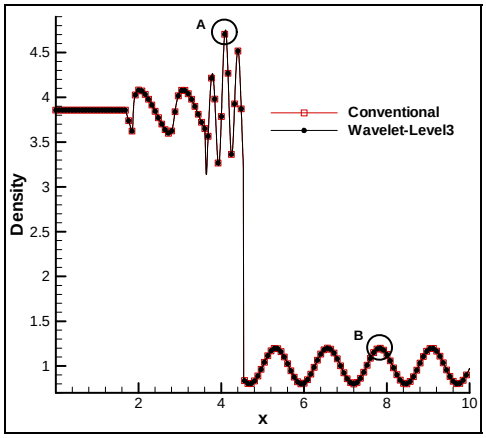

Fig. 3-2 Comparison of density distribution of the shock-sine wave interaction problem at t=1sec.

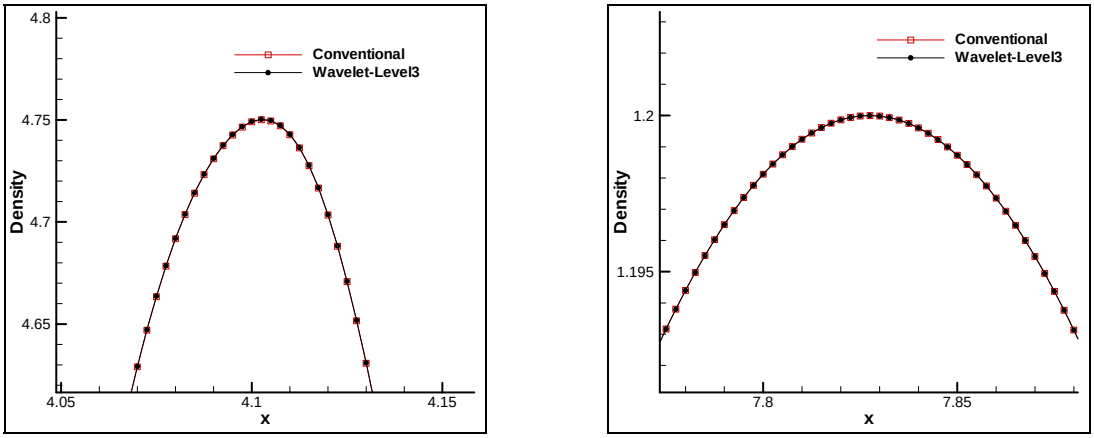

(a) Magnified pressure plots in the region of A (b) Magnified pressure plots in the region of B

Fig. 3-3 Detailed density distribution.

3-1-2. Shock-Vortex Interaction Problem

To assess the accuracy and efficiency of the higher order accurate adaptive wavelet method in more complicated case, it is applied to a shock-vortex interaction problem [23]. The domain is set as $-20 \le x \le 5$ and $-20 \le y \le 10$ with a 600×600 grid. The initial velocity, density and pressure distributions of a vortex flow are presented in Eq. (3-2).

$$
\begin{aligned}
&\text{Tangential velocity: } u_\theta = M_v r \exp[(1-r^2)/2], \\
&\text{Radial velocity: } u_r = 0, \\
&\text{Vorticity: } \omega(r) = M_v(2-r^2)\exp[(1-r^2)/2], \\
&\text{Pressure: } p(r) = \frac{1}{\gamma}[1-\frac{\gamma-1}{2}M_v^2\exp(1-r^2)]^{\gamma/(\gamma-1)}, \\
&\text{Density: } \rho(r) = \frac{1}{\gamma}[1-\frac{\gamma-1}{2}M_v^2\exp(1-r^2)]^{1/(\gamma-1)}.
\end{aligned}
\tag{3-2}
$$

The Mach number of vortex is 0.39 and the initial vortex core is located at (-5,-5). The normal shock with Mach number of 1.29 is propagated to the vortex from right boundary of the computational domain. Fig. 3-4 shows the schematic diagram of shock-vortex interaction problem; in step1, the shock wave deforms as the shock-vortex interaction develops. In step2, the shock wave deforms more and more with the development of the interaction and reflected waves emanate. Finally in step3, slip lines are formed and the lines meet the reflected wave and normal shock at the triple points. For the simulation of this complicated flow problem, AUSMPW+ method combined with 3rd order interpolation with TVD limiting function was used for spatial discretization and 3rd order of Runge-Kutta method was for time integration, respectively.

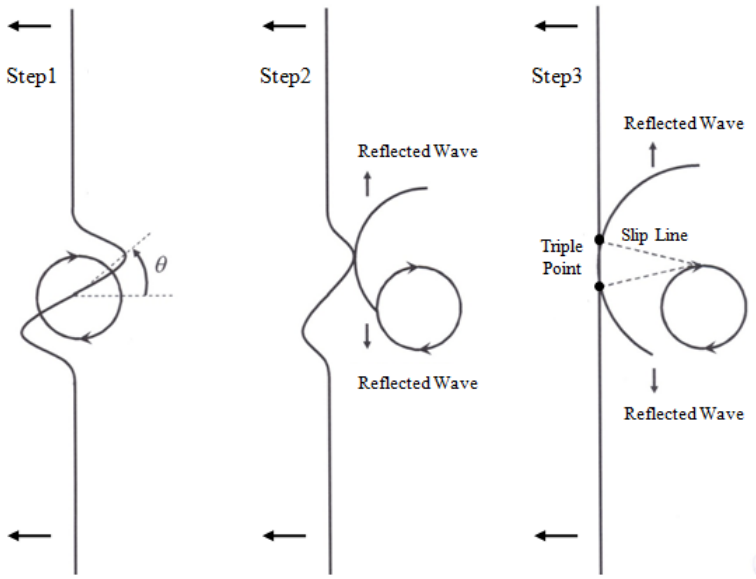

Fig. 3-4 Schematics of shock-vortex interaction problem.

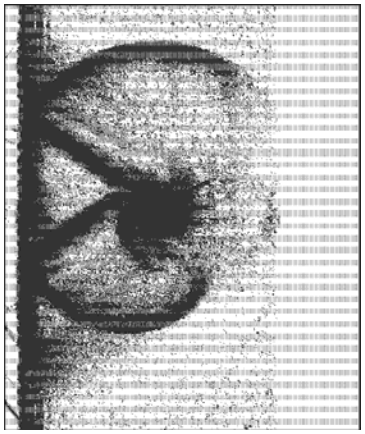

(a) Level 1

(b) Level 2

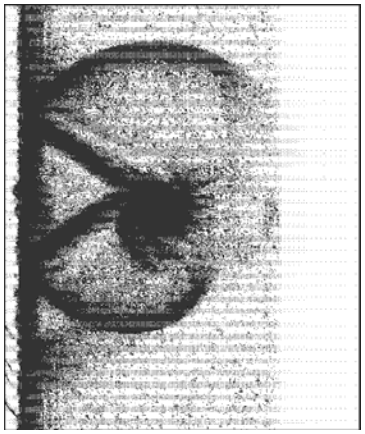

(c) Level 3

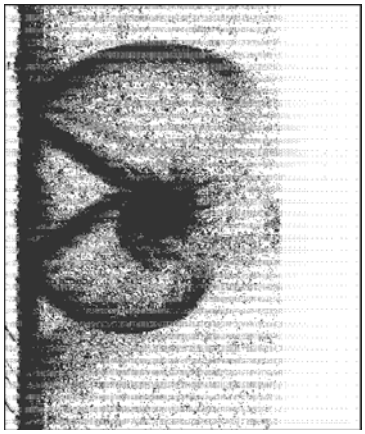

(d) Level 4

Fig. 3-5 Adaptive datasets of shock-vortex interaction problem according to wavelet decomposition level at t=18.

After the non-dimensional time of 18, the adaptive dataset according to the level of wavelet decomposition are represented in Fig. 3-5. It is shown in these figures that the dataset follows the local features of the solution, accurately; many cells are automatically remained near the vortex core, normal shock regions, reflected wave region, and slip lines, etc. according to the crucial flow features. In the other smooth regions, the changes if the flow properties are negligible and the remaining cells are sparsely distributed. Here, the adaptive datasets between level 3 and 4 are very similar. There is a proper level of wavelet resolution according to the solution complexity and the appropriate level is 3 in this case. After the construction of an adaptive dataset, operation with high cost such as high order interpolation and flux evaluation are performed only at the remaining cells, which enhance the computational efficiency.

Fig. 3-6 shows the density contours of a conventional 2^{nd} order accurate solver, 3^{rd} order accurate solver and the adaptive wavelet method with 3 level of wavelet decomposition after the non-dimensional time of 18. In this figure, it is shown that the contour of 2^{nd} order accurate conventional solver is smeared comparing with that of 3^{rd} order accurate solver. However, the 3^{rd} order accurate adaptive wavelet method can maintain the original features of a solution; the contours of slip line, reflected wave pattern, etc. are clearly presented not only in the results of the 3^{rd} order accurate solver but also in the adaptive wavelet method.

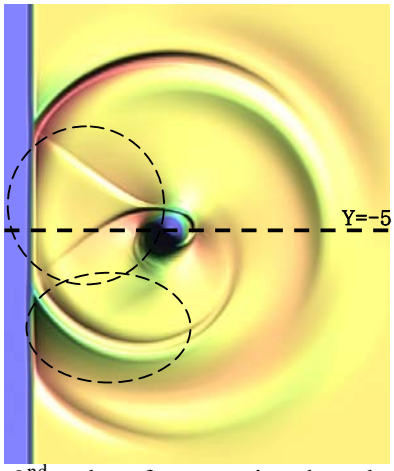

(a) 2nd order of conventional method

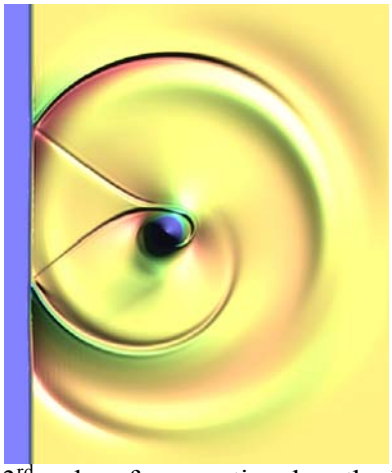

(b) 3rd order of conventional method

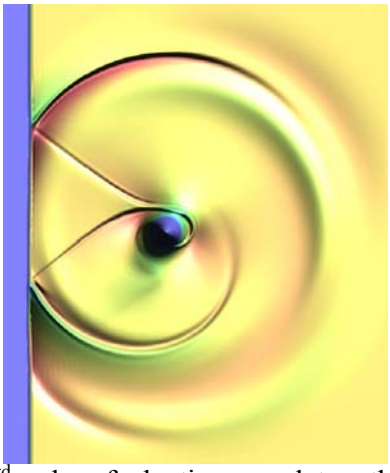

(c) 3rd order of adaptive wavelet method

Fig. 3-6 Comparison of density contours of shock vortex interaction problem at t=18

Fig. 3-7 shows the detailed density distributions of 2nd order accurate solver, 3rd order accurate solver, the adaptive wavelet method at y=-5 and they are compared with the result of dense grid system. In the result of 2nd order accurate solver, the vortex and reflected wave is dissipated compared with the 3rd order accurate conventional solver and the wavelet method. However, by using 3rd order accurate method, the density distributions are clearly represented; the results of 3rd order accurate method follows that of dense grid system more accurately though small number of grid points is used. Therefore, it can be verified in this test that the adaptive wavelet method can maintain the numerical accuracy of the 3rd order accurate conventional solver; it presents higher order accurate results compared with that of the 2nd order accurate solver.

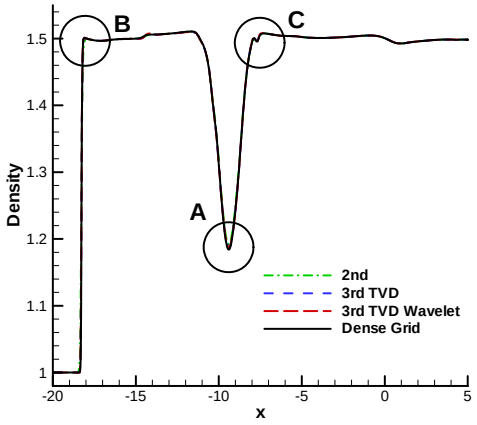

(a) Density distribution at y=-5

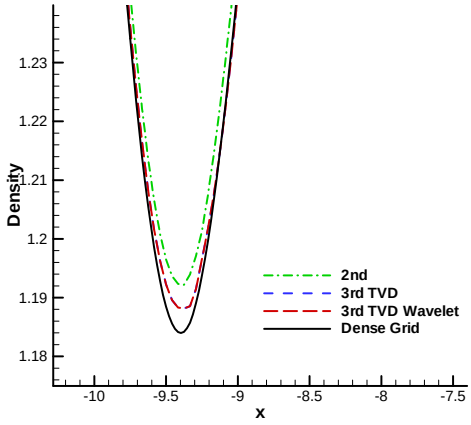

(b) Detailed density distribution at A region

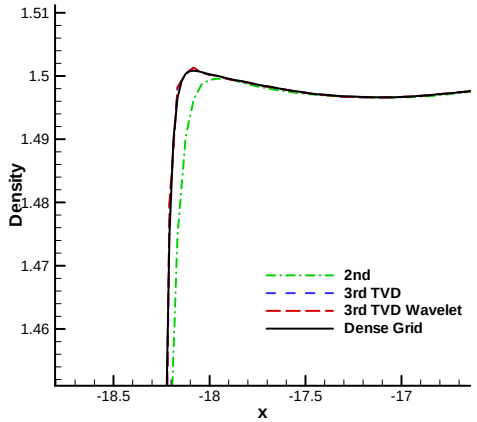

(c) Detailed density distribution at B region

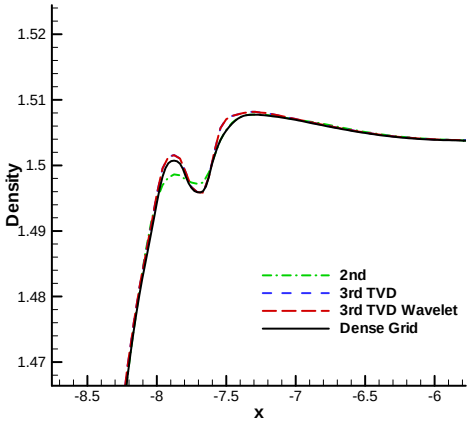

(d) Detailed density distribution at C region

Fig. 3-7 Comparison of density distribution at y=-5.

The CPU times of conventional solver and adaptive wavelet method and L2 error norm between the results of 3rd order accurate conventional solver and adaptive wavelet method are summarized in Table 3-2. In this table, the order of L2 error norm is very small, that is, the results of adaptive wavelet method are nearly similar to that of the 3rd order accurate solver. On the other hand, there is the substantial enhancement of the computational efficiency by using the adaptive wavelet method; in case of the 3rd order accurate solver, the computational speed is only about 80% of the speed of the 2nd order accurate solver due to the operational cost of high order interpolation. However, the computational time of adaptive wavelet method with l level of wavelet decomposition becomes somewhat faster than the 2nd order accurate solver. The cost of high order interpolation and flux evaluation decreases because high order interpolation and flux evaluation are not performed at the excluded cells in the adaptive dataset. As the wavelet resolution level increases, the adaptive wavelet method with 3rd order accuracy becomes more efficient than 2nd order accurate solver as well as 3rd order accurate solver; the computational time of adaptive wavelet method is about 1.4 times faster than the 2nd order accurate conventional solver and 1.9 times faster than the 3rd order accurate solver at maximum when the resolution level of wavelet is 3.

Table 3-2 Results of efficiency improvements in the shock-vortex interaction problem; Grid size is 601×601

Wavelet Decomposition	L2 Error	CPU Time	Time Ratio
2nd Order Conventional		8080	
3rd Order Conventional		10446	0.77
Level 1	6.90×10^{-8}	7837	1.03
Level 2	8.65×10^{-8}	6048	1.34
Level 3	8.46×10^{-8}	5603	1.44
Level 4	7.42×10^{-8}	5676	1.42

3-1-3. Isentropic vortex problem

In order to assess the adaptive wavelet analysis in continuous problem, it was applied to an isentropic vortex problem. The vortex model was defined as Eq. (3-3) [26].

$$\begin{aligned} &\text{Tangential velocity: } u_\theta = M_v r \exp\left[\frac{1-r^2}{2}\right], \\ &\text{Radial velocity: } u_r = 0, \\ &\text{Density velocity: } \rho(r) = \left(1-\frac{\gamma-1}{2}M_v^2\exp[1-r^2]\right)^{1/(\gamma-1)}, \\ &\text{Pressure distribution: } p(r) = \rho^\gamma/\gamma. \end{aligned} \tag{3-3}$$

Here, the computational domain ranged from (-5,-5) to (5,5) with equal grid spacing and the vortex core was located at (0,0). The vortex Mach number, M_v was 1.0 and the number of grid points was 201×201. The CFL number was 0.5 and the boundary was fixed with initial values. For a simulation, a third-order spatial interpolation with a MLP limiting function was utilized for the evaluation of cell interface values and AUSMPW+ was for flux calculation. Then time integration by the 3rd order of Runge-Kutta method was applied. After a non-dimensional time of 50, the density distributions were plotted.

Through the thresholding, many cells are remained near the vortex core as shown in Fig. 3-8. Fig. 3-9 shows the density distribution of second-order accurate solver, third-order accurate solver, and the adaptive wavelet with 3 level of resolution along y=0. The density distribution of second order accurate solver is damped out near the vortex core region. However, third order accurate solver and adaptive wavelet can offer improved steepness near the vortex core region.

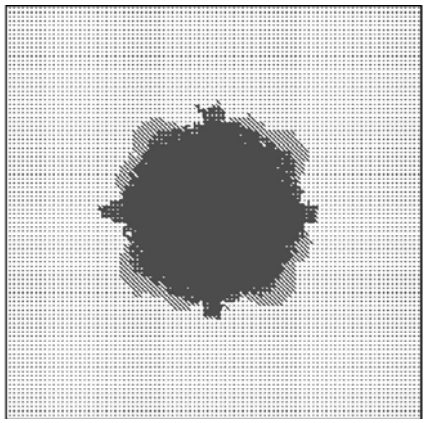

(a) Level 1

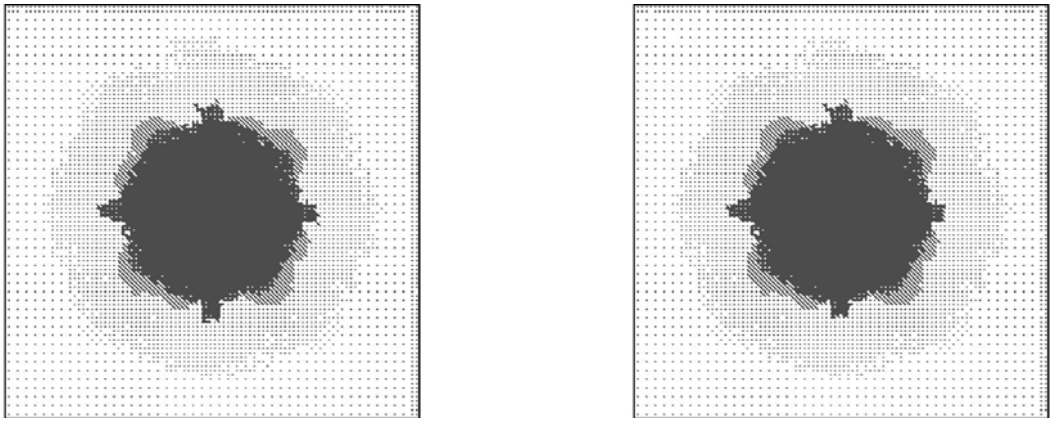

(b)Level 2 (c) Level 3

Fig. 3-8 Adaptive datasets of the isentropic vortex flow according to resolution level.

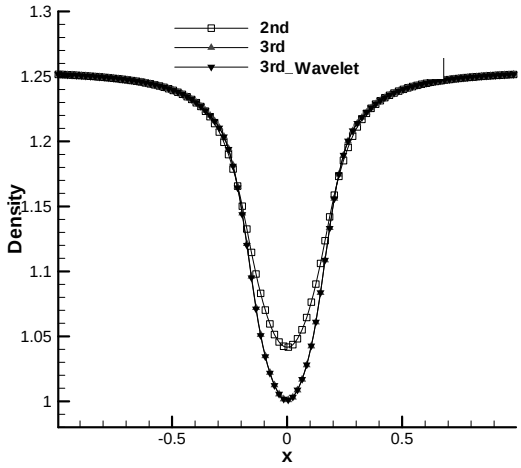

Fig. 3-9 Comparison of the density distributions at y=0.

The computational time of second order solver, third order solver and adaptive wavelet method and the L2 error norm between the results of the third-order solver and the multi-resolution analysis are summarized in Table 6-3. It is shown that the computation of multi-resolution analysis with 3 level of resolution becomes 1.7 times faster than third order accurate solver while the L2 error norms are nearly small. Hence, multi-resolution analysis can enhances the accuracy of a solution compared with a second order accurate solver as well as it improves the computational efficiency of a third order accurate solver.

Table 3-3. Results of efficiency improvements in the isentropic vortex problem; Grid size of 201×201.

Adaptive wavelet	L2 Error	CPU Time	Time Ratio 2^{nd} / wavelet(3^{rd})
Second-Order Conventional		4081	
Third-Order Conventional		7054	
Level 1	6.81×10^{-7}	5107	1.38
Level 2	8.03×10^{-7}	4549	1.55
Level 3	7.80×10^{-7}	4266	1.65

3-2 High accurate adaptive wavelet with e-MLP

3-2-1 Shock-Vortex Interaction Problem

First, the higher order accurate adaptive wavelet method was tested with the shock-vortex interaction problem in Eq. (3-2). The domain is set as $-20 \le x \le 5$ and $-20 \le y \le 10$ with a 400×400 grid. The Mach number of vortex is 0.39 and the initial vortex core is located at (-5,-5). The normal shock with Mach number of 1.29 is propagated to the vortex and ε is set as 10^{-5}. The CPU times of 2nd order accurate TVD computation, 3rd order accurate TVD computation, 3rd order accurate e-MLP computation, and 3rd order accurate e-MLP computation with adaptive wavelet method are summarized in Table 3-4. In this table, it is definitely shown that 3rd order accurate TVD and e-MLP computations need more computational time than 2nd order accurate TVD computation. Also, e-MLP spends 20% of additional computational cost comparing with the result of 3rd order TVD solver because of the complexity of the calculation of MLP coefficients, $\alpha_{L,R}$ in nonlinear discontinuous regions.

Table 3-4. Comparison of CPU times in shock-vortex interaction problem.

Level	CPU Time				Time Ratio
	2nd order	3rd order	e-MLP (3rd)	Wavelet	2nd / wavelet(3rd)
Level 1				1962	0.886
Level 2	1738	2092	2498	1537	1.131
Level 3				1478	1.176

However, the CPU time of e-MLP solver with 1 level of wavelet resolution becomes smaller than that of 3rd order TVD solver as well as e-MLP solver though it is still larger than that of 2nd order TVD solver. It is because the region which needs high order accurate flux evaluation including e-MLP decreases by the wavelet transformation. The decrease of CPU time in flux evaluation exceeds the increase of CPU time caused by wavelet transformation and the application of e-MLP. By increasing the wavelet resolution level, then the computational efficiency is substantially enhanced and the computation becomes faster than the 2nd order accurate TVD solver; the CPU time of wavelet method became about 1.2 times faster than the 2nd order accurate TVD solver at maximum when the resolution level of wavelet is 3.

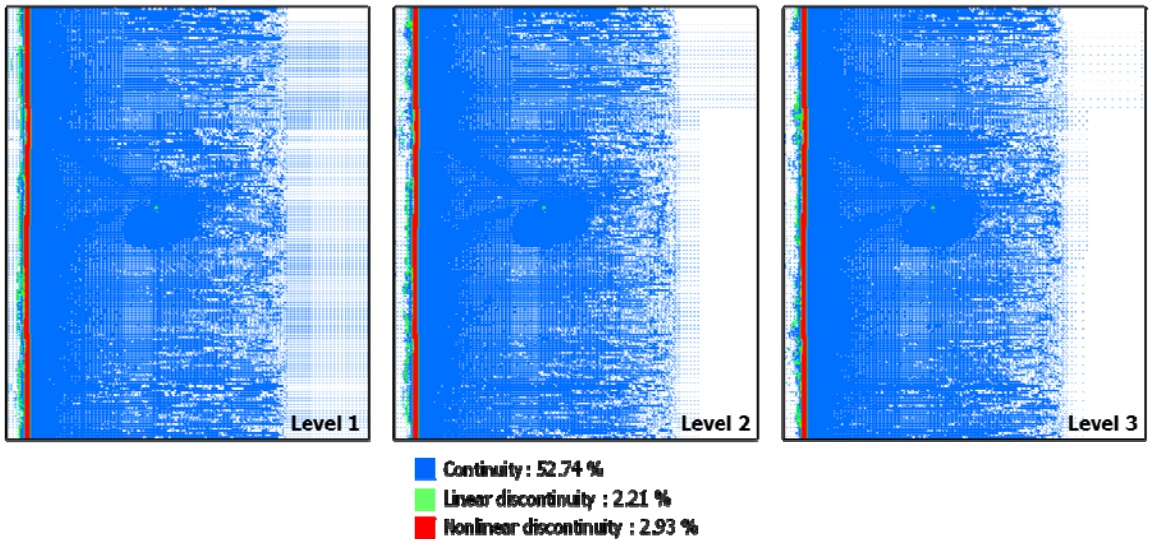

Fig. 3-10 Adaptive dataset by the wavelet transformation at t=18.

The adaptive dataset by the wavelet transformation is constructed so as to follow these physical features of the solution accurately as Fig. 3-10; many cells are remained near the vortex and shock regions. In the other smooth regions, the changes of the flow properties are negligible and the remaining cells are sparsely distributed. By the wavelet transformation, the remaining cells in the adaptive dataset are about 58% of the whole computational domain where fluxes are calculated. Here, the remaining regions are divided into continuous, linear dis-continuous and nonlinear discontinuous regions; 53% of the whole computational domain is continuous region, 2% is linear discontinuous region, and 3% is nonlinear discontinuous region. Then in the continuous region, there is no application of limiting function. In the linear discontinuous region and non-linear discontinuous region, TVD and MLP limiting function are used for oscillation removal, respectively. Due to the combination of wavelet and e-MLP, the computational efficiency is substantially enhanced.

Fig. 3-11 shows the density contours of 2^{nd} order TVD solver, 3^{rd} order TVD solver, 3rd order e-MLP solver and 3^{rd} order e-MLP solver with the wavelet method after the non-dimensional time of 18. In these figures, it is shown that the contour of 2^{nd} order accurate TVD solver is smeared comparing with that of 3^{rd} order accurate solvers. However, the 3^{rd} order e-MLP with the wavelet method can maintain the original features of a solution; the contours of slip lines, reflected wave pattern, etc. are clearly presented.

(a) 2nd order TVD

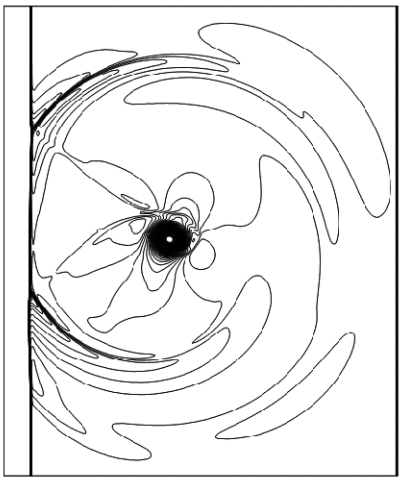

(b) 3rd order TVD

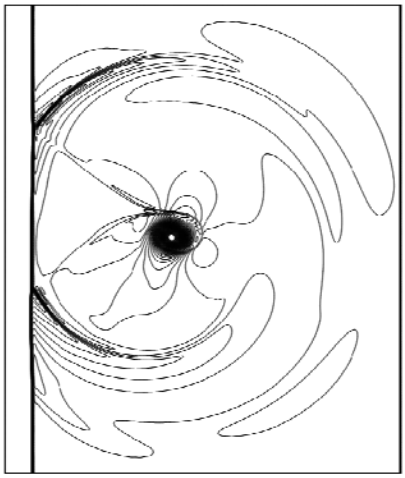

(c) 3rd order e-MLP

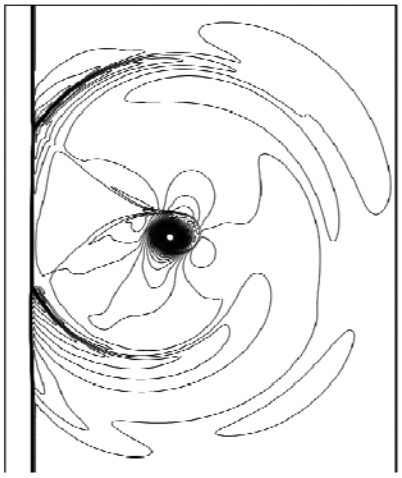

(d) 3rd order e-MLP + wavelet

Fig. 3-11 Comparison of the density distributions at y=0.

Fig. 3-12 shows the detailed density distributions of 2nd order TVD solver, 3rd order TVD and e-MLP solver, and the e-MLP with adaptive wavelet method at y=-5. And they are compared with the result of dense grid system with 2nd order accurate solver. In the result of 2nd order TVD computation, the vortex and reflected wave is dissipated compared with the 3rd order accurate solvers and the wavelet method. However, in case of the 3rd order TVD, e-MLP methods and the wavelet method, the density distributions follow that of dense grid system accurately.

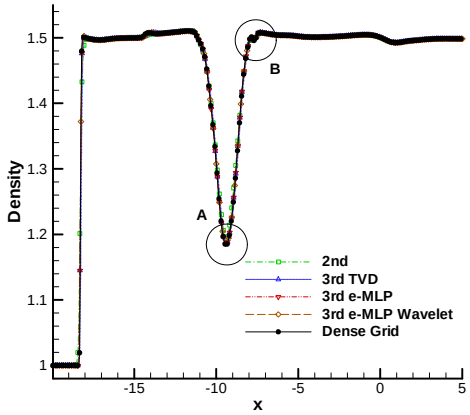

(a) Density distribution at y=-5

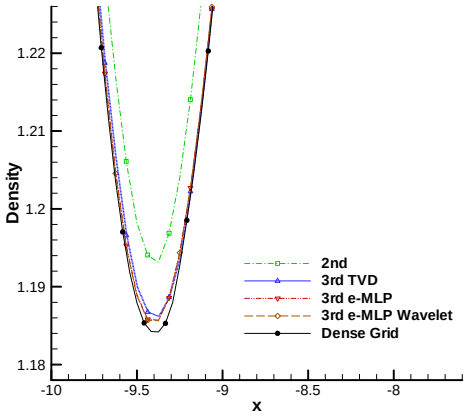

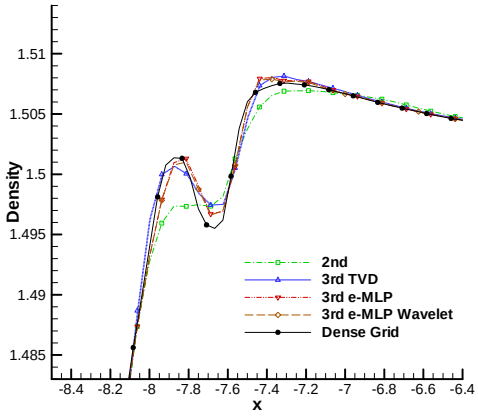

(c) Detailed density distribution at A region (d) Detailed density distribution at B region

Fig. 3-12 Comparison of density distribution at y=-5.

3-2-2. Viscous shock tube Problem

The second test is unsteady viscous shock tube problem [27, 28]. The computational domain is set to be $0 \le x \le 1,\ 0 \le y \le 0.5$, and the total number of grids is 401×201. For boundary conditions, symmetric boundary conditions are applied at $y = 0.5$. Then at the other sides, wall boundary conditions are enforced. The initial conditions of this problem are given as Eq. (3-4).

$$(\rho, u, v, p) = (120,0,0,\frac{120}{\gamma}) \text{ where } 0 \le x \le 0.5, 0 \le y \le 0.5,$$
$$(\rho, u, v, p) = (1.2,0,0,\frac{1.2}{\gamma}) \text{ where } 0.5 < x \le 1, 0 \le y \le 0.5, \quad (3\text{-}4)$$

with $\gamma = 1.4,\ \mathrm{Re} = 200,$ and $\mu = \text{constant}$.

In this problem, the governing equation is two-dimensional Navier-Stokes' equations. Inviscid fluxes are discretized by AUSMPW+ & e-MLP. Viscous fluxes are calculated by the 2nd order of spatial accuracy. For a time integration, the 4th order of Runge-Kutta method with CFL number=0.4 is applied and ε is 10^{-5}.

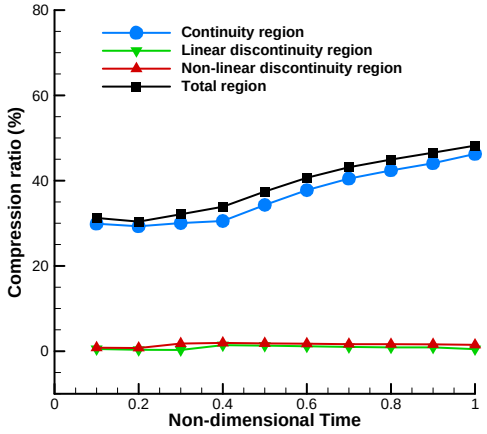

(a) Level 1

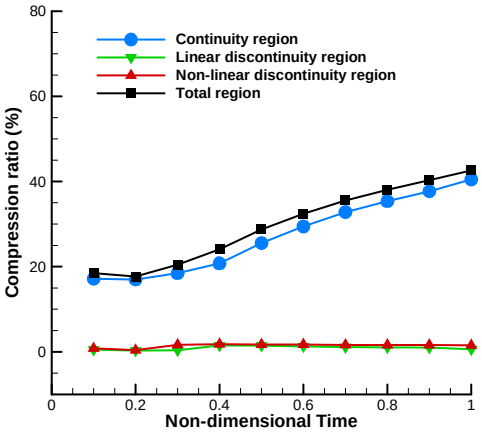

(b) Level 2

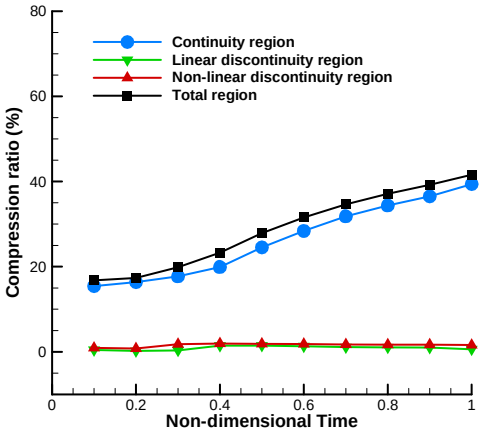

(c) Level 3

Fig. 3-13 Compression ratio of shock tube problem at each time

Fig. 3-13 shows the compression ratio at each time. Due to the moving shock and interactions between the shock and the boundary layer, the total compression ratio increase as time goes further. Especially, the compression ratio in continuity region influences total compression ratio most, because the flow features become very complex. However, the compression ratio in linear discontinuity region and non-linear discontinuity region are few changes of ratio.

Fig. 3-14 shows the adaptive dataset according to the level of wavelet resolution at t=1. At the beginning, the strong shock is propagated to the right wall, and then reflected and re-propagated again to the left accompanying complex shock-shear-boundary layer interactions. Here, the dataset is seen to follow the flow feature effectively. Near shock discontinuities and the vortex region, there remain many grid points to manifest the crucial features of solution.

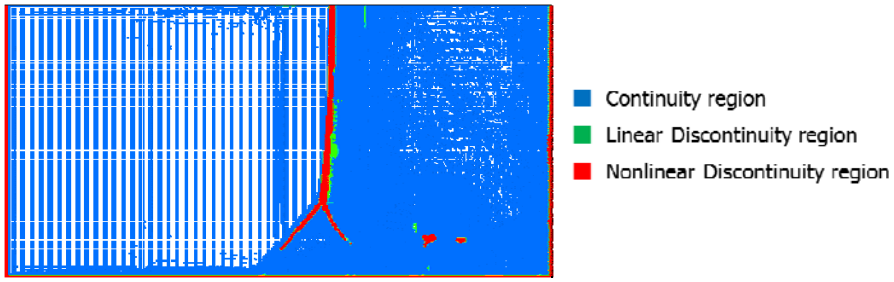

(a) Level 1

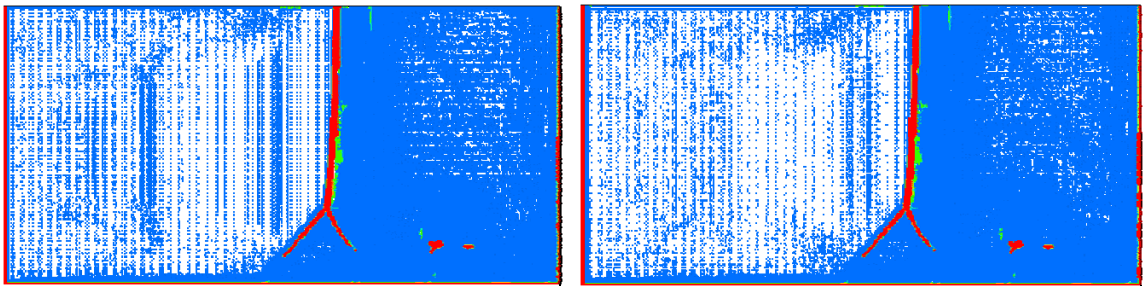

(b) Level 2 (c) Level 3

Fig. 3-14 Adaptive dataset according to the wavelet decomposition at t=1.

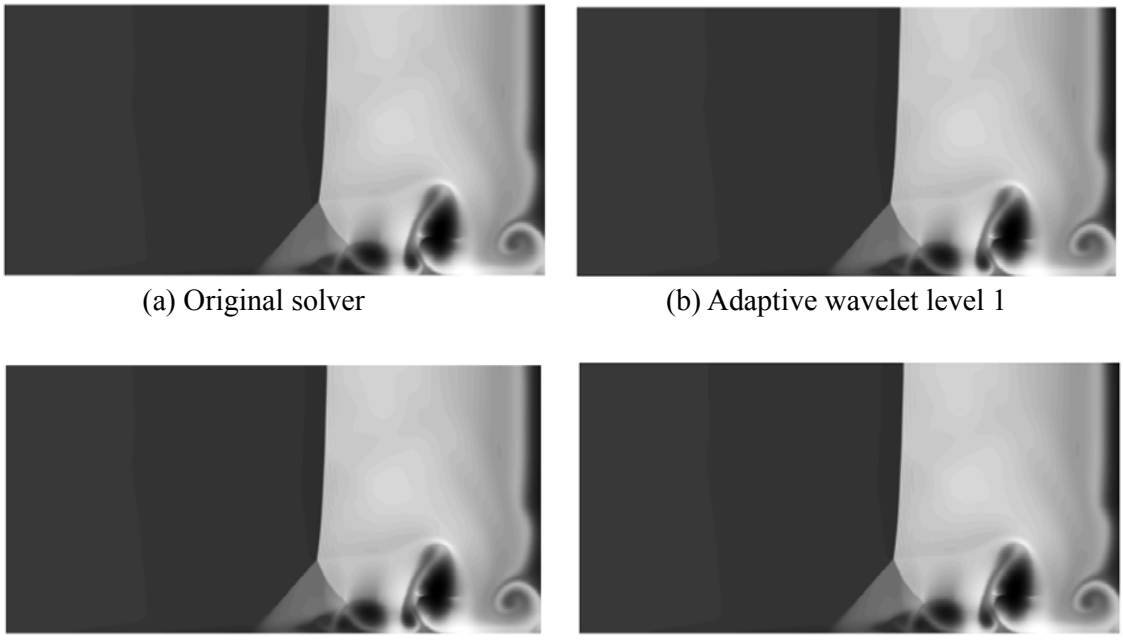

(a) Original solver (b) Adaptive wavelet level 1

(c) Adaptive wavelet level 3 (d) Adaptive wavelet level 3

Fig. 3-15 Density contours of shock tube problem at t=1.

In Fig. 3-15, the density contours of the original solver and the adaptive wavelet method are presented at t=1sec. In these figures, the 3rd order accurate adaptive wavelet method can maintain the original features of a solution; the contours of slip line, reflected wave pattern, etc. are very similar to the contour of the 3rd order accurate original solver. Fig. 3-16 shows the detailed

density distributions of 3rd order accurate original solver and the adaptive wavelet method at y=0.153, In Fig. 3-15 (a), the density distributions of adaptive wavelet method follows that of original solver accurately. But, in Fig. 3-15 (b), (c), and (d), the results of adaptive wavelet method are slightly different with the original solver because of thresholding process in adaptive wavelet algorithm.

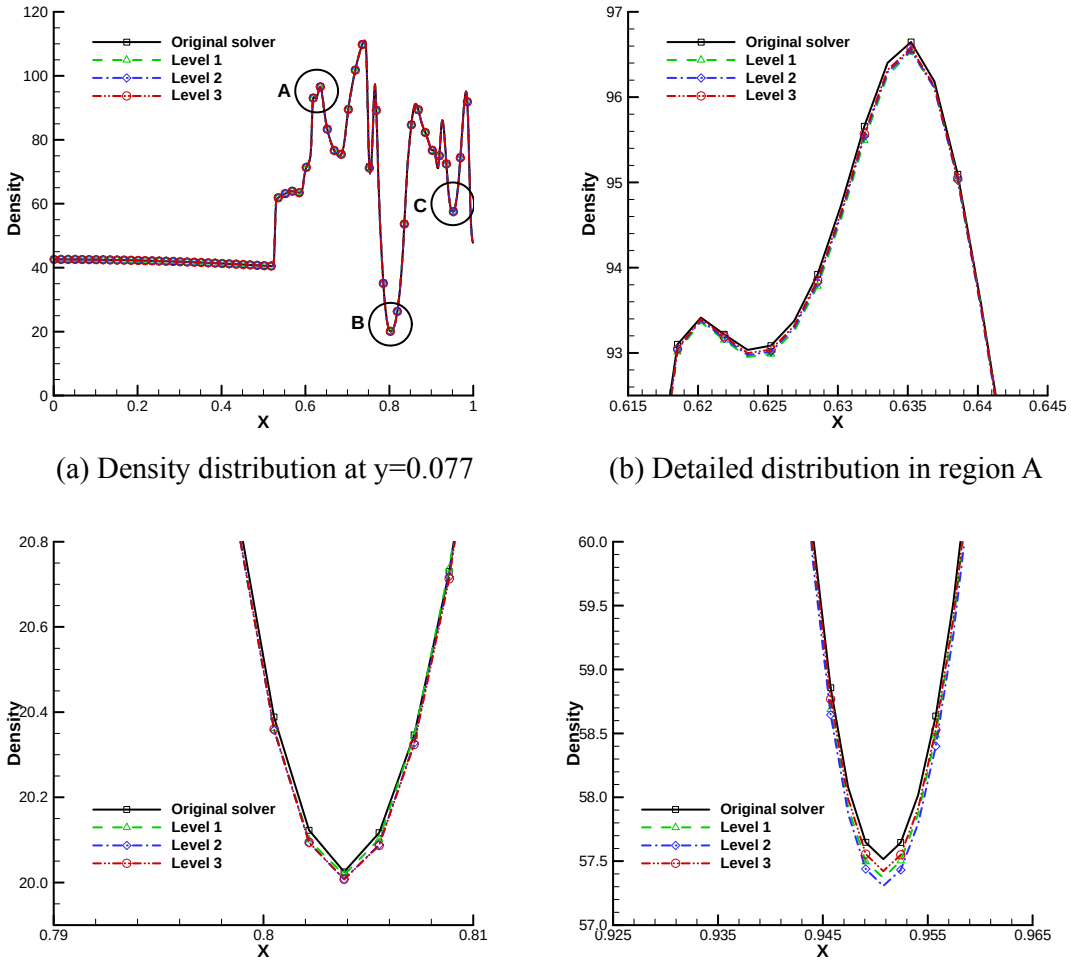

(a) Density distribution at y=0.077

(b) Detailed distribution in region A

(c) Detailed distribution in region B

(d) Detailed distribution in region C

Fig. 3-16 Comparison of density distribution at y=0.077

The overall efficiency improvement according to wavelet resolution level is summarized in Table 3-5. In this table, the computational time with 1 level of wavelet resolution is larger than that of 2nd order accurate conventional solver. It is because the additional CPU time of wavelet transformation is larger than the decrease of CPU time of flux evaluation. By increasing the wavelet resolution level, the adaptive wavelet method with 3rd order accuracy becomes more efficient than 2nd order accurate solver as well as 3rd order accurate original solver; the computational time of wavelet method became about 1.4 times faster than the 3rd order of e-MLP method at maximum when the resolution level of wavelet is 3.

Table 3-5. Comparison of CPU times in shock tube problem; Grid size (600×300)

	Total Comp. Ratio	CPU Time (Sec.)		Time Ratio
		e-MLP (3rd)	Adaptive Wavelet	
Level 1	48.21 %		28,531	1.181
Level 2	42.51 %	33,982	25,114	1.353
Level 3	41.58 %		24,763	1.372

4. Conclusions

In this research, high order accurate method for numerical flow analysis using adaptive non-linear wavelets is developed. For the objective, the non-linear wavelet basis is proposed and applied to accurate data representation method. The CFD solution algorithm using adaptive wavelet is also developed and implemented to high accurate schemes of TVD and e-MLP respectively. The proposed adaptive wavelet methods are proved to be efficient and preserve the high accuracy through the following numerical exercises.

1. Using the developed non-linear wavelet basis, the original data was compressed for two applications of sine function and a Gaussian and pressure distribution around the transonic airfoil. In sine function and a Gaussian, only 57 grid points can represent original 1025 grid points. In pressure distribution around transonic airfoil, about 40% of data can represent original data.

2. The constructed adaptive wavelet algorithm is applied to typical problems containing the two-dimensional Euler equations. Throughout computations of a NACA0012 airfoil and shock-vortex interaction problems, the computational efficiency is enhanced as follows. In NACA0012 airfoil problems, by applying the adaptive wavelet method to the LU-SGS time integration method, the computation is 2.1 times faster in the subsonic case and 1.5 times in the transonic case compared with the results of the reference solver. In shock-vortex interaction problem, the computation becomes 2 times faster.

3. The higher order accurate adaptive wavelet method with TVD scheme was applied to one-dimensional shock-sine wave interaction, two-dimensional shock-vortex interaction, and the isentropic vortex problems. In case of shock-sine wave interaction problem, it was verified that the original numerical accuracy of the 3rd order conventional solver is preserved with enhanced computational efficiency. Through the computation of shock-vortex interaction problem, it was shown that adaptive datasets are constructed so as to capture local features of solution automatically. Also, the higher order accurate adaptive wavelet method speeds up the simulation 1.4 times faster than that of the 2nd order accurate solver while the 3rd order numerical accuracy of a solution is maintained. Also, the proposed 3rd order method was about 1.65 times faster than 2nd order conventional solver while preserving 3rd order of spatial accuracy in isentropic vortex problem.

4. The higher order accurate adaptive wavelet method with e-MLP scheme was applied to two-dimensional shock-vortex interaction and the viscous shock tube problems. In the shock-vortex interaction problem, the proposed 3rd order adaptive wavelet method can present much better efficiency (1.2 times faster) and accuracy compared with 2nd order accurate computation by decreasing the computational time of 3rd order accurate e-MLP

method. In the viscous shock tube problem, the adaptive wavelet method with 3rd order accuracy becomes more efficient than 2nd order accurate solver as well as 3rd order accurate original solver; the computational time of wavelet method became about 1.4 times faster than the 3rd order of e-MLP method.

The developed high accurate adaptive wavelet method was confirmed to improve the computational efficiency of the reference solver and to improve the numerical accuracies compared to the similar computation workload problem. These capabilities of the proposed algorithm were successfully enhanced by adopting three techniques for the adaptive wavelet method.

1. The threshold value is modified to consider the grid spacing and the size of temporal step. As a result, it is realized that the adaptive wavelet method preserves the spatial and the temporal accuracies of the reference solver.

2. The stabilization technique is applied to the construction process of an adaptive dataset in order to improve the compression ratio. Also, residual interpolation is performed at the n time step, not at the $n+1$ time step. It enables the process of arbitrary addition of adjacent cells to a $I(\varepsilon')^n$ dataset to be excluded from the wavelet process. Therefore, the $I(\varepsilon')^n$ dataset can be automatically constructed without the user's arbitrary adjustment of the threshold value.

3. In the time integration, if the variations of the flow variables are smaller than the threshold value ε', they are controlled by adopting a weighting factor. This restriction technique enhances the convergence rate of steady state calculations.

References

[1] Harten A., "High resolution schemes for hyperbolic conservation laws," J. Comput. Phys., Vol. 49, pp. 357– 393, 1983.

[2] Kim K. and Kim C., "Accurate, efficient and monotonic numerical methods for multi-dimensional compressible flows. Part II: Multi-dimensional Limiting Process," J. Comput. Phys., Vol. 208, pp. 570– 615, 2005.

[3] Kang H., Kim K. and Lee D., "A new approach of a limiting process for multi-dimensional flows," J. Comput. Phys., Vol. 229, pp. 7102-7128, 2010.

[4] Harten A, "Adaptive multiresolution schemes for shock computation", Journal of computational Physics, Vol. 115, pp. 319-338, 1994.

[5] Holmström, M., "Solving hyperbolic PDEs using interpolation wavelets", SIAM Journal on scientific computing, Vol. 21, No. 2, pp. 405-420, 1999.

[6] Sjögreen B., "Numerical experiments with the multiresolution scheme for the compressible Euler equations", Journal of computational physics, Vol. 117, pp. 251-261, 1995.

[7] Vasilyev O. V. and Paolucci S., A fast adaptive wavelet collocation algorithm for multidimensional PDEs, Journal of Computational Physics, vol. 138, pp. 16-56, 1997.

[8] Vasilyev O. V. and Kevlahan N. K.-R., An adaptive multilevel wavelet collocation method for elliptic problems, Journal of Computational Physics, vol. 206, pp. 412-431, 2005.

[9] Cohen A., Dahmen W. and Devore R., Adaptive wavelet methods for elliptic operator equations: Convergence rates, Mathematics of Computation, vol. 70, pp. 27-75, 2000.

[10] Bacry E., Mallat S. and Papanicolaou G., A wavelet based space-time adaptive numerical method for partial differential equation, Mathematical Modelling and Numerical Analysis, vol. 26, pp. 793-834, 1992.
[11] Holmström M. and Walden J., Adaptive wavelet method for hyperbolic PDEs, Journal of Scientific Computing, vol. 13, pp. 19-49, 1998.
[12] Beylkin G. and Keiser J. M., On the adaptive numerical solution of nonlinear partial differential equations in wavelet bases, Journal of Computational Physics, vol. 132, pp. 233-259, 1997.
[13] Chiavassa G. and Donat R., Point value multiscale algorithms for 2D compressible flows, SIAM Journal on Scientific Computing, vol. 23, pp. 805-823, 2001.
[14] Kang H., Kim K., Lee D. and Lee D., "Improvement in computational efficiency of Euler equations via a modified Sparse Point Representation method," Compu. and Fluids, Vol. 37, pp. 265-280, 2008.
[15] Kang H., Kim K., Lee D. and Lee D., "Improved computational efficiency of unsteady flow problems via the modified wavelet method," AIAA J. Vol. 46, pp. 1191-1203, 2008.
[16] Kim K., Kim C. and Rho O., Methods for the accurate computations of hypersonic flows: I. AUSMPW+ scheme, Journal of Computational Physics, vol. 174, pp. 38-80, 2001.
[17] Yoon S. and Kwak D., Three-dimensional incompressible Navier-Stokes solver using Lower-Upper Symmetric-Gauss-Seidel algorithm, AIAA Journal, vol. 29, pp. 874-875, 1991.
[18] Inoue O. and Hattori Y., Sound generation by shock-vortex interactions, Journal of Fluid Mechanics, Vol. 380, pp. 81-116, 1999.
[19] Jameson A., Schmidt W. and Turkel E., Numerical solution of the Euler equations by finite volume methods using Runge-Kutta time-stepping schemes, AIAA 14th fluid and plasma dynamics conference, Palo Alto, California, June, 1981.
[20] A. Harten, High Resolution Schemes for Hyperbolic Conservation Laws, Journal of Computational Physics,Vol. 49, pp. 357-393, 1983.
[21] P. K. Sweby, High Resolution Schemes Using Flux Limiters for Hyperbolic Conservation Laws, SIAM Journal on Numerical Analysis, Vol. 21, pp. 995-1011, 1984.
[22] C. Hirsch, Numerical Computation of Internal and External Flows, Vol. 1 & 2, Wiley, Berlin, 1990.
[23] A. Harten, B. Enquist, S. Osher, and S. R. Chakravarthy, Uniformly High Order Accurate Essentially Non-oscillatory Schemes, III, Journal of Computational Physics, Vol. 71, pp. 231-303, 1987.
[24] C. W. Shu, TVB Uniformly High-Order Schemes for Conservation Laws, Mathematics of Computation, Vol. 49, pp. 105-121, 1987.
[25] Shu CW., Osher S., "Efficient implementation of essentially non-oscillatory shock-capturing schemes," J. Comput. Phys., Vol. 77, pp. 439-471, 1988.
[26] H. C. Yee, N. D. Sandham and M.J. Djomehri, Low-Dissipative High-Order Shock-Capturing Methods Using Characteristic-Based Filters, J. Comput. Phys., Vol. 150, pp. 199-238, 1999.
[27] Sjögreen B., and Yee H. C., Grid convergence of high order methods for multiscale complex unsteady viscous compressible flows, Journal of Computational Physics, vol. 185, pp. 1-26, 2003.
[28] Kim K. H. and Kim C., Accurate, efficient and monotonic numerical methods for multi-dimensional compressible flows. Part I. Spatial discretization, Journal of Computational Physics, Vol. 208, pp. 527-569, 2005.

List of Publications and Significant Collaborations:

1. Papers published in conference proceedings

- H.M. Kang, D.H. Lee, D.H. Lee, D.C. Kwak, J. Seo, "Efficiency Enhancement in High Order Accurate Euler Computation Via AWM," *Computational Fluid Dynamics 2010* (ICCFD6), pp. 495-500, 2011.
- H.M. Kang, S.W. Kim, D.H. Lee, D.H. Lee, "The application of wavelet algorithm to high order accurate flow computations," *KSME, Proceedings of 2010 spring conference*, pp. 267-268, 2010. (*Korean version, not attached*)
- H.M. Kang, J.H. Jeong, K.H. Park, K.H. Kim, D.H. Lee, D.H. Lee, "The Application of the Adaptive Wavelet Method for High Order Accurate Flow Computation," *KSAS*, *Proceedings of 2010 fall conference*, pp. 29-32, 2010. (*Korean version, not attached*)
- H.M. Kang, K.H. Park, D.H. Lee, K.H. Kim, S.H. Park, D.H. Lee, "THE APPLICATION OF ADAPTIVE WAVELET METHOD TO MUTI-DIMENSIONAL LIMITING PROCESS FOR ENHANCEMENT OF COMPUTATIONAL EFFICIENCY," *Proceedings of ASME-JSME-KSME 2011 Joint Fluids Engineering Conference* (AJK2011), pp. 1089-1094, 2011.
- K.H. Park, H.M. Kang, J.H. Jeong, K.H. Kim, D.H. Lee, D.H. Lee, "Research on the Adaptive Wavelet Method for the Enhancement of Computational Efficiency of Three Dimensional Flows," *Proceedings of 42nd AIAA Fluid Dynamics Conference and Exhibit*, AIAA-2012-3065, 2012. (*Online published*)
- K.H. Park, H.M. Kang, D.H. Lee, D.H. Lee, D.C. Kwak "Study on the Computational Efficiency of Three Dimensional Euler Equations by Multi-Resolution Analysis," *Computational Fluid Dynamics 2012*, ICCFD7, ICCFD7-1806, 2012. (*Online published*)

2. Conference presentations

- H.M. Kang, S.W. Kim, D.H. Lee, D.H. Lee, D.C. Kwak, "High Order Accurate and Efficient Computation Via Wavelet Transformation Method," *International Conference on Intelligent Unmanned Systems*(ICIUS) , ICIUS -2010-0158.

3. List of interactions

- Dr. Dochan Kwak visited Hanyang university and Seoul national university on Oct. 20, 2010 and Oct. 21, 2010.
  - Discussion on the subject of "Efficient CFD solution algorithm via adaptive wavelet".
  - Prof. Dohyung Lee (Hanyang university), Kyunghyun Park (Seoul national university)
- Dr. Dochan Kwak visited Seoul national university and Hanyang university on April 27, 2012 and April 30, 2012.
  - Discussion on the subject of "Efficient and high accurate CFD schemes based on adaptive wavelet".
  - Prof. Dohyung Lee (Hanyang university), Kyunghyun Park (Seoul national university)

Published Paper in ICCFD6

Efficiency Enhancement in High Order Accurate Euler Computation Via AWM

Hyungmin Kang, Dongho Lee, Dohyung Lee, Dochan Kwak and John Seo

1 Introduction

Recently, in various aerospace transportation and exploration system, there have been strong demands for accurate computations of flow features including supersonic or hypersonic flow phenomena. These demands for accurate computations oblige the developments in Computational Fluid Dynamics (CFD) modeling and simulation technologies. As a result, CFD tools have been widely used in the aerospace engineering and have become indispensable in the part of design stage of aerospace vehicles.

However, the current level of technology does not meet the requirement of the CFD field yet. For the enhancement of the prediction capability of CFD tools, it is essential to perform high fidelity simulations with many grid points and high order accurate algorithms. Then, the increment of computational cost is inevitable, especially in unsteady calculations. In order to extend the availability of high fidelity simulations, it is necessary to alleviate the computational cost through the advancement of CFD algorithms.

From the viewpoint of computational efficiency, the adaptive wavelet method can be a good remedy. The crucial idea of the adaptive wavelet method is as follows: in a CFD dataset, the majority of region is smooth except some rapidly changing region

Hyungmin Kang, Dongho Lee
School of Mechanical and Aerospace Engineering, Seoul National University, Seoul, S. Korea,

Dohyung Lee
Department of Mechanical Engineering, Hanyang University, Ansan, S. Korea e-mail: dohyung@hanyang.ac.kr

Dochan Kwak
NAS Applications Branch, NASA Ames Research Center, CA 94035-1000, USA

John Seo
Asian Office of Aerospace Research and Development, Air Force Office of Scientific Research, Tokyo, JAPAN

such as shock, boundary layer, vortices, etc. Then the wavelet coefficients computed from decomposition process are compared with the threshold value, ε'. If these values are larger than ε', points become remained in an adaptive dataset. Through these processes, the adaptive wavelet method can present the automatic adaptation of a dataset based on the local feature of a CFD solution [1-3]. Then, flux evaluation is performed only at the sparsely remaining points in an adaptive dataset, which substantially reduces the computational time. However, by the thresholding process, additional errors are added to a solution and may cause the deterioration of the numerical accuracy of conventional CFD schemes if the additional errors are larger than the truncation errors of the spatial discretization and time integration methods. To overcome this defect, Kang et al. present the modified threshold value which considers the temporal accuracy as well as the spatial accuracy of the conventional CFD schemes. And they applied it to the 2nd order accurate unsteady flow problems [2,3].

In this paper, the objective is the high order accurate Euler computation with enhancing the computational efficiency. For this purpose, 3rd order accurate Euler solver is constructed with AUSMPW+ spatial discretization method and 3rd order Runge-Kutta time integration scheme [4,5]. And Multi-dimensional Limiting Process (MLP) is used in order to remove numerical oscillation [6]. This 3rd order accurate Euler solver is combined with the adaptive wavelet method as follows: first, the threshold value is modified to be adequate for maintaining 3rd order spatial and temporal accuracy of a current CFD solver. Second, the general adaptive wavelet transformation procedure is changed by adopting residual interpolation. Throughout these processes, the higher order accuracy of a conventional solver is conserved and the computational cost is substantially reduced. In order to demonstrate the efficiency and the accuracy of the developed method, the method is applied to a complicated shock-vortex interaction problem [7].

2 Numerical Algorithm of the Adaptive Wavelet Method

In this research, the two-dimensional Euler equations are used as the governing equations of unsteady flow problems. The generalized coordinate transformed two-dimensional Euler equations are written as Eq. (1).

$$\frac{\partial \overline{Q}}{\partial \tau} = -[\frac{\partial \overline{E}}{\partial \xi} + \frac{\partial \overline{F}}{\partial \eta}] = -R^n_{i,j}, \tag{1}$$

$$with \quad \overline{Q} = \frac{Q}{J},\ \overline{E} = \frac{1}{J}[\xi_t Q + \xi_x E + \xi_y F],\ \overline{F} = \frac{1}{J}[\eta_t Q + \eta_x E + \eta_y F].$$

For constructing 3rd order accurate conventional solver, AUSMPW+ with MLP limiting function is used for spatial discretization and 3rd order Runge-Kutta method is for time integration [4-6].

Then, by the decomposition process, the estimation of flow variables is performed. If we assume that (i,j) cell is even numbered cell and $(i+1,j)$, $(i,j+1)$ and $(i+1,j+1)$ are odd numbered cells, the values at even numbered cell is saved to a point in the coarser level grid. At odd numbered cells, we approximate the original values by interpolating polynomial. In this research, 6th order of interpolating polynomial is used for maintaining the 3rd order accuracy of a conventional solver. The equations with 6th order of accuracy for the approximation procedure of two dimensional flow problems are presented in Eq. (2).

$$\begin{aligned}
\widetilde{Q}^n_{i+1,j} &= \frac{1}{256}\times(3Q^n_{i-4,j}-25Q^n_{i-2,j}+150Q^n_{i,j}+150Q^n_{i+2,j}-25Q^n_{i+4,j}+3Q^n_{i+6,j})\\
\widetilde{Q}^n_{i,j+1} &= \frac{1}{256}\times(3Q^n_{i,j-4}-25Q^n_{i,j-2}+150Q^n_{i,j}+150Q^n_{i,j+2}-25Q^n_{i,j+4}+3Q^n_{i,j+6})\\
\widetilde{Q}^n_{i+1,j+1} &= \frac{1}{512}\times(3Q^n_{i,j-4}+3Q^n_{i+2,j-4}+2Q^n_{i-2,j-2}-27Q^n_{i,j-2}-27Q^n_{i+2,j-2}\\
&+2Q^n_{i+4,j-2}+3Q^n_{i-4,j}-27Q^n_{i-2,j}+174Q^n_{i,j}+174Q^n_{i+2,j}-27Q^n_{i+4,j}+3Q^n_{i+6,j}\cdot\\
&+3Q^n_{i-4,j+2}-27Q^n_{i-2,j+2}+174Q^n_{i,j+2}+174Q^n_{i+2,j+2}-27Q^n_{i+4,j+2}+3Q^n_{i+6,j+2}\\
&+2Q^n_{i-2,j+4}-27Q^n_{i,j+4}-27Q^n_{i+2,j+4}+2Q^n_{i+4,j+4}+3Q^n_{i,j+6}+3Q^n_{i+2,j+6}
\end{aligned} \tag{2}$$

Then, difference values between original values and approximation values are calculated and compared with threshold value. In this research, in order to maintain the accuracy of a conventional solver, the modified threshold value, ε' is defined as Eq. (3).

$$\varepsilon' = min[\varepsilon, max((\Delta x)^3, max(|U|,|V|)\cdot CFL^3\cdot(\Delta x)^3)]. \tag{3}$$

If difference value is larger than ε', the point is included in the adaptive dataset; if not, the point is excluded from the dataset. Throughout this process, the dataset is adapted to the flow features while maintaining the numerical accuracy of conventional schemes. After thresholding process, flux values are only calculated at the included cells in the adaptive dataset by AUSMPW+ with MLP limiting function with 3rd order accuracy. At excluded cells in the dataset, residual values are interpolated by using the same interpolating polynomial as Eq. (2). And 3rd order of Runge-Kutta time integration is performed on the whole computational domain.

3 Numerical Test and Discussion

In order to assess the numerical accuracy and efficiency of the higher order accurate adaptive wavelet method, it is applied to a shock-vortex interaction problem [7]. The computational domain is set as $-20 \le x \le 5$ and $-20 \le y \le 10$ with a 600×600 grid. The Mach number of vortex is 0.39 and the initial vortex core is located at (-5,-5). This vortex is propagated to a stationary normal shock with the Mach number of 1.29. Here, ε is set as 10^{-5}.

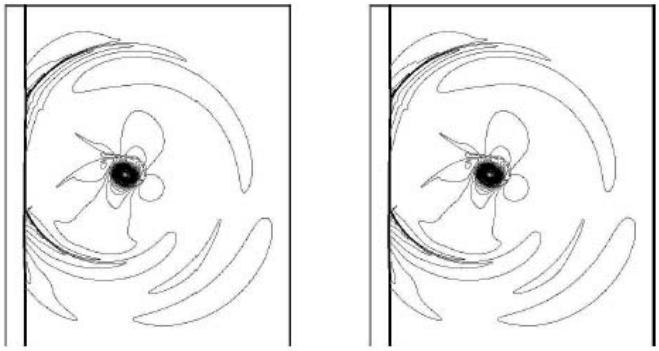

(a) Conventional method (b) Modified wavelet method

Fig. 1 Density contours of shock-vortex interaction problem at t=18sec; the wavelet decomposition level is 3.

Figure 1 shows the density contours of a conventional 3rd order accurate solver and the adaptive wavelet scheme after the non-dimensional time of 18. It is shown that they are almost same. The adaptive wavelet method can maintain the original features of a solution such as the vortex pattern, the position and strength of shock, etc. Figure 2 shows the detailed density distributions of 2nd order accurate solver, 3rd order accurate solver, the adaptive wavelet method at y=-5 and they are compared with the result of dense grid system. In case of 2nd order accurate case, the distribution is smeared compared with 3rd order accurate cases. However, the results of 3rd accurate solver and 3rd order accurate adaptive wavelet method present more accurate distributions than 2nd order accurate solver.

Figure 3 represents the adaptive dataset with wavelet decomposition level=3. The dataset follows the flow features accurately and many cells are remained near the vortex and shock regions. In the other smooth regions, the changes of the flow properties are negligible and the remaining cells are sparsely distributed. Fluxes are calculated only at the remaining points, which enhances the computational efficiency as shown in Table 1. In this table, the 3rd order accurate adaptive wavelet method presents better computational efficiency than the 2nd order accurate solver. Therefore, the present adaptive wavelet method can present high order accurate results with better efficiency than conventional CFD solvers.

4 Conclusion

Throughout this research, the higher order accurate adaptive wavelet method is proposed for the flow computations which need higher order accuracy and efficiency. For this purpose, 6th order accurate interpolating polynomial is implemented to the

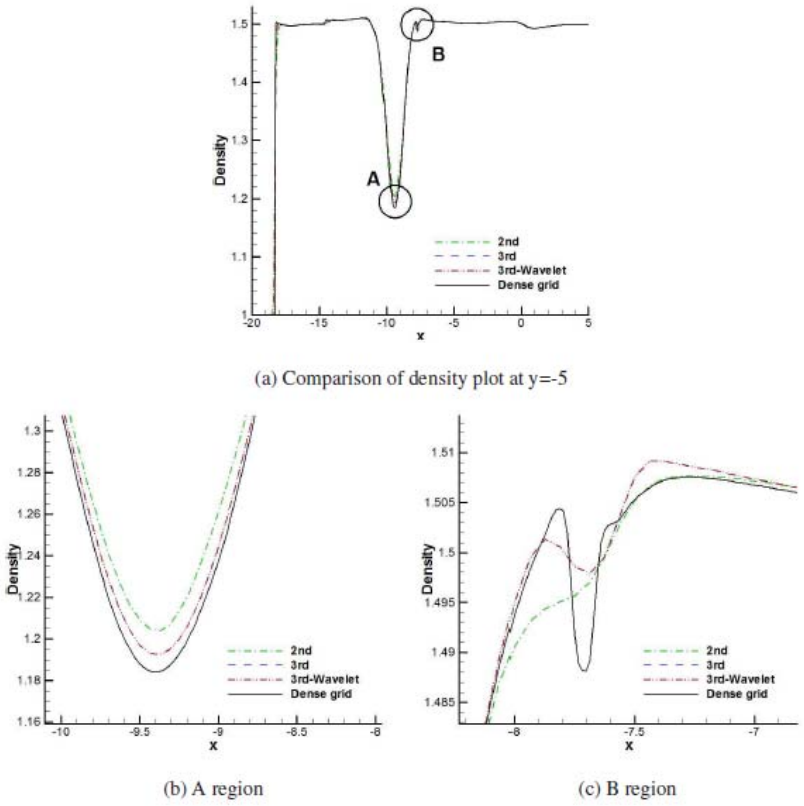

(a) Comparison of density plot at y=-5

(b) A region

(c) B region

Fig. 2 Comparison of density plots of shock-vortex interaction problem at t=18sec; the wavelet decomposition level is 3.

wavelet decomposition process. Also, the threshold value is modified in order to

Table 1 Results of efficiency improvements and L2error for the shock-vortex interaction problem

Wavelet Level	CPU Time	Time Ratio
Third Order	12411.3	
Level 1	9086.0	1.37
Level 2	6798.5	1.83
Level 3	6020.1	2.06
Level 4	6053.6	2.05
Second Order	8079.2	1.54

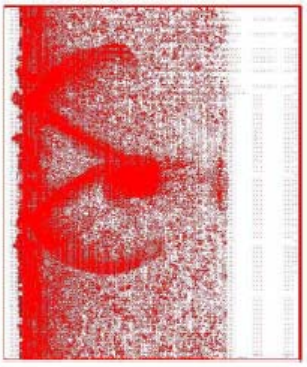

Fig. 3 Adaptive datasets of shock-vortex interaction problem with wavelet decomposition level=3 at t=18

maintain the 3rd order accuracy of conventional CFD schemes. This higher order accurate adaptive wavelet method is applied to the shock-vortex interaction problem. And it can present much better computational efficiency than a 2nd order accurate scheme while maintaining the higher order numerical accuracy.

Acknowledgements This work was supported by the Asian Office of Aerospace R&D (AOARD) project (Award No: FA2386-10-1-4001).

References

1. Sjögreen, B.: Numerical experiments with the multiresolution scheme for the compressible Euler equations. J. Comput. Phys., **117**, 251-261 (1995)
2. Kang H., Kim K., Lee D. and Lee D.: Improvement in computational efficiency of Euler equations via a modified Sparse Point Representation method. Computers and Fluids **37**, 265-280 (2008)
3. Kang H., Kim K., Lee D. and Lee D.: Improved computational efficiency of unsteady flow problems via the modified wavelet method. AIAA J. **46**, 1191-1203 (2008)
4. Kim K., Kim C. and Rho O.: Methods for the accurate computations of hypersonic flows: I. AUSMPW+ scheme. J. Comput. Phys., **174**, 38-80 (2001)
5. Kim K. and Kim C.: Accurate, efficient and monotonic numerical methods for multi-dimensional compressible flows Part I: Spatial discretization. J. Comput. Phys., **208**, 527-569 (2005)
6. Kim K. and Kim C.: Efficient and monotonic numerical methods for multi-dimensional compressible flows Part II: Multi-dimensional limiting process. J. Comput. Phys., **208**, 570-615 (2005)
7. Inoue O. and Hattori Y.: Sound generation by shock-vortex interactions. J. Fluid Mech. **380**, 81-116 (1999)

Published Paper in AJK 2011

High Order Accurate and Efficient Computation Via Wavelet Transformation Method

Hyungmin Kang*, Sangwoo Kim[1], Dongho Lee[2], Dohyung Lee[=] and Dochan Kwak[3]

*Chief Scientist, Advanced Aerodynamics and Structure Department
Korea Aerospace Research Institute, Daejeon, S. Korea
e-mail: avdlkang@kari.re.kr

[=]Professor, Department of Mechanical Engineering, Hanyang University, Ansan, KyungKi-Do, S. Korea
e-mail: dohyung@hanyang.ac.kr (corresponding author)

[1]Department of Mechanical Engineering, Hanyang University, Ansan, KyungKi-Do, S. Korea

[2]Professor, School of Mechanical and Aerospace Engineering, Seoul National University, Seoul, S. Korea

[3]Nas Application Branch, NASA Ames Research Center, Moffett Field, CA 94305, USA

Abstract

An adaptive wavelet transformation method with high order accuracy is proposed to enable efficient and accurate flow computations. The main algorithm is as follows; 3rd order of wavelet decomposition and thresholding are applied to a CFD dataset and the positions of crucial features in the dataset are searched with maintaining the original numerical accuracy of a conventional solver and the dataset is automatically adapted to local features of a solution. After the wavelet transformation, 3rd order spatial and temporal accurate high order interpolation scheme with Multi-dimensional Limiting Process (MLP) are performed only at the included points in the adapted dataset. In the other points, high order of interpolation method is utilized in order to construct residual values. This high order interpolation scheme with high order adaptive wavelet transformation was applied to unsteady Euler flow computations. Through these processes, both computational efficiency and numerical accuracy are guaranteed in case of high order accurate unsteady flow computations.

1 Introduction

Recently, there have been strong demands for accurate flow computations including supersonic/hypersonic phenomena based on the enhancement of analysis systems. Especially in various aerospace transportation and exploration systems, the prediction capability of flow phenomena becomes important for cost reduction during the part of design stage of aerospace vehicles. For the satisfaction of these demands, accurate modeling algorithms and simulation technologies with vast size of grids have been forced in Computational Fluid Dynamics (CFD). As a result, CFD algorithms have been widely used in various filed including the aerospace engineering.

However, the current level of technology is often insufficient for the satisfaction of the requirement of the CFD field. Still, complexity of the flow phenomena and shape of the models becomes the obstruction in terms of accuracy and efficiency. To enhance the prediction capability of CFD algorithms, high fidelity algorithms with many grid points are essential; the increment of computing cost is inevitable, especially in unsteady calculations. Hence, it is necessary to accurately calculate the flow phenomena and efficiently alleviate the computational cost through the advancement of the CFD algorithms.

From the viewpoint of computational efficiency, the adaptive wavelet method can be a good remedy [1-3].The crucial idea of the adaptive wavelet method is as follows; generally, the usage of dense grid system in the whole computational domain becomes a waste of resources because the majority of the domain consists of smooth regions. A dense grid system is only needed in the rapidly changing regions such as shock waves, boundary layers, etc. Through the wavelet transformation, wavelet coefficients become larger than threshold value ε in these crucial regions. Then, the dataset is automatically adapted to the local features of a solution [1-3]. Flux values are calculated only at the remaining points in an adaptive dataset, which reduces the computational time.

However, the accuracy of the adaptive wavelet method is sensitive to ε value. By the wavelet transformation, additional numerical errors might be added to the solution and the numerical accuracy of a conventional CFD solver becomes deteriorated if the order of additional error is larger than that of truncation errors of the spatial discrete-

zation and time integration method. In order to resolve this defect, modified threshold value is presented by considering the spatial and temporal accuracies of numerical schemes [2, 3].

In this paper, our main objective is to efficiently compute the Euler flows with higher order of accuracy. For this purpose, higher order of wavelet transformation process applicable to the 3rd order accurate solver is constructed as follows; first, the 6th order of interpolating polynomial is introduced to wavelet decomposition process. Second, the threshold value is modified in order to maintain the 3rd order of spatial and temporal accuracies of a solver. This adaptive wavelet method is fed into the 3rd order accurate Euler solver and applied to several numerical tests. Through the application of the higher order accurate adaptive wavelet method, the accuracy of the conventional solver is conserved and the cost is substantially reduced.

This paper is organized as follows; after the introduction, the overall adaptive wavelet method including the higher order of decomposition and thresholding is described. Then, to assess the developed method, several numerical experiments are performed such as one-dimensional shock-sine interaction problem and two-dimensional shock-vortex interaction problem. Finally, a conclusion is drawn.

2 The overall implementation of the adaptive wavelet method

The two dimensional Euler equation is written as follows:

$$\frac{\partial Q}{\partial t}+\frac{\partial E}{\partial x}+\frac{\partial F}{\partial y}=0, \qquad (1)$$

with $Q=\begin{bmatrix}\rho\\ \rho u\\ \rho v\\ \rho e_t\end{bmatrix}$, $E=\begin{bmatrix}\rho u\\ \rho u^2+p\\ \rho uv\\ (\rho e_t+p)u\end{bmatrix}$, $F=\begin{bmatrix}\rho v\\ \rho uv\\ \rho v^2+p\\ (\rho e_t+p)v\end{bmatrix}$ and

$$e_t=\frac{a^2}{\gamma(\gamma-1)}+\frac{1}{2}(u^2+v^2),$$

where all properties and governing equations are non-dimensionalized. By the generalized coordinate transformation, Eq. (2) is derived.

$$\frac{\partial \overline{Q}}{\partial \tau}=-[\frac{\partial \overline{E}}{\partial \xi}+\frac{\partial \overline{F}}{\partial \eta}]=-R^n_{i,j}, \qquad (2)$$

with $\overline{Q}=\frac{Q}{J}$, $\overline{E}=\frac{1}{J}[\xi_t Q+\xi_x E+\xi_y F]$ and

$$\overline{F}=\frac{1}{J}[\eta_t Q+\eta_x E+\eta_y F].$$

The flow chart in figure 1 shows the overall processes of the implementation of the adaptive wavelet method to a two-dimensional Euler solver.

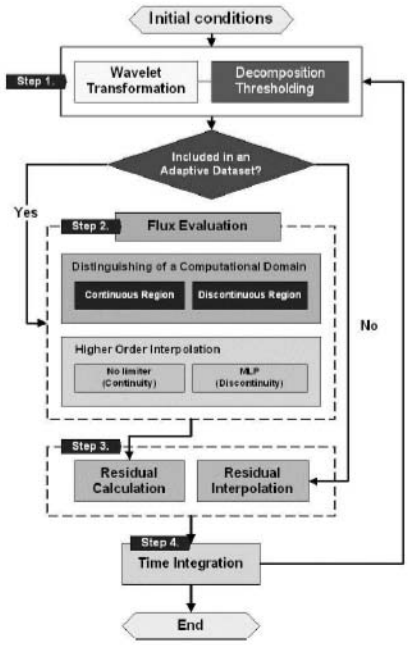

Figure 1: Overall procedure of the adaptive wavelet method.

2.1 Wavelet transformation

At first, assume a two-dimensional dyadic gridset as figure 2. Here, positions of the symbol ○ are even numbered grids and the other positions of symbols □, △, and X are odd numbered grid points. Then, values at even numbered cell are saved to a point in the coarser level grid. At odd numbered cells, 6th order of interpolating polynomial is used for maintaining the 3rd order accuracy of a conventional solver as shown in Eq. (3).

$$\square:\ \tilde{Q}^n_{i+1,j}=\frac{1}{256}(3Q^n_{i-4,j}-25Q^n_{i-2,j}+150Q^n_{i,j}+150Q^n_{i+2,j}-25Q^n_{i+4,j}+3Q^n_{i+6,j})$$

$$\triangle:\ \tilde{Q}^n_{i+1,j}=\frac{1}{256}(3Q^n_{i,j-4}-25Q^n_{i,j-2}+150Q^n_{i,j}+150Q^n_{i,j+2}-25Q^n_{i,j+4}+3Q^n_{i,j+6}) \qquad (3)$$

$$\mathrm{X}:\ \tilde{Q}^n_{i+1,j}=\frac{1}{512}(3Q^n_{i,j-4}+3Q^n_{i+2,j-4}+2Q^n_{i-2,j-2}-27Q^n_{i,j-2}-27Q^n_{i+2,j-2}+2Q^n_{i+4,j-2}+3Q^n_{i-4,j}-27Q^n_{i-2,j}+174Q^n_{i,j}+174Q^n_{i+2,j}-27Q^n_{i+4,j}+3Q^n_{i+6,j}+3Q^n_{i-4,j+2}-27Q^n_{i-2,j+2}+174Q^n_{i,j+2}+174Q^n_{i+2,j+2}-27Q^n_{i+4,j+2}+3Q^n_{i+6,j+2}+2Q^n_{i-2,j+4}-27Q^n_{i,j+4}-27Q^n_{i+2,j+4}+2Q^n_{i+4,j+4}+3Q^n_{i,j+6}+3Q^n_{i+2,j+6})$$

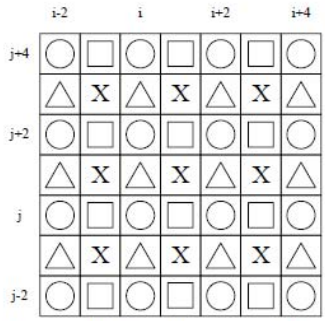

Figure 2: Example of two-dimensional dyadic grid.

The difference values are calculated as Eq. (4).

$$\begin{aligned} \square&: \; d^n_{i+1,j} = Q^n_{i+1,j} - \widetilde{Q}^n_{i+1,j}, \\ \triangle&: \; d^n_{i,j+1} = Q^n_{i,j+1} - \widetilde{Q}^n_{i,j+1}, \\ \mathrm{X}&: \; d^n_{i+1,j+1} = Q^n_{i+1,j+1} - \widetilde{Q}^n_{i+1,j+1}. \end{aligned} \tag{4}$$

This wavelet decomposition process is performed by multi-resolution and until the coarser level of gridset is obtained.

After wavelet decomposition, the wavelet coefficients are compared with the threshold value; if the values are larger than the threshold value, the points become remained in an adaptive dataset. Through these processes, the dataset follows the local feature of a CFD solution. However, the thresholding process inevitably results in the additional $O(\varepsilon)$ numerical errors because of the data loss below $O(\varepsilon)$. If $O(\varepsilon)$ error is larger than the truncation errors of the spatial discretization and time integration method, the accuracy of a conventional CFD scheme should be deteriorated. In order to overcome this defect, the thresholding method is modified by considering the order of truncation errors as Eq. (5).

$$\varepsilon' = \min[\varepsilon, \max(\Delta x^3, CFL^3 \cdot \Delta x^3)]. \tag{5}$$

If a wavelet coefficient is smaller than ε' at some point, the grid point doesn't belong to the dataset. In the other case, the point is included in the dataset; an adaptive dataset is constructed according to the local features of the dataset with 3rd order of accuracy. Through these higher order of wavelet decomposition and modified threshold value, 3rd order of spatial and temporal accuracies of a conventional CFD solver are guaranteed.

2.2 Flux evaluation

After the wavelet transformation, flux values are only calculated at the included cells in the adaptive dataset with 3rd order of accuracy. In order to construct a 3rd order accurate solver, AUSMPW+ scheme is utilized [4, 5]. Also, for oscillation removal due to numerical discontinuities, Multi-dimensional Limiting Process (MLP) is applied [6]. However, there is no need of the application of limiting function to the continuous regions; dissipation due to limiting function may damage the solution's accuracy in the continuous region though it is indispensible for the oscillation removal due to higher order accurate scheme in the discontinuous region. Also, it is a waste of the computational resources to use limiting function in continuous region.

In order to resolve this problem, the adaptive dataset is divided into two regions: continuous and discontinuous regions [7]. In the continuous region, there is no application of limiting process and only higher order of interpolation is applied. On the other hand, in discontinuous region, MLP is utilized for the removal of numerical oscillation. Through this switching of limiting function, accurate and efficient calculation of flux values is possible.

2.3 Residual interpolation

At excluded cells in the dataset, residual values are interpolated by using the 6th order of interpolating polynomial as Eq. (6).

$$\begin{aligned} \square&: \; \widetilde{R}^n_{i+1,j} = \frac{1}{256}(3R^n_{i-4,j} - 25R^n_{i-2,j} + 150R^n_{i,j} \\ &\qquad + 150R^n_{i+2,j} - 25R^n_{i+4,j} + 3R^n_{i+6,j}), \\ \triangle&: \; \widetilde{R}^n_{i+1,j} = \frac{1}{256}(3R^n_{i,j-4} - 25R^n_{i,j-2} + 150R^n_{i,j} \\ &\qquad + 150R^n_{i,j+2} - 25R^n_{i,j+4} + 3R^n_{i,j+6}), \\ \mathrm{X}&: \; \widetilde{R}^n_{i+1,j} = \frac{1}{512}(3R^n_{i,j-4} + 3R^n_{i+2,j-4} + 2R^n_{i-2,j-2} - 27R^n_{i,j-2} \\ &\qquad - 27R^n_{i+2,j-2} + 2R^n_{i+4,j-2} + 3R^n_{i-4,j} - 27R^n_{i-2,j} \\ &\qquad + 174R^n_{i,j} + 174R^n_{i+2,j} - 27R^n_{i+4,j} + 3R^n_{i+6,j} \\ &\qquad + 3R^n_{i-4,j+2} - 27R^n_{i-2,j+2} + 174R^n_{i,j+2} + 174R^n_{i+2,j+2} \\ &\qquad - 27R^n_{i+4,j+2} + 3R^n_{i+6,j+2} + 2R^n_{i-2,j+4} - 27R^n_{i,j+4} \\ &\qquad - 27R^n_{i+2,j+4} + 2R^n_{i+4,j+4} + 3R^n_{i,j+6} + 3R^n_{i+2,j+6}) \end{aligned} \tag{6}$$

By using this 6th order of interpolating polynomial, the error caused by interpolation becomes smaller than the truncation errors of the numerical schemes. After constructing residual distributions in the whole computational domain, 3rd order of Runge-Kutta time integration is performed [4, 5].

3 Numerical results and discussion

In order to assess the accuracy of the higher order accurate wavelet transformation, it is applied to shock-sine wave interaction problem. The initial conditions for the shock-sine wave interaction problem are given in the following Eq. (7). Here, ε is set as 10^{-5}.

$$\begin{aligned} &(\rho, U, p) = (3.8571, 2.6294, 10.333) \;\text{ where }\; 0 \le x \le 1, \\ &(\rho, U, p) = (1 + 0.2\sin(5(x-5)), 0, 1) \;\text{ where }\; 1 \le x \le 10. \end{aligned} \tag{7}$$

The CPU times of the higher order adaptive wavelet method are compared to those of a conventional 3rd order accurate CFD solver according to the resolution level in Table 1.

Table. 1 Comparison of CPU times in shock-sine wave interaction problem.

Level	Grid Number	CPU Time		Compression Ratio
		Original	Wavelet	
1	1001	70.656	73.828	1.672
	2001	139.422	144.547	1.756
	4001	277.359	286.344	1.775
	8001	550.453	571.547	1.789
2	1001	70.656	50.531	2.304
	2001	139.422	97.000	2.548
	4001	277.359	189.594	2.649
	8001	550.453	377.844	2.695
3	1001	70.656	48.547	2.381
	2001	139.422	84.891	2.829
	4001	277.359	143.047	3.396
	8001	550.453	285.641	3.507
4	1001	70.656	------	------
	2001	139.422	83.984	2.857
	4001	277.359	140.594	3.413
	8001	550.453	272.813	3.675

In the case of the adaptive wavelet method with a 1st level resolution, the CPU time rather increases. This is because the increase in CPU time due to additional computations for the adaptive wavelet method exceeds the decrease in CPU time from the flux evaluation step. On the other hand, in the case of the adaptive wavelet method with a 2nd level resolution, the decrease in CPU time for the evaluation of fluxes is dominant and the overall CPU time decreases. For example, in a 2nd level resolution with 8001 grid points, the computation of the wavelet method is 1.46 times faster than that of a conventional solver.

Figure 3 shows the solutions of a conventional solver and the higher order adaptive wavelet method at t=1. The original solution of a conventional solver and that of the wavelet method are almost same. In order to verify it more precisely, the density contours of a conventional solver and the wavelet method are enlarged at positions A and B and compared in figure 4. At A and B regions, the results of adaptive wavelet method show good agreement with those of a conventional solver.

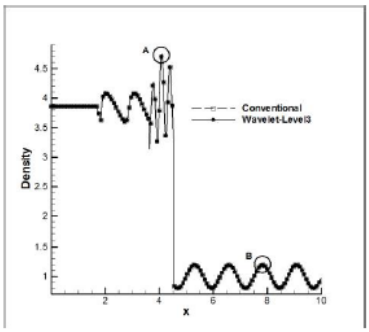

Figure 3: Density distribution of the shock-sine wave interaction problem at t=1.

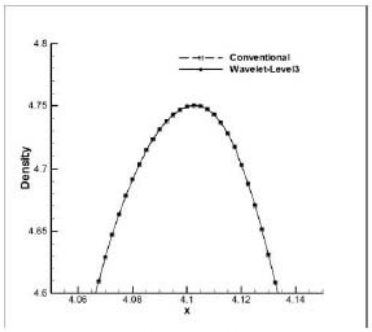

(a) A region.

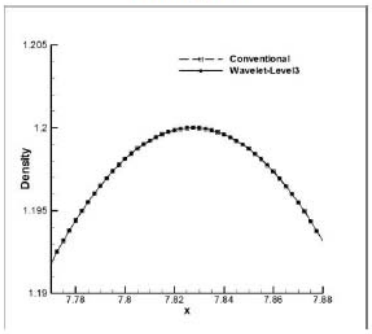

(b) B region.

Figure 4: Detailed density comparison.

Finally, in order to confirm the spatial accuracy of this method, grid convergence tests are performed and the results are shown in figure 5. From figure 5, the higher order accurate adaptive wavelet method maintains the 3rd order of accuracy of a conventional solver by setting the thresholding values as Eq. (5).

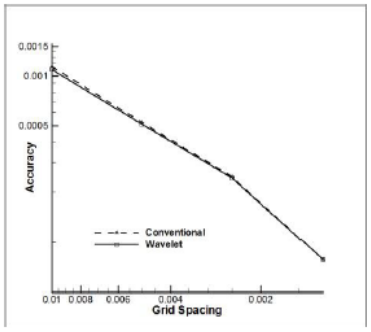

Figure 5: The result of grid convergence test.

To assess the accuracy and efficiency of the higher order accurate adaptive wavelet method in more complicated case, it is applied to a shock-vortex interaction problem [8]. The domain is set as $-20 \le x \le 5$ and $-20 \le y \le 10$ with a

400X400 grid. The initial velocity, density and pressure distributions of a vortex flow are presented in Eq. (8) [8].

$$\text{Tangential velocity: } u_\theta = M_v r \exp[(1-r^2)/2],$$

$$\text{Radial velocity: } u_r = 0,$$

$$\text{Vorticity: } \omega(r) = M_v(2-r^2)\exp[(1-r^2)/2], \quad (8)$$

$$\text{Pressure: } p(r) = \frac{1}{\gamma}[1-\frac{\gamma-1}{2}M_v^2\exp(1-r^2)]^{\gamma/(\gamma-1)},$$

$$\text{Density: } \rho(r) = \frac{1}{\gamma}[1-\frac{\gamma-1}{2}M_v^2\exp(1-r^2)]^{1/(\gamma-1)}.$$

The Mach number of vortex is 0.39 and the initial vortex core is located at (-5,-5). The normal shock with Mach number of 1.29 is propagated to the vortex and ε is set as 10^{-5}.

The overall efficiency improvement according to wavelet resolution level is summarized in Table 2. In this table, the computational time with 1 level of resolution is larger than that of 2nd order accurate conventional solver. It is because the additional CPU time of wavelet transformation is larger than the decrease of CPU time of flux evaluation, as mentioned in the previous example. By increasing the wavelet resolution level, the adaptive wavelet method with 3rd order accuracy becomes more efficient than 2nd order accurate solver as well as 3rd order accurate solver; the computational time became about 2.0 times faster at maximum when the resolution level of wavelet is 3.

Table. 2 Comparison of CPU times in shock-vortex interaction problem.

Level	CPU Time			Computational Efficiency (CPU time_Con/ CPU time_Wav)
	Conventional (2nd order)	Conventional (3rd order)	Wavelet (3rd order)	
1	8079.2	12411.3	9086.0	1.37
2			6798.5	1.83
3			6020.1	2.06
4			6053.6	2.05

Figure 6 represents the adaptive dataset with wavelet decomposition level=3. The dataset follows the flow features accurately and many cells are remained near the vortex and shock regions. In the other smooth regions, the changes of the flow properties are negligible and the remaining cells are sparsely distributed. Fluxes are calculated only at the remaining points, which enhance the computational efficiency.

Figure 7 shows the density contours of a conventional 2nd order accurate solver, 3rd order accurate solver and the adaptive wavelet scheme after the non-dimensional time of 18. In these figures, it is shown that the contour of 2nd order accurate conventional solver is smeared comparing with that of 3rd order accurate solver. However, the 3rd order accurate adaptive wavelet method can maintain the original features of a solution; the contours of slip line, reflected wave pattern, etc. are clearly presented in the results of the 3rd order accurate solver and the adaptive wavelet method. Figure 8 shows the detailed density distributions of 2nd order accurate solver, 3rd order accurate solver, the adaptive wavelet method at y=-5 and they are compared with the result of dense grid system with 2nd order accurate solver. In the result of 2nd order accurate solver, the vortex and reflected wave is dissipated compared with the 3rd order accurate conventional solver and the wavelet method. However, by using 3rd order accurate method, the density distributions are clearly represented; the results of 3rd order accurate method follows that of dense grid system more accurately though small number of grid points is used.

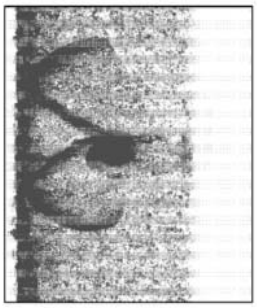

Figure 6: An adaptive dataset with wavelet level=3.

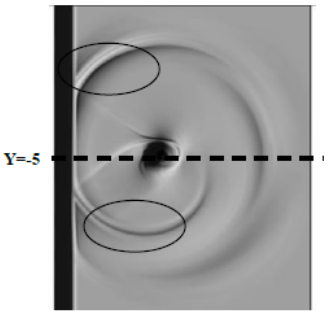

(a) Conventional solver (2nd order).

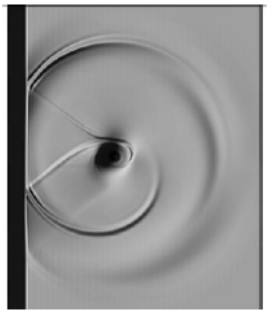

(b) Conventional solver (3rd order).

(c) Adaptive wavelet method.

Figure 7: Comparison of density contour.

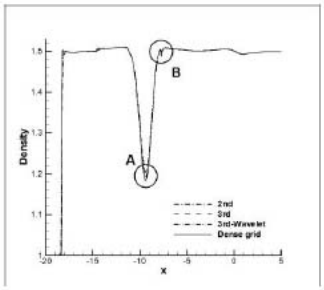

(a) Density distribution at y=-5.

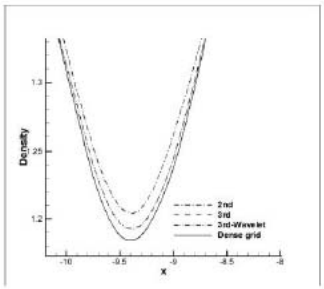

(b) Detailed density distribution at A region.

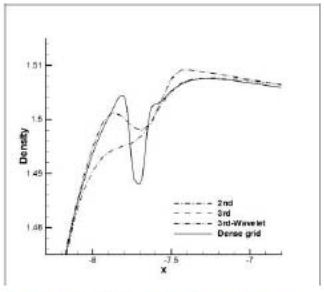

(c) Detailed density distribution at B region.

Figure 8: Comparison of density distribution at y=-5.

4 Conclusions

Through this research, the higher order accurate adaptive wavelet method is proposed for enhancing the prediction capability of CFD with better efficiency. For this purpose, 6^{th} order accurate interpolating polynomial is implemented to the wavelet decomposition process. Also, the threshold value is modified in order to conserve the 3rd order accuracy of conventional CFD schemes. This higher order accurate adaptive wavelet method is applied to one-dimensional shock-sine wave interaction and two-dimensional shock-vortex interaction problems. In these test, the adaptive wavelet method can present much better computational efficiency than a 2nd order accurate scheme while maintaining the higher order numerical accuracy of a conventional CFD solver.

Acknowledgments

We appreciate the support of the Asian Office of Aerospace R&D (AOARD) project (Award No:FA2386-10-1-4001)

References

[1] B. Sjögreen, Numerical experiments with the multiresolution scheme for the compressible Euler equations, J. Comput. Phys., Vol. 117, pp. ~251--261, 1995.

[2] H. Kang, K. Kim, D. Lee and D. Lee, Improvement in computational efficiency of Euler equations via a modified Sparse Point Representation method. Compu. and Fluids, Vol. 37, pp. ~265--280, 2008.

[3] H. Kang, K. Kim, D. Lee and D. Lee, Improved computational efficiency of unsteady flow problems via the modified wavelet method, AIAA J. Vol. 46, pp. ~1191--1203, 2008.

[4] K. Kim, C. Kim and O. Rho, Methods for the accurate computations of hypersonic flows: I. AUSMPW+ scheme. J. Comput. Phys., Vol. 174, pp. ~38--80, 2001.

[5] K. Kim and C. Kim, Accurate, efficient and monotonic numerical methods for multi-dimensional compressible flows Part I: Spatial discretization. J. Comput. Phys., Vol. 208, pp. ~527--569, 2005.

[6] K. Kim and C. Kim, Efficient and monotonic numerical methods for multi-dimensional compressible flows Part II: Multi-dimensional limiting process. J. Comput. Phys., Vol. 208, pp ~570--615, 2005.

[7] H. Kang, K. Kim and D. Lee, A new approach of a limiting process for multi-dimensional flows, J. Comput. Phys., Vol. 229, pp ~7102—7128, 2010.

[8] O. Inoue and Y. Hattori, Sound generation by shock-vortex interactions. J. Fluid Mech. Vol. 380, pp ~81--116, 1999.

primary burdens which decrease the computational efficiency, especially in unsteady calculations. It is necessary to accurately compute the flow phenomena and efficiently alleviate the computational cost through the advancement of the CFD algorithms. The adaptive wavelet method can be a good solution by alleviating the computational cost of the spatial discretization [5-7]. The crucial idea of the adaptive wavelet method is that the crucial locations in the CFD dataset such as shock, vortex core, etc. are automatically and accurately searched by the wavelet transformation. Then, the dataset is automatically adapted to the local features of a solution [5-7]. Flux values are computed only at the remaining points in an adaptive dataset, which enhances the computational efficiency.

In this paper, out target is to efficiently and accurately compute the Euler flows with shock discontinuities. For this purpose, the adaptive wavelet method is applied to a high order accurate CFD solver. For preserving the accuracy of the original solver, higher order accurate wavelet transformation is constructed as follows; first, the 6th order of interpolating polynomial is introduced to wavelet decomposition process. Second, the threshold value is modified in order to maintain higher order accuracy of the solver. This higher order accurate adaptive wavelet method is fed into the high order accurate CFD solver. That is, a spatial discretization scheme including the 3rd order accurate interpolations with e-MLP limiting function is performed at the crucial positions in the CFD dataset. In the other positions, simple interpolating polynomials are used to compute the residual values. To assess the accuracy and efficiency of the adaptive wavelet method, it was applied to a shock-vortex interaction problem. Through the application of the higher order accurate adaptive wavelet method, the accuracy of the conventional solver is conserved and the cost is substantially reduced.

NOMENCLATURE

a = speed of sound
$d_{l,k}$ = wavelet coefficient at $x_{l,k}$
$d^n_{i,j}$ = wavelet coefficient at (i,j) cell of n time step
$L^n_{i,j}$ = (ρ, p, u, v) at (i,j) cell of n time step
$\tilde{L}^n_{i,j}$ = interpolated value of $L^n_{i,j}$
p = pressure
$R^n_{i,j}$ = residual values at (i,j) cell of n time step
$\tilde{R}^n_{i,j}$ = interpolated value of $R^n_{i,j}$
u, v = components of the velocity vector

Subscript

i, j = position of a cell

Superscript

n = current time step

Greek

ε = threshold value
ε' = modified threshold value
γ = ratio of specific heat (1.4 for air)
ρ = density

THE OVERALL PROCEDURE OF THE ADAPTIVE WAVELET METHOD

The two dimensional Euler equation is written as follows:

$$\frac{\partial Q}{\partial t}+\frac{\partial E}{\partial x}+\frac{\partial F}{\partial y}=0, \tag{1}$$

$$\text{with } Q=\begin{bmatrix}\rho\\ \rho u\\ \rho v\\ \rho e_t\end{bmatrix},\ E=\begin{bmatrix}\rho u\\ \rho u^2+p\\ \rho uv\\ (\rho e_t+p)u\end{bmatrix},\ F=\begin{bmatrix}\rho v\\ \rho uv\\ \rho v^2+p\\ (\rho e_t+p)v\end{bmatrix} \text{ and}$$

$$e_t=\frac{a^2}{\gamma(\gamma-1)}+\frac{1}{2}(u^2+v^2),$$

where all properties and governing equations are non-dimensionalized. By the generalized coordinate transformation, Eq. (2) is derived.

$$\frac{\partial \overline{Q}}{\partial \tau}=-[\frac{\partial \overline{E}}{\partial \xi}+\frac{\partial \overline{F}}{\partial \eta}]=-R^n_{i,j}, \tag{2}$$

$$\text{with } \overline{Q}=\frac{Q}{J},\ \overline{E}=\frac{1}{J}[\xi_t Q+\xi_x E+\xi_y F] \text{ and}$$

$$\overline{F}=\frac{1}{J}[\eta_t Q+\eta_x E+\eta_y F].$$

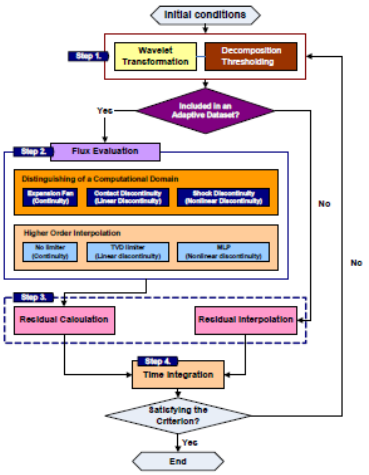

FIGURE 1. OVERALL PROCEDURE OF THE ADAPTIVE WAVELET METHOD

The flow chart in figure 1 shows the overall process of the implementation of the adaptive wavelet method to a two-dimensional high order accurate Euler solver.

Wavelet Transformation

At first, assume a two-dimensional dyadic gridset as figure 2. Here, values at O cells are saved to the position in the coarser level gridset. At the other cells of □, △ and X positions, the 6th order of interpolating polynomial is used for maintaining the 3rd order accuracy of a conventional solver as shown in Eq. (3).

$$\square:\ \tilde{Q}^n_{i+1,j}=\frac{1}{256}(3Q^n_{i-4,j}-25Q^n_{i-2,j}+150Q^n_{i,j}+150Q^n_{i+2,j}-25Q^n_{i+4,j}+3Q^n_{i+6,j})$$

$$\triangle:\ \tilde{Q}^n_{i+1,j}=\frac{1}{256}(3Q^n_{i,j-4}-25Q^n_{i,j-2}+150Q^n_{i,j}+150Q^n_{i,j+2}-25Q^n_{i,j+4}+3Q^n_{i,j+6}) \qquad (3)$$

$$\begin{aligned}\text{X}:\ \tilde{Q}^n_{i+1,j}=\frac{1}{512}(&3Q^n_{i,j-4}+3Q^n_{i+2,j-4}+2Q^n_{i-2,j-2}-27Q^n_{i,j-2}\\&-27Q^n_{i+2,j-2}+2Q^n_{i+4,j-2}+3Q^n_{i-4,j}-27Q^n_{i-2,j}\\&+174Q^n_{i,j}+174Q^n_{i+2,j}-27Q^n_{i+4,j}+3Q^n_{i+6,j}\\&+3Q^n_{i-4,j+2}-27Q^n_{i-2,j+2}+174Q^n_{i,j+2}+174Q^n_{i+2,j+2}\\&-27Q^n_{i+4,j+2}+3Q^n_{i+6,j+2}+2Q^n_{i-2,j+4}-27Q^n_{i,j+4}\\&-27Q^n_{i+2,j+4}+2Q^n_{i+4,j+4}+3Q^n_{i,j+6}+3Q^n_{i+2,j+6})\end{aligned}$$

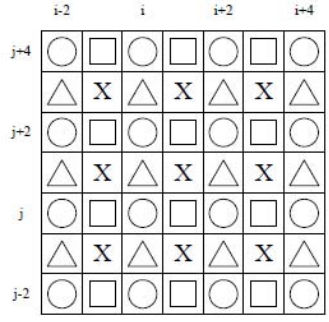

FIGURE 2. TWO-DIMENSIONAL DYADIC GRID

The difference values are calculated as Eq. (4).

$$\square:\ d^n_{i+1,j}=Q^n_{i+1,j}-\tilde{Q}^n_{i+1,j},$$

$$\triangle:\ d^n_{i,j+1}=Q^n_{i,j+1}-\tilde{Q}^n_{i,j+1}, \qquad (4)$$

$$\text{X}:\ d^n_{i+1,j+1}=Q^n_{i+1,j+1}-\tilde{Q}^n_{i+1,j+1}.$$

After wavelet decomposition, the wavelet coefficients are compared with the threshold value; if the values are larger than the threshold value, the points become remained in an adaptive dataset. Through these processes, the dataset follows the local feature of a CFD solution. However, the thresholding process inevitably results in the additional $O(\varepsilon)$ numerical errors because of the data loss below $O(\varepsilon)$. In order to overcome this defect, the thresholding method is modified by considering the order of truncation errors as Eq. (5) [7].

$$\varepsilon'=\min[\varepsilon,\max(\Delta x^3,CFL^3\cdot\Delta x^3)]. \qquad (5)$$

If a wavelet coefficient is smaller than ε', the cell doesn't belong to the dataset. In the other case, the cell is included in the dataset; an adaptive dataset is constructed according to the local features of the dataset with 3rd order of accuracy. Through these higher order wavelet decomposition and modified threshold value, 3rd order of accuracy of a conventional CFD solver is guaranteed.

Flux Evaluation

After the wavelet transformation, flux values are only calculated at the included cells in the adaptive dataset with 3rd order of accuracy. In order to construct a 3rd order accurate spatial discretization, e-MLP limiting function is used for the oscillation removal of the 3rd order interpolation scheme [4]. The primary features of e-MLP are as follows; in the CFD, the majority of the regions are so continuous that there is no need of applying the limiting functions. Rather, the dissipation due to limiting function may damage the solution's accuracy in the continuous region. Thus, there is no application of limiting function in continuous regions. In the discontinuous regions, the regions can be divided into linear and nonlinear discontinuous regions by the types of discontinuities. Then, by the switching of limiting function between TVD and MLP, TVD is used in the linear discontinuous regions and MLP is in the nonlinear dis-continuous regions.

The brief summary of 3rd order accurate interpolation with e-MLP is shown in Eq. (6-9) [4].

(a) 3rd order accuracy

$$\beta_L=\frac{1+2r_{L,i}}{3},\quad \beta_R=\frac{1+2r_{R,i+1}}{3}, \qquad (6a)$$

$$\text{where}\ \ r_{L,i}=\frac{\overline{\Phi}_{i+1}-\overline{\Phi}_i}{\overline{\Phi}_i-\overline{\Phi}_{i-1}}\ \ r_{R,i+1}=\frac{\overline{\Phi}_{i+1}-\overline{\Phi}_i}{\overline{\Phi}_{i+2}-\overline{\Phi}_{i+1}}.$$

(b) Continuous region: No limiting function

$$\mathbf{\Phi}_L = \overline{\mathbf{\Phi}}_i + 0.5\beta_L \Delta\mathbf{\Phi}_{i-\frac{1}{2}}, \tag{7a}$$

$$\mathbf{\Phi}_R = \overline{\mathbf{\Phi}}_{i+1} - 0.5\beta_R \Delta\mathbf{\Phi}_{i+\frac{3}{2}}. \tag{7b}$$

(c) Linear discontinuous region:
TVD criterion, $\phi(r) = \max(0, \min(2, 2r))$

$$\mathbf{\Phi}_L = \overline{\mathbf{\Phi}}_i + 0.5\max(0, \min(2\Delta\mathbf{\Phi}_{i+\frac{1}{2}}, 2\Delta\mathbf{\Phi}_{i-\frac{1}{2}}, \beta_L \Delta\mathbf{\Phi}_{i-\frac{1}{2}})), \tag{8a}$$

$$\mathbf{\Phi}_R = \overline{\mathbf{\Phi}}_{i+1} - 0.5\max(0, \min(2\Delta\mathbf{\Phi}_{i+\frac{1}{2}}, 2\Delta\mathbf{\Phi}_{i+\frac{3}{2}}, \beta_R \Delta\mathbf{\Phi}_{i+\frac{3}{2}})). \tag{8b}$$

(d) Nonlinear discontinuous region:
MLP limiter, $\phi(r) = \max(0, \min(\alpha, \alpha r))$

$$\mathbf{\Phi}_L = \overline{\mathbf{\Phi}}_i + 0.5\max(0, \min(\alpha_L \Delta\mathbf{\Phi}_{i+\frac{1}{2}}, \alpha_L \Delta\mathbf{\Phi}_{i-\frac{1}{2}}, \beta_L \Delta\mathbf{\Phi}_{i-\frac{1}{2}})), \tag{9a}$$

$$\mathbf{\Phi}_R = \overline{\mathbf{\Phi}}_{i+1} - 0.5\max(0, \min(\alpha_R \Delta\mathbf{\Phi}_{i+\frac{1}{2}}, \alpha_R \Delta\mathbf{\Phi}_{i+\frac{3}{2}}, \beta_R \Delta\mathbf{\Phi}_{i+\frac{3}{2}})), \tag{9b}$$

where $\alpha_{L,R}$ are MLP coefficients.

After the interpolation of primitive variables at the cell interface, AUSMPW+ scheme is applied for the spatial discretization [8, 9].

Residual Interpolation

At unimportant cells in the dataset, residual values are interpolated by using the 6th order of interpolating polynomial as Eq. (10).

$$\square: \quad \tilde{R}^n_{i+1,j} = \frac{1}{256}(3R^n_{i-4,j} - 25R^n_{i-2,j} + 150R^n_{i,j} + 150R^n_{i+2,j} - 25R^n_{i+4,j} + 3R^n_{i+6,j})$$

$$\triangle: \quad \tilde{R}^n_{i+1,j} = \frac{1}{256}(3R^n_{i,j-4} - 25R^n_{i,j-2} + 150R^n_{i,j} + 150R^n_{i,j+2} - 25R^n_{i,j+4} + 3R^n_{i,j+6}) \tag{10}$$

$$\begin{aligned} X: \quad \tilde{R}^n_{i+1,j} = \frac{1}{512}(&3R^n_{i,j-4} + 3R^n_{i+2,j-4} + 2R^n_{i-2,j-2} - 27R^n_{i,j-2} \\ &- 27R^n_{i+2,j-2} + 2R^n_{i+4,j-2} + 3R^n_{i-4,j} - 27R^n_{i-2,j} \\ &+ 174R^n_{i,j} + 174R^n_{i+2,j} - 27R^n_{i+4,j} + 3R^n_{i+6,j} \\ &+ 3R^n_{i-4,j+2} - 27R^n_{i-2,j+2} + 174R^n_{i,j+2} + 174R^n_{i+2,j+2} \\ &- 27R^n_{i+4,j+2} + 3R^n_{i+6,j+2} + 2R^n_{i-2,j+4} - 27R^n_{i,j+4} \\ &- 27R^n_{i+2,j+4} + 2R^n_{i+4,j+4} + 3R^n_{i,j+6} + 3R^n_{i+2,j+6}) \end{aligned}$$

By using this 6th order of interpolating polynomial, the error caused by interpolation becomes smaller than the truncation errors of the numerical schemes. After constructing residual distributions in the whole computational domain, 3rd order of Runge-Kutta time integration is performed [8, 9].

NUMERICAL RESULTS AND DISCUSSION

In order to assess the efficiency of the higher order accurate adaptive wavelet method, it is applied to a shock-vortex inter-action problem [10]. The domain is set as $-20 \le x \le 5$ and $-20 \le y \le 10$ with a 400×400 grid. The initial velocity, density and pressure distributions of a vortex flow are presented in Eq. (11) [10].

$$\text{Tangential velocity:} \quad u_\theta = M_v r \exp[(1-r^2)/2],$$

$$\text{Radial velocity:} \quad u_r = 0,$$

$$\text{Vorticity:} \quad \omega(r) = M_v(2-r^2)\exp[(1-r^2)/2], \tag{11}$$

$$\text{Pressure:} \quad p(r) = \frac{1}{\gamma}[1 - \frac{\gamma-1}{2}M_v^2 \exp(1-r^2)]^{\gamma/(\gamma-1)},$$

$$\text{Density:} \quad \rho(r) = \frac{1}{\gamma}[1 - \frac{\gamma-1}{2}M_v^2 \exp(1-r^2)]^{1/(\gamma-1)}.$$

The Mach number of vortex is 0.39 and the initial vortex core is located at (-5,-5). The normal shock with Mach number of 1.29 is propagated to the vortex and ε is set as 10^{-5}.

The overall efficiency improvement according to wavelet resolution level is summarized in Table 1. In this table, the computational time with 1 level of wavelet resolution is larger than that of 2nd order accurate conventional solver. It is because the additional CPU time of wavelet transformation is larger than the decrease of CPU time of flux evaluation. By increasing the wavelet resolution level, the adaptive wavelet method with 3rd order accuracy becomes more efficient than 2nd order accurate solver as well as 3rd order accurate solver; the computational time of wavelet method became about 1.7 times faster than the 3rd order of e-MLP method at maximum when the resolution level of wavelet is 3.

TABLE 1. COMPARISON OF CPU TIMES IN SHOCK-VORTEX INTERACTION PROBLEM

Level	CPU Time			Computational Efficiency (CPU time_e-MLP / CPU time_Wav)
	2nd order	e-MLP (3rd)	Wavelet	
1	1737.6	2498.2	1961.9	1.273
2			1537.1	1.625
3			1477.7	1.691

Figure 3 represents the adaptive dataset with wavelet decomposition level=3. The dataset follows the flow features accurately and many cells are remained near the vortex and shock regions. In the other smooth regions, the changes of the flow properties are negligible and the remaining cells are sparsely distributed. By the wavelet transformation, the remaining cells in the CFD dataset is about 58% of the whole computational domain where fluxes are calculated. In the other regions, residual interpolation is performed. Here, the remaining regions are divided into continuous, linear discontinuous and nonlinear discontinuous regions; 53% of the whole computational domain is continuous region, 2% is linear discontinuous region, and 3% is nonlinear discontinuous region. Then in the continuous region, there is no application of limiting function. In the linear discontinuous region and nonlinear discontinuous region, TVD and MLP limiting function are used for oscillation removal, respectively. Due to the combination of wavelet and e-MLP, the computational efficiency is substantially enhanced.

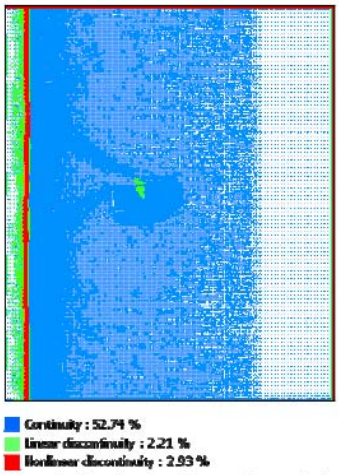

FIGURE 3. Adaptive dataset with wavelet resolution level=3

Figure 4 shows the density contours of a conventional 2nd order accurate solver, 3rd order accurate solver and the adaptive wavelet scheme after the non-dimensional time of 18. In these figures, it is shown that the contour of 2nd order accurate conventional solver is smeared comparing with that of 3rd order accurate solver. However, the 3rd order accurate adaptive wavelet method can maintain the original features of a solution; the contours of slip line, reflected wave pattern, etc. are clearly presented in the results of the 3rd order accurate solver and the adaptive wavelet method. Figure 5 shows the detailed density distributions of 2nd order accurate solver, 3rd order accurate solver, the adaptive wavelet method at y=-5 and they are compared with the result of dense grid system with 2nd order accurate solver. In the result of 2nd order accurate computation, the vortex and reflected wave is dissipated compared with the 3rd order accurate conventional solver and the wavelet method. However, by using 3rd order accurate method, the density distributions follows that of dense grid system more accurately.

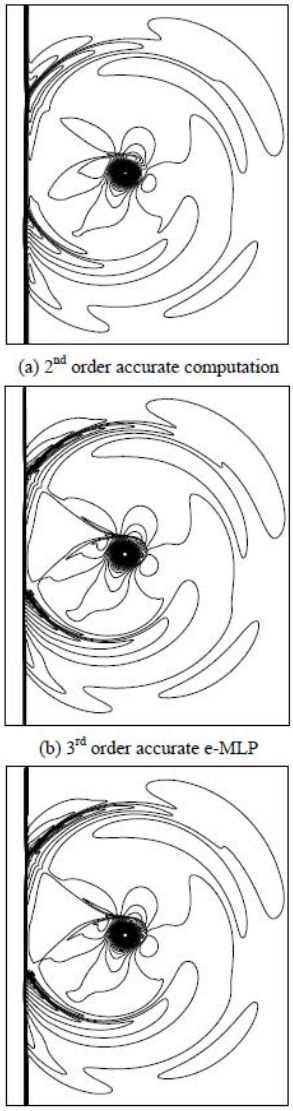

(a) 2nd order accurate computation

(b) 3rd order accurate e-MLP

(c) 3rd order accurate e-MLP with adaptive wavelet method

FIGURE 4. Comparison of density contours with wavelet resolution level=3

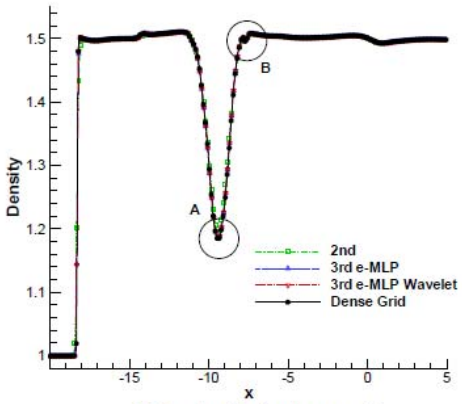

(a) Density distribution at y=-5.

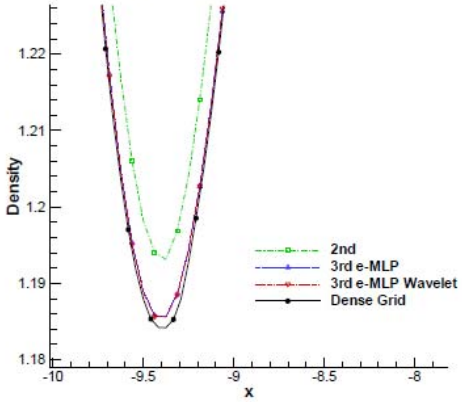

(b) Detailed density distribution at A region.

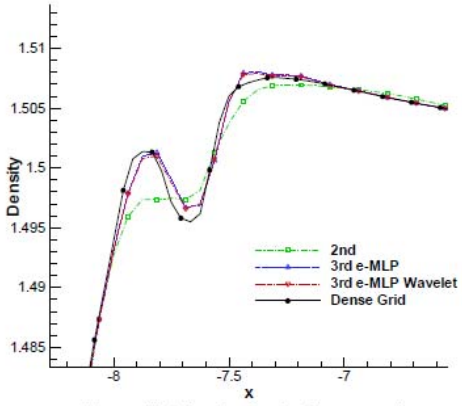

(c) Detailed density distribution at B region.

FIGURE 5. Comparison of density distribution at y=-5

CONCLUSIONS

Through this research, the higher order accurate adaptive wavelet method is proposed for enhancing the computational efficiency of e-MLP method. For this purpose, higher order accurate wavelet transformation is proposed including the wavelet decomposition with 6th order accurate interpolating polynomial and modified threshold value. This higher order accurate adaptive wavelet method is applied to two-dimensional shock-vortex interaction problems. In these test, the adaptive wavelet method can present much better efficiency and accuracy compared with 2nd order accurate computation by decreasing the computational time of 3rd order accurate e-MLP method.

ACKNOWLEDGMENTS

This work was supported by the second stage of the Brain Korea 21 Project in 2011 and partially supported by the Asian Office of Aerospace R&D (AOARD) project (Award No: FA2386-10-1-4001).

REFERENCES

[1] Harten, A., 1983. "High resolution schemes for hyperbolic conservation laws." *J. Comput. Phys.*, **49**, pp. 357-393.

[2] Harten, A., Enquist, B., Osher, S. and Chakravarthy, S.R., 1987. "Uniformly high order accurate essentially non-oscillatory schemes, III." *J. Comput. Phys.*, **71**, pp. 231-303.

[3] Kim, K. and Kim, C., 2005. "Efficient and monotonic numerical methods for multi-dimensional compressible flows Part II: Multi-dimensional limiting process." *J. Comput. Phys.*, **208**, pp. 570–615.

[4] Kang, H., Kim, K. and Lee, D., 2010. "A new approach of a limiting process for multi-dimensional flows." *J. Comput. Phys.*, **229**, pp. 7102–7128.

[5] Sjögreen, B., 1995. "Numerical experiments with the multi-resolution scheme for the compressible Euler equations," *J. Comput. Phys.*, **117**, pp. 251–261.

[6] Kang, H., Kim, K., Lee, D. and Lee, D., 2008. "Improvement in computational efficiency of Euler equations via a modified Sparse Point Representation method". *Compu. and Fluids*, **37**, pp. 265–280.

[7] Kang, H., Kim, K., Lee, D. and Lee, D., 2008. "Improved computational efficiency of unsteady flow problems via the modified wavelet method", *AIAA J.* **46**, pp. 1191–1203.

[8] Kim, K., Kim, C. and Rho, O., 2001. "Methods for the accurate computations of hypersonic flows: I. AUSMPW+ scheme". *J. Comput. Phys.*, **174**, pp. 38–80.

[9] Kim, K. and Kim, C., 2005. "Accurate, efficient and monotonic numerical methods for multi-dimensional compressible flows Part I: Spatial discretization". *J. Comput. Phys.*, **208**, pp. 527–569.

[10] Inoue, O. and Hattori, Y., 1999. "Sound generation by shock-vortex interactions". *J. Fluid Mech.* **380**, pp ~81–116.

Published Paper in AIAA 2012 Fluid Dynamics Conference

42nd AIAA Fluid Dynamics Conference and Exhibit
25 - 28 June 2012, New Orleans, Louisiana

AIAA 2012-3065

Research on the Adaptive Wavelet Method for the Enhancement of Computational Efficiency of Three Dimensional Flows

Kyung-Hyun Park[1]
School of Mechanical and Aerospace Engineering, College of Engineering, Seoul National University, Seoul 151-744, Republic of Korea

Hyung-Min Kang[2]
Advanced Aerodynamics and Structures Department, Korea Aerospace Research Institute, 115 Gwahangno, Yuseong-gu, Daejeon, 301-333, Republic of Korea

Ji-Hoon Jeong.[3], Kyu-Hong Kim.[4]

School of Mechanical and Aerospace Engineering, College of Engineering, Seoul National University, Seoul 151-744, Republic of Korea

Do-Hyung Lee[5]
Department of Mechanical Engineering, Hanyang University, Ansan 426-791, KyungKi-Do, Republic of Korea

and

Dong-Ho Lee[6]
School of Mechanical and Aerospace Engineering, College of Engineering, Seoul National University, Seoul 151-744, Republic of Korea

The adaptive wavelet method is studied for the enhancement of computational efficiency of three-dimensional flows. Three-dimensional wavelet decomposition process is introduced based on the previous two-dimensional method. The order of numerical accuracy of an original solver is preserved by applying a proper thresholding technique. The proposed algorithm is applied to the computation of flow field around ONERA-M6 wing in transonic regime. Through the application, it is confirmed that the three-dimensional adaptive wavelet method can reduce the computational time with conserving the numerical accuracy of an original solver.

Nomenclature

English

[1] Graduate Student, School of Mechanical and Aerospace Engineering, BD 312-202, San 56-1, Shinlim-dong, Gwanak-gu / pkh365@snu.ac.kr.
[2] Ph. D, Advanced Aerodynamics and Structures Department, Aeronautics Technology Devision, 115 Gwahangno, Yuseong-gu / kangm@snu.ac.kr.
[3] Ph. D, School of Mechanical and Aerospace Engineering, BD 312-202, San 56-1, Shinlim-dong, Gwanak-gu / pkh365@snu.ac.kr.
[4] Professor, School of Mechanical and Aerospace Engineering and Institute of Advanced Aerospace Technology, BD 302-628, San 56-1, Shinlim-dong, Gwanak-gu / aerocfd1@snu.ac.kr, AIAA Member.
[5] Professor, Department of Mechanical Engineering, 1271 Sa 1 Dong / dohyung@hanyang.ac.kr, AIAA Member.
[6] Professor, School of Mechanical and Aerospace Engineering and Institute of Advanced Aerospace Technology, BD 301-1302, San 56-1, Shinlim-dong, Gwanak-gu / donghlee@snu.ac.kr, AIAA Member.

$d^n_{i,j,k}$ = wavelet coefficient at (i, j, k) cell of n time step
$f_{l,k}$ = $f(x_{l,k})$, exact function value at $x_{l,k}$
$Q^n_{i,j,k}$ = (ρ, p, u, v, w) at (i, j, k) cell of n time step
$\widetilde{Q}^n_{i,j,k}$ = approximated value by interpolating polynomial
$\mathrm{P}_l f(x)$ = Set of original values at V_l
p = pressure
$R^n_{i,j,k}$ = residual values at (i, j, k) cell of n time step
$\widetilde{R}^n_{i,j,k}$ = interpolated value of $R^n_{i,j,k}$ given by interpolating polynomial
u, v, w = components of the velocity vector
V_l = Dyadic grid set with l^{th} wavelet resolution level
$x_{l,k}$ = k^{th} cell on V_l
Z = Integer

Subscript
i, j, k = position of a cell

Superscript
n = current time step

Greek
ε = threshold value
ε' = modified threshold value
γ = ratio of specific heat (1.4 for air)
ρ = density

I. Introduction

RECENTLY in aerospace fields, high fidelity simulations have been strongly demanded for the accurate analysis of complicated flows related with transonic/supersonic flow phenomena. These demands emphasize the accurate and robust flow computation with vast size of grids in Computational Fluid Dynamics (CFD). However, the current level of technologies in CFD is often insufficient in terms of accuracy and efficiency; a large number of grid points and higher order accurate algorithms result in a substantial burden in computation. Sometimes, the consideration of computational efficiency and vice versa restricts the enhancement of numerical accuracy.

For solving these problems, many numerical approaches have been applied in various CFD fields. Among these approaches, the adaptive wavelet method has been studied as very useful CFD tools for solutions algorithms, feature extraction, and data compression, etc. In the adaptive wavelet approach, wavelet decomposition is performed to calculate the wavelet coefficients and some coefficients which are smaller than thresholding value, ε are cut-off in the dataset. In most cases, the wavelet coefficients are small in the smooth region and large in the rapidly changing regions such as shock, vortex and boundary layer, etc. Therefore, the crucial features in the CFD solutions are automatically searched by wavelet transformation and an adaptive dataset is constructed so as to follow these local features with $O(\varepsilon)$ errors. Then, high cost calculation such as flux evaluation is only performed in these important regions and low cost interpolation polynomial is applied in the other regions. Because the major parts of CFD solutions show smooth flow patterns, adaptive wavelet method can present crucial advantages in the computational efficiency.

Due to this significant advantage, there have been many researches about adaptive wavelet methods; Harten presented an adaptive multi-resolution scheme for computing the discontinuous solutions of hyperbolic PDEs.[1] Holmström proposed the algorithm that uses the interpolating wavelet transformation to organize an adaptive dataset.[2] Sjögreen also used a multi-resolution scheme based on the interpolating wavelet transformation to solve the

compressible Euler equations.[3] Kang et. al. implanted modified threshold value in adaptive wavelet methods, applied the method to two-dimensional flows, and enhance the computational efficiency of the simulation with the conservation of the numerical accuracy of the solutions.[4, 5] D. Wirasaet et al. simulated three dimensional flow within a differentially heated cavity using adaptive wavelet algorithm.[6]

However, for more practical applications such as three-dimensional flow analysis for design optimization or sensitivity analysis, the adaptive wavelet algorithm should be simple to be implanted in an original solver, enhance the computational efficiency, and preserve the numerical accuracy of the solver. For these purposes, the adaptive wavelet method proposed by Kang et al.[4, 5] is extended to three dimensional analysis. Because this adaptive wavelet method utilizes the 4th order interpolation coefficients as wavelet basis, it is very simple to be united with an original solver. Also, the numerical accuracy of an original solver can be preserved by the modified thresholding value. In order to assess the method, it is applied to a flow simulation around the ONERA-M6 wing in transonic regime. Consequently, it is confirmed that the proposed three-dimensional adaptive wavelet method can enhance the computational efficiency of an original solver with preservation of the numerical accuracy of the solver.

II. Preliminary background of the adaptive wavelet method

In this research, the adaptive wavelet method based on the interpolating polynomial is used.[2] At first, let us assume a dyadic grid set as shown in Eq. (1).

$$V_l = \{x_{l,k} \in R : x_{l,k} = 2^{-l}k, k \in Z\},\ l \in Z\ . \tag{1}$$

The key idea of the adaptive wavelet method is that the smoothness of flow pattern can be easily determined by the magnitude of difference value between original function value and approximated value by using neighboring cells. That is, the original value can be accurately approximated by the values at neighboring cells in the smooth region but not vice versa in rapidly changing region. Here, interpolating polynomial is used at the odd numbered cells for approximation of original function values and then the dyadic dataset is decomposed as Eq. (2).

$$\begin{cases} \widetilde{f}_{l+1,2k} = f_{l,k} \\ \widetilde{f}_{l+1,2k+1} = P_{l+1,2k+1}(f_{l,k-\frac{p}{2}+1}, \cdots, f_{l,k}, f_{l,k+1}, \cdots, f_{l,k+\frac{p}{2}}) \end{cases} \tag{2}$$

where $P_{l,k}$ is the order of interpolating polynomial; the 4th order of interpolating polynomial is shown in Eq. (3).

$$\widetilde{f}_{l+1,2k+1} = -\frac{1}{16}f_{l,k-1} + \frac{9}{16}f_{l,k} + \frac{9}{16}f_{l,k+1} - \frac{1}{16}f_{l,k+2}\ . \tag{3}$$

After the approximation, the difference can be computed as Eq. (4).

$$d_{l,k} = f_{l+1,2k+1} - \widetilde{f}_{l+1,2k+1},\ \forall k \in Z\ . \tag{4}$$

In smooth region, the order of difference value is very small and the corresponding cell can be partially rejected in the whole dataset; an adaptive dataset is acquired according to the local features of solution. And the maximum error is bounded within the order of threshold value as Eq. (5).

$$\left|d_{l,k}\right|_\infty = \left|f_{l,k} - \widetilde{f}_{l,k}\right|_\infty < O(\varepsilon)\ . \tag{5}$$

III. Implementation of Adaptive Wavelet Method on the Three-Dimensional Euler Equations

In this research, the three-dimensional Euler equations are used as the governing equations of the flow problem. The three-dimensional Euler equations are written as Eq. (6).

$$\frac{\partial Q}{\partial t}+\frac{\partial E}{\partial x}+\frac{\partial F}{\partial y}+\frac{\partial G}{\partial z}=0 \tag{6}$$

$$\text{with } Q=\begin{bmatrix}\rho\\ \rho u\\ \rho v\\ \rho w\\ \rho e_t\end{bmatrix},\ E=\begin{bmatrix}\rho u\\ \rho u^2+p\\ \rho uv\\ \rho uw\\ (\rho\rho_t+p)u\end{bmatrix},\ F=\begin{bmatrix}\rho v\\ \rho vu\\ \rho v^2+p\\ \rho vw\\ (\rho\rho_t+p)v\end{bmatrix},\ G=\begin{bmatrix}\rho w\\ \rho wu\\ \rho wv\\ \rho w^2+p\\ (\rho\rho_t+p)w\end{bmatrix} \text{ and}$$

$$e_t=\frac{a^2}{\gamma(\gamma-1)}+\frac{1}{2}(u^2+v^2+w^2),$$

where all properties and governing equations are non-dimensionalized. By the generalized coordinate transformation, Eq. (6) is rewritten as Eq. (7).

$$\frac{\partial \overline{Q}}{\partial \tau}=-[\frac{\partial \overline{E}}{\partial \xi}+\frac{\partial \overline{F}}{\partial \eta}+\frac{\partial \overline{G}}{\partial \varsigma}]=-R^n_{i,j,k} \tag{7}$$

$$\text{with } \overline{Q}=\frac{Q}{J},\ \overline{E}=\frac{1}{J}[\xi_t Q+\xi_x E+\xi_y F+\xi_z G],\ \overline{F}=\frac{1}{J}[\eta_t Q+\eta_x E+\eta_y F+\eta_z G] \text{ and}$$

$$\overline{G}=\frac{1}{J}[\zeta_t Q+\zeta_x E+\zeta_y F+\zeta_z G].$$

In order to apply the wavelet procedure to CFD algorithms of three dimensional Euler equations, the three-dimensional wavelet decomposition procedure is implemented to the algorithms. For preservation of the numerical accuracy of the solution, the modified threshold value is applied by considering the grid spacing. The flow chart in Fig. 1 shows the overall procedure of implementation of the adaptive wavelet method to a three-dimensional Euler solver. The details of all steps are as follows:

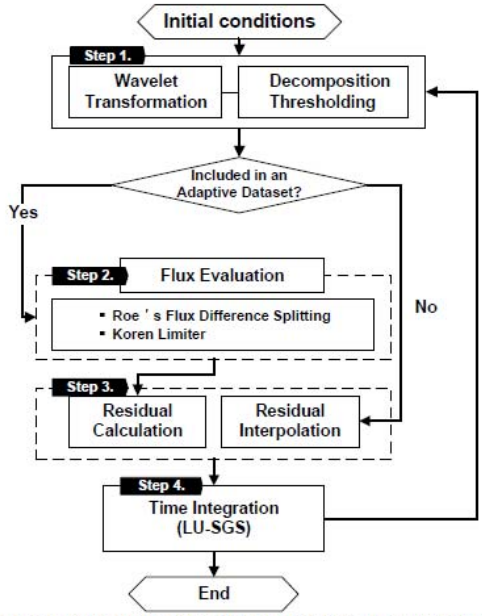

Figure 1 Overall procedure of the three-dimensional Euler solver with adaptive wavelet method.

A. Wavelet Transformation

Assume a three-dimensional dyadic gridset with level l as shown in Fig. 2.

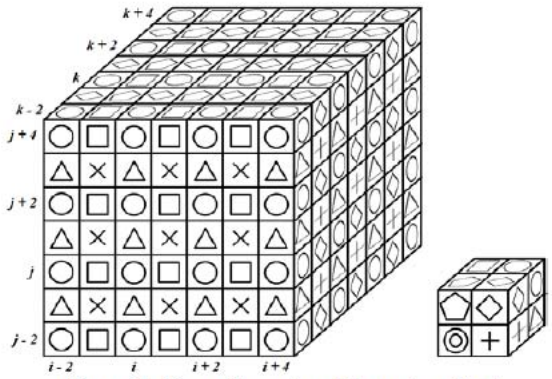

Figure 2 Three-dimensional dynamic gridset.

Here, values at ○ cells are saved in the coarser level gridset, and 4th order of interpolating polynomial is employed at the other cells (□, △, ◇, ×, +, ⬠, ◎) as Eq. (8).

$$
\begin{aligned}
\square:\ & \widetilde{Q}^n_{i+1,j,k} = \frac{1}{16}\left(-Q^n_{i-2,j,k} + 9Q^n_{i,j,k} + 9Q^n_{i+2,j,k} - Q^n_{i+4,j,k}\right),\\
\triangle:\ & \widetilde{Q}^n_{i,j+1,k} = \frac{1}{16}\left(-Q^n_{i,j-2,k} + 9Q^n_{i,j,k} + 9Q^n_{i,j+2,k} - Q^n_{i,j+4,k}\right),\\
\diamond:\ & \widetilde{Q}^n_{i,j,k+1} = \frac{1}{16}\left(-Q^n_{i,j,k-2} + 9Q^n_{i,j,k} + 9Q^n_{i,j,k+2} - Q^n_{i,j,k+4}\right),\\
\times:\ & \widetilde{Q}^n_{i+1,j+1,k} = \frac{1}{32}\left(-Q^n_{i-2,j-2,k} + 9Q^n_{i,j,k} + 9Q^n_{i+2,j+2,k} - Q^n_{i+4,j+4,k}\right.\\
& \qquad \left. - Q^n_{i-2,j+4,k} + 9Q^n_{i,j+2,k} + 9Q^n_{i+2,j,k} - Q^n_{i+4,j-2,k}\right),\\
+:\ & \widetilde{Q}^n_{i,j+1,k+1} = \frac{1}{32}\left(-Q^n_{i,j-2,k-2} + 9Q^n_{i,j,k} + 9Q^n_{i,j+2,k+2} - Q^n_{i,j+4,k+4}\right.\\
& \qquad \left. - Q^n_{i,j-2,k+4} + 9Q^n_{i,j,k+2} + 9Q^n_{i,j+2,k} - Q^n_{i,j+4,k-2}\right),\\
\pentagon:\ & \widetilde{Q}^n_{i+1,j,k+1} = \frac{1}{32}\left(-Q^n_{i-2,j,k-2} + 9Q^n_{i,j,k} + 9Q^n_{i+2,j,k+2} - Q^n_{i+4,j,k+4}\right.\\
& \qquad \left. - Q^n_{i-2,j,k+4} + 9Q^n_{i,j,k+2} + 9Q^n_{i+2,j,k} - Q^n_{i+4,j,k-2}\right),\\
\text{◎}:\ & \widetilde{Q}^n_{i+1,j+1,k+1} = \frac{1}{64}\left(-Q^n_{i-2,j-2,k-2} + 9Q^n_{i,j,k} + 9Q^n_{i+2,j+2,k+2} - Q^n_{i+4,j+4,k+4}\right.\\
& \qquad - Q^n_{i-2,j-2,k+4} + 9Q^n_{i,j,k+2} + 9Q^n_{i+2,j+2,k} - Q^n_{i+4,j+4,k-2}\\
& \qquad - Q^n_{i-2,j+4,k-2} + 9Q^n_{i,j+2,k} + 9Q^n_{i+2,j,k+2} - Q^n_{i+4,j-2,k+4}\\
& \qquad \left. - Q^n_{i+4,j-2,k-2} + 9Q^n_{i+2,j,k} + 9Q^n_{i,j+2,k+2} - Q^n_{i-2,j+4,k+4}\right)
\end{aligned}
\tag{8}
$$

After the interpolation of each cell, the difference values are computed as Eq. (9).

$$\begin{aligned}
&\square: d^n_{i+1,j,k} = Q^n_{i+1,j,k} - \widetilde{Q}^n_{i+1,j,k},\\
&\triangle: d^n_{i,j+1,k} = Q^n_{i,j+1,k} - \widetilde{Q}^n_{i,j+1,k},\\
&\diamond: d^n_{i,j,k+1} = Q^n_{i,j,k+1} - \widetilde{Q}^n_{i,j,k+1},\\
&\times: d^n_{i+1,j+1,k} = Q^n_{i+1,j+1,k} - \widetilde{Q}^n_{i+1,j+1,k},\\
&+: d^n_{i,j+1,k+1} = Q^n_{i,j+1,k+1} - \widetilde{Q}^n_{i,j+1,k+1},\\
&\pentagon: d^n_{i+1,j,k+1} = Q^n_{i+1,j,k+1} - \widetilde{Q}^n_{i+1,j,k+1},\\
&\circledcirc: d^n_{i+1,j+1,k+1} = Q^n_{i+1,j+1,k+1} - \widetilde{Q}^n_{i+1,j+1,k+1}.
\end{aligned} \tag{9}$$

Then the difference values are compared with the threshold value, ε; if the values are larger than the threshold value, the points are remained in an adaptive dataset. If the difference values are smaller than ε, the cells don't belong to the adaptive dataset. That is, an adaptive dataset is constructed so as to follow the local feature of a CFD solution.

However due to approximation and data loss from thresholding, some $O(\varepsilon)$ error is added to the solution and deteriorate the numerical accuracy of a original solver. In order to prevent the addition of this $O(\varepsilon)$ error, the thresholding method is modified by considering the order of truncation errors.[4-5] The details are as follows. In this paper, because a second order of MUSCL scheme is applied to the flux evaluation, the flux at (*i, j, k*) cell can be written based on the real value as Eq. (10).

$$E^n_{\frac{1}{2}} = E^n_{\frac{1}{2},real} + O(\Delta x^2),\ F^n_{\frac{1}{2}} = F^n_{\frac{1}{2},real} + O(\Delta y^2),\ G^n_{\frac{1}{2}} = G^n_{\frac{1}{2},real} + O(\Delta z^2) \tag{10}$$

According to the definition of $R^n_{i,j,k}$ in Eq. (7) and Eq. (10), $R^n_{i,j,k}$ is derived as Eq. (11).

$$R^n_{i,j,k} \approx R^n_{i,j,k,real} + O(\Delta x^4)_1. \tag{11}$$

Also, O(ε) error due to thresholding is added to the solution as Eq. (12).

$$\widetilde{E}^n_{\frac{1}{2}} = E^n_{\frac{1}{2}} + O(\varepsilon),\ \widetilde{F}^n_{\frac{1}{2}} = F^n_{\frac{1}{2}} + O(\varepsilon),\ \widetilde{G}^n_{\frac{1}{2}} = G^n_{\frac{1}{2}} + O(\varepsilon). \tag{12}$$

Consequently, $R^n_{i,j,k}$ can be written as Eq. (13).

$$\widetilde{R}^n_{i,j,j} = R^n_{i,j,k} + O(\Delta x^2 \varepsilon). \tag{13}$$

The third type of error is due to residual interpolation at the excluded points of a SPR dataset. In this case, the error order is about $O(\Delta x^4)$ because a 4th order of interpolating polynomial is used for the calculation of the residual values. Therefore, the error order at the excluded points of a SPR dataset is finally derived as Eq. (14).

$$\widetilde{R}^n_{i,j} = R^n_{i,j,real} + O(\Delta x^4) + O(\Delta x^2 \varepsilon). \tag{14}$$

From Eq. (14), $O(\varepsilon) < O(\Delta x^2)$ condition has to be satisfied to conserve the second order spatial accuracy. Therefore, for switching the threshold value associated to grid spacing, the threshold value need to be modified as Eq. (15).

$$\varepsilon' = min(\varepsilon, \Delta x^2) \tag{15}$$

In this study, ε is set to 1×10^{-5}, so $\varepsilon' = min(10^{-5}, \Delta x^2)$.

B. Flux Evaluation

After the wavelet transformation, flux values are only calculated at the included cells in the adaptive dataset. In this research, Finite Volume Method (FVM) is used to calculate the numerical fluxes; flux values are then computed on all sides of the cell with 2nd order accuracy.

C. Residual Interpolation & Time Integration

At unimportant cells which doesn't belong to the adaptive dataset, residual values are interpolated by 4th order of interpolating polynomial as Eq. (16).

$$
\begin{aligned}
\square:\ & \widetilde{R}^n_{i+1,j,k} = \frac{1}{16}\left(-R^n_{i-2,j,k} + 9R^n_{i,j,k} + 9R^n_{i+2,j,k} - R^n_{i+4,j,k}\right),\\
\triangle:\ & \widetilde{R}^n_{i,j+1,k} = \frac{1}{16}\left(-R^n_{i,j-2,k} + 9R^n_{i,j,k} + 9R^n_{i,j+2,k} - R^n_{i,j+4,k}\right),\\
\diamond:\ & \widetilde{R}^n_{i,j,k+1} = \frac{1}{16}\left(-R^n_{i,j,k-2} + 9R^n_{i,j,k} + 9R^n_{i,j,k+2} - R^n_{i,j,k+4}\right),\\
\times:\ & \widetilde{R}^n_{i+1,j+1,k} = \frac{1}{32}\left(-R^n_{i-2,j-2,k} + 9R^n_{i,j,k} + 9R^n_{i+2,j+2,k} - R^n_{i+4,j+4,k}\right.\\
& \qquad \left. - R^n_{i-2,j+4,k} + 9R^n_{i,j+2,k} + 9R^n_{i+2,j,k} - R^n_{i+4,j-2,k}\right),\\
+:\ & \widetilde{R}^n_{i,j+1,k+1} = \frac{1}{32}\left(-R^n_{i,j-2,k-2} + 9R^n_{i,j,k} + 9R^n_{i,j+2,k+2} - R^n_{i,j+4,k+4}\right.\\
& \qquad \left. - R^n_{i,j-2,k+4} + 9R^n_{i,j,k+2} + 9R^n_{i,j+2,k} - R^n_{i,j+4,k-2}\right),\\
\pentagon:\ & \widetilde{R}^n_{i+1,j,k+1} = \frac{1}{32}\left(-R^n_{i-2,j,k-2} + 9R^n_{i,j,k} + 9R^n_{i+2,j,k+2} - R^n_{i+4,j,k+4}\right.\\
& \qquad \left. - R^n_{i-2,j,k+4} + 9R^n_{i,j,k+2} + 9R^n_{i+2,j,k} - R^n_{i+4,j,k-2}\right),\\
\circledcirc:\ & \widetilde{R}^n_{i+1,j+1,k+1} = \frac{1}{64}\left(-R^n_{i-2,j-2,k-2} + 9R^n_{i,j,k} + 9R^n_{i+2,j+2,k+2} - R^n_{i+4,j+4,k+4}\right.\\
& \qquad - R^n_{i-2,j-2,k+4} + 9R^n_{i,j,k+2} + 9R^n_{i+2,j+2,k} - R^n_{i+4,j+4,k-2}\\
& \qquad - R^n_{i-2,j+4,k-2} + 9R^n_{i,j+2,k} + 9R^n_{i+2,j,k+2} - R^n_{i+4,j-2,k+4}\\
& \qquad \left. - R^n_{i+4,j-2,k-2} + 9R^n_{i+2,j,k} + 9R^n_{i,j+2,k+2} - R^n_{i-2,j+4,k+4}\right)
\end{aligned}
\tag{16}
$$

After residual interpolation, time integration such as LU-SGS method is applied.

IV. Numerical Tests and Discussion

For the assessment of the computational efficiency and numerical accuracy of the three-dimensional adaptive wavelet algorithm, it is applied to the computation of flow field around the ONERA-M6 wing with Mach number of 0.8395 and angle of attack of 3.06°.[7] After the computations, the adaptive dataset of all level of resolution are shown at Fig. 3. These figures show that the dataset follows the local features of the solution; many cells remain near the wing and downstream. In other smooth regions, the remaining cells are sparsely distributed because the changes in the flow properties are negligible.

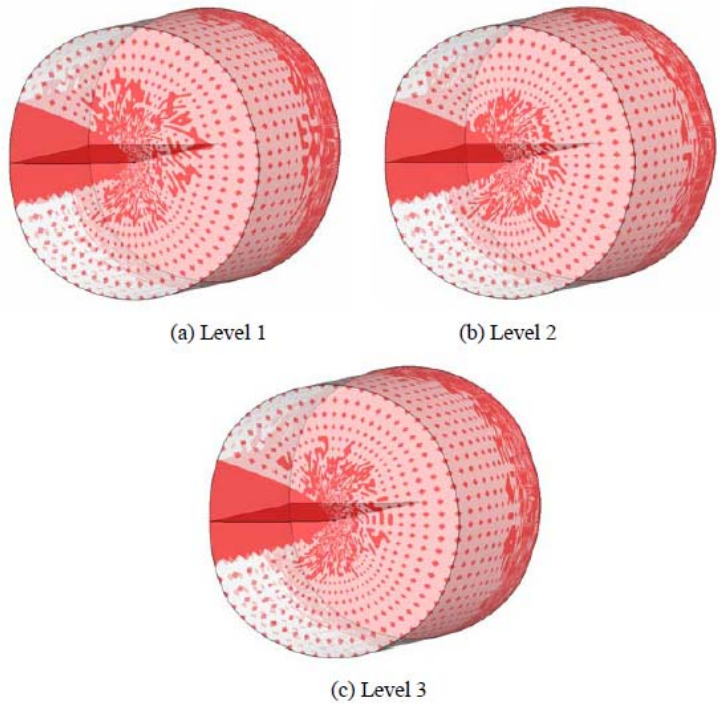

(a) Level 1 (b) Level 2

(c) Level 3

Figure 3. Adaptive datasets of ONERA-M6 wing flow problem.

The overall efficiency improvement and the L_2 error according to the wavelet resolution level are summarized in Table 1. Here, the computation speed of adaptive wavelet method becomes about 3 times faster than the reference CFD method. And the L_2 errors between the results of reference method and adaptive wavelet methods are only about $O(10^{-7})$. Throughout this implementation, it is substantiated that the adaptive wavelet method can enhance the computational efficiency of the steady state three dimensional Euler flow computation while numerical accuracy of the reference CFD solver is preserved.

Table 1. Results of efficiency improvements and L_2 error

		Iteration	SPR Pt.	CPU Time	Time Ratio	L_2 Error
Reference Solver		10764	·	29329.3	·	·
Adaptive Wavelet	1 Level	3206	64.61%	9192.5	3.19	2.51×10^{-7}
	2 Level	3267	64.57%	9438.4	3.11	3.14×10^{-7}
	3 Level	3205	64.74%	9251.8	3.17	3.49×10^{-7}

Fig. 4 shows the pressure contours on the upper surfaces of ONERA-M6 wings computed by reference CFD method and adaptive wavelet method. In both contours, the patterns of lambda shock which is the crucial feature of ONERA-M6 wing are very similar. For more detailed comparison of the results, pressure distributions of reference method and adaptive wavelet method at the positions of 50% and 80% of wing span are presented at Fig. 5. In the figures, it is shown that the positions of shock, shock strength and pressure distributions, etc. are almost same. Through the application, it is verified that the three-dimensional adaptive wavelet method can present much better efficiency with the maintenance of numerical accuracy of a solution.

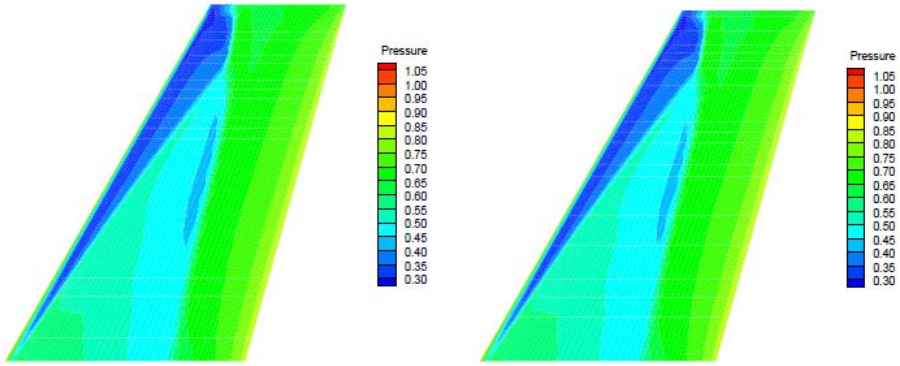

(a) Reference solver (b) Adaptive wavelet – 2 level of resolution

Figure 4. Pressure contour on the upper surface of wing.

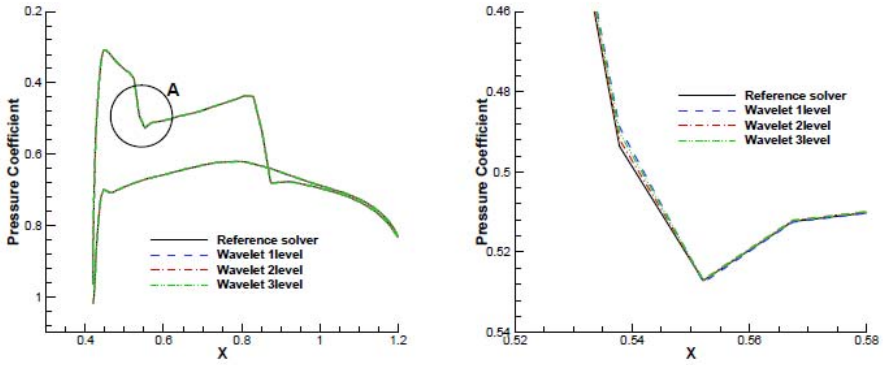

(a) Pressure distribution at 0.5 of span (b) Detailed pressure distribution at A region

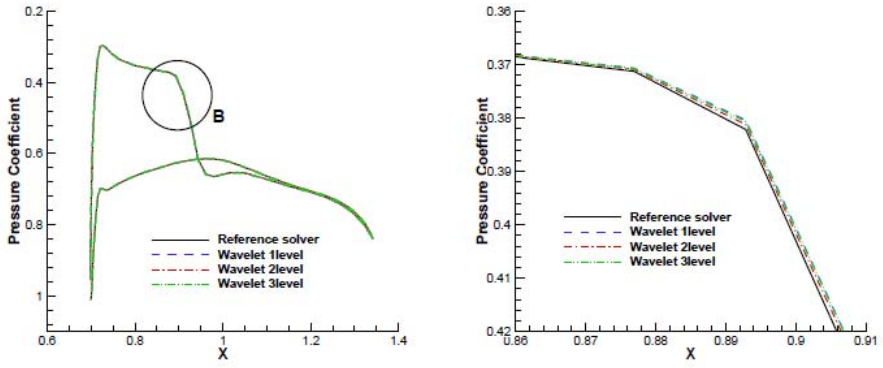

(a) Pressure distribution at 0.8 of span (b) Detailed pressure distribution at B region

Figure 5. Pressure distribution on the surface of wing.

V. Conclusion

In this research, the three-dimensional adaptive wavelet method is presented for enhancing the computational efficiency of three-dimensional Euler flow simulations in transonic regime. To this end, the previous adaptive algorithm proposed by Kang et al. is extended to three-dimensional adaptive wavelet properly; three-dimensional wavelet decomposition process and modified threshold value based on the switching between ε and Δx^2 is introduced to the method. The developed three-dimensional adaptive wavelet method is applied to ONERA-M6 wing in transonic regime. Through the application, it is shown that adaptive wavelet dataset are constructed so as to follow local features of solution automatically. Also, it enhances the computational efficiency about 3 times faster than that of reference solver with preservation of numerical accuracy of a solution.

Acknowledgments

We appreciate the support of Defense Acquisition Program Administration and Agency for Defense Development for this study to be completed under the contract UD070041AD, the National Research Foundation of Korea (NRF) grant funded by the Korea government(MEST) (No. 20110001227), the Ministry of Education, Science and Technology, subjected to the project EDISON (EDucation-research Integration through Simulation On the Net, Grant No.: 2011-0020562), the Asian Office of Aerospace R&D (AOARD) project (Award No:FA2386-10-1-4001), and the second stage of the Brain Korea 21 Project in 2012.

References

[1]Harten A., "Adaptive multiresolution schemes for shock computation," *Journal of Computational Physics*, Vol. 115, 1994, pp. 319-338.

[2]Holmström M., "Solving hyperbolic PDEs using interpolation wavelets," *SIAM journal on Scientific Computing*, Vol. 21, 1999, pp. 405-420.

[3]Sjögreen B., "Numerical experiments with the multi-resolution scheme for the compressible Euler equations," *Journal of Computational Physics*, Vol. 117, 1995, pp. 251-261.

[4]H. Kang, K. Kim, D. Lee and D. Lee, "Improvement in computational efficiency of Euler equations via a modified Sparse Point Representation method," *Compu. and Fluids*, Vol. 37, 2008, pp. 265-280.

[5]H. Kang, K. Kim, D. Lee and D. Lee, "Improved computational efficiency of unsteady flow problems via the modified wavelet method," *AIAA Journal*, Vol. 46, 2008, pp. 1191-1203.

[6]D. Wirasaet and S. Paolucci, "Three-dimensional Flow in the Differentially Heated Cavity Using an Adaptive Wavelet Method," " *9th AIAA/ASME Joint Thermophysics and Heat Transfer Conference*, San Francisco, California, 2006, AIAA-2006-3924.

[7]V. Schmitt and F. Charpin, "Pressure Distributions on the ONERA-M6-Wing at Transonic Mach Numbers," Experimental Data Base for Computer Program Assessment. Report of the Fluid Dynamics Panel Working Group 04, AGARD AR 138, May 1979.

Seventh International Conference on Computational Fluid Dynamics (ICCFD7), Big Island, Hawaii, July 9-13, 2012

ICCFD7-2012-1806

Study on the Computational Efficiency of Three Dimensional Euler Equations by Multi-Resolution Analysis

K. Park*, H. Kang**, D. Lee*, D. Lee*** and D. Kwak****
Corresponding author: dohyung@hanyang.ac.kr

* Seoul National University, Korea
** Korea Aerospace Research Institute, Korea
*** Hanyang University, Korea
**** NASA Ames Research Center, USA

Abstract: Based on the multi-resolution analysis, efficient computational algorithm for three dimensional Euler equations is developed. A proper thresholding technique is applied to preserve the order of the accuracy of the original solver. In order to assess the efficiency of the proposed algorithm, the method is applied to the computation of flow field around ONERA-M6 wing in transonic regime. The computation time is significantly reduced by the proposed multi-resolution numerical method, compared to the original solver.

Keywords: Multi-resolution analysis, Wavelets, Computational Efficiency, Three Dimensional Euler Equations.

1 Introduction

New design of various aeronautical and aerospace transportation systems calls for accurate computations of transonic/supersonic flow, that may encompass more physically correct and detailed flow structures. However, current level of Computational Fluid Dynamics (CFD) modeling and simulation technology still falls short of practical implementation for a full scale or integrated design. For enhancement of prediction capability of CFD tools, it is indespensible to preform high fidelity simulations with concentrated grid point clustering and high order accurate algorithms. However, three dimensional flow analysis and unsteady flow computation have to face substantial increase of computational cost. Thereby, it is important to develop an advanced numerical method that should produce accurate simulation output and at the same time, that alleviate overall computational cost.

The computational efficiency issue has been reserached by numerical algorithms via multi-resolution analysis using wavelet basis. Especially, the wavelets have been studied as useful CFD tools for solution algorithms, feature extraction, and data compression, etc. Harten presented an adaptive multi-resolution scheme for computing the discontinuous solutions of hyperbolic PDEs [1]. Holmström proposed the algorithm that uses the interpolating wavelet transformation to organize an adaptive dataset [2]. Sjögreen also used a multi-resolution scheme based on the interpolating wavelet transformation to solve the compressible Euler equations [3]. Lee extended 1D supercompact wavelets concept to multidimensions and demonstrated big compression ratio for massive flow field simulation data [4]. Kang & Lee proposed modified threshold value in adaptive wavelet methods and enhance the computational efficiency even with the preservation of the numerical accuracy of original algorithm [5, 6, 7].

In the multi-resolution analysis using wavelets, wavelet decomposition is performed to compute the scale and wavelet coefficients. In most cases, quite many wavelet coefficients are smaller than a certain value. Even with cutting-off these small wavelets coefficients, the reconstructed data is not

much different from the original dataset. By using efficient wavelet data representation, a variety of solution algorithms have been developed based on multi-resolution analysis. However, practical applications such as three-dimensional wavelet analysis for Euler and Navier-Stokes equations are pretty rare, compared to the efforts on fundamental wavelet analysis. D. Wirasaet et al. extended the adaptive wavelet method to solve three-dimensional flows [8]. Then, they simulated the unsteady three dimensional flow within a differentially heated cavity using adaptive wavelet algorithm to demonstrate the versatility and efficiency of the method. However, for more successful practical implementations, the multi-resolution algorithm should be simple to implement in original solver and should be robust in applying to non-uniform and distorted grid system with various shapes.

In this study our previous two-dimensional adaptive wavelet algorithm [5, 6, 7] is extended to three-dimensional flow analysis. To this end, three-dimensional wavelet decomposition process and an appropriate modified thresholding function are proposed. The developed multi-resolution method is applied to flow field simulation around ONERA-M6 wing in transonic regime. From the application, it is confirmed that the proposed algorithm is about 3 times faster than original flow solver and preserves order of accuracy of the reference solver. In addition, the limitation of current three-dimensional algorithm and on-going approaches are discussed.

2 Multi-Resolution Analysis Using Wavelets for Three-Dimensional Euler Equations

In this study, the three-dimensional Euler equations are used as the governing equations to solve the flow problem. The three-dimensional Euler equations are as follows.

$$\frac{\partial Q}{\partial t}+\frac{\partial E}{\partial x}+\frac{\partial F}{\partial y}+\frac{\partial G}{\partial z}=0$$

$$\text{with } Q=\begin{bmatrix}\rho\\ \rho u\\ \rho v\\ \rho w\\ \rho e_t\end{bmatrix},\ E=\begin{bmatrix}\rho u\\ \rho u^2+p\\ \rho uv\\ \rho uw\\ (\rho\rho_t+p)u\end{bmatrix},\ F=\begin{bmatrix}\rho v\\ \rho vu\\ \rho v^2+p\\ \rho vw\\ (\rho\rho_t+p)v\end{bmatrix},\ G=\begin{bmatrix}\rho w\\ \rho wu\\ \rho wv\\ \rho w^2+p\\ (\rho\rho_t+p)w\end{bmatrix} \text{ and}$$

$$e_t=\frac{a^2}{\gamma(\gamma-1)}+\frac{1}{2}(u^2+v^2+w^2),$$

where all properties and governing equations are non-dimensionalized. By the generalized coordinate transformation, above equations are rewitten as

$$\frac{\partial \overline{Q}}{\partial \tau}=-[\frac{\partial \overline{E}}{\partial \xi}+\frac{\partial \overline{F}}{\partial \eta}+\frac{\partial \overline{G}}{\partial \varsigma}]=-R^n_{i,j}$$

$$\text{with } \overline{Q}=\frac{Q}{J},\ \overline{E}=\frac{1}{J}[\xi_t Q+\xi_x E+\xi_y F+\xi_z G],\ \overline{F}=\frac{1}{J}[\eta_t Q+\eta_x E+\eta_y F+\eta_z G] \text{ and}$$

$$\overline{G}=\frac{1}{J}[\zeta_t Q+\zeta_x E+\zeta_y F+\zeta_z G].$$

In order to apply the multi-resolution analysis to CFD algorithms of three dimensional Euler equations, the three-dimensional wavelet decomposition procedure is implemented to the algorithms. For preservation of the numerical accuracy of the solution, the modified threshold value is derived by considering the grid spacing. Also, three-dimensional restriction method [5] is applied in time integration for enhancement of the convergence of the solution. The procedure of multi-resolution analysis algorithm is as shown in Figure 1.

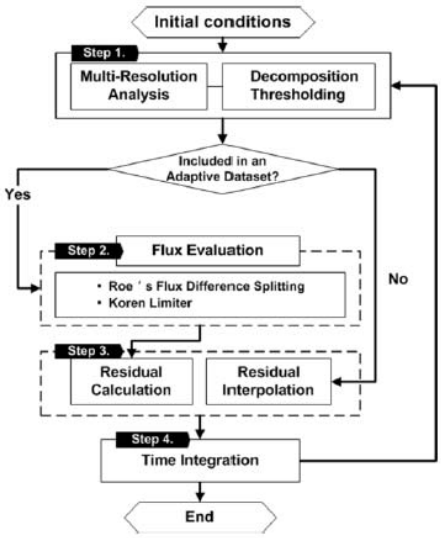

Figure 1: Overall procedure of multi-resolution analysis algorithm.

- **Step 1**: The multi-resolution analysis is performed; by the decomposition and thresholding, computational domain is adapted to follow the local features of the solution such as shock, vortex, etc. Then, the positions of crucial features are included in the adaptive dataset.

- **Step 2**: The flux evaluation is performed in the including cells in the adaptive dataset with conventional methods.

- **Step 3**: In the excluded cells in the adaptive dataset, the residual is computed from the results of Step 2 by residual interpolation.

- **Step 4**: The time integration is carried out. Then, restriction method is applied to the solution; negligible flow variations are restricted and the convergence of the solution is enhanced.

2.1 Wavelet transformation

2.1.1 Sparse Representation (SPR)

In this study, the multi-resolution analysis based on the interpolating polynomial is used [2]. Assume a dyadic grid set as shown in below equation.

$$V_l = \{x_{l,k} \in \boldsymbol{R} : x_{l,k} = 2^{-l}k, k \in Z\},\ l \in Z\ .$$

The dyadic dataset is decomposed into two types of coefficient as follows.

$$\begin{cases} \tilde{f}_{l+1,2k} = f_{l,k} \\ \tilde{f}_{l+1,2k+1} = \mathrm{P}_{l+1,2k+1}(f_{l,k-\frac{p}{2}+1}, \cdots, f_{l,k}, f_{l,k+1}, \cdots, f_{l,k+\frac{p}{2}}) \end{cases}$$

where $\mathrm{P}_{i,j}$ is the order of interpolating polynomial in an even number. The 4^{th} order of interpolating polynomial is

$$\tilde{f}_{l+1,2k+1} = -\frac{1}{16}f_{l,k-1} + \frac{9}{16}f_{l,k} + \frac{9}{16}f_{l,k+1} - \frac{1}{16}f_{l,k+2}\ .$$

Then, the wavelet coefficients are defined as

$$d_{l,k} = f_{l+1,2k+1} - \tilde{f}_{l+1,2k+1},\ \forall k \in Z\ .$$

In the thresholding process, the wavelet coefficients corresponding to regions of less importance are partially rejected, accordingly sparse wavelet representation is obtained. Through the sparse

wavelet representation, a compressed dataset is constructed with remaining data points. This compressed dataset is the set of function values that survive after thresholding as

$$\left|d_{l,k}\right|_{\infty} = \left|f_{l,k} - \tilde{f}_{l,k}\right|_{\infty} < O(\varepsilon).$$

2.1.2 Three dimensional wavelet trasformation

Assume a three-dimensional dyadic gridset with level 1 as shown in Figure 2.

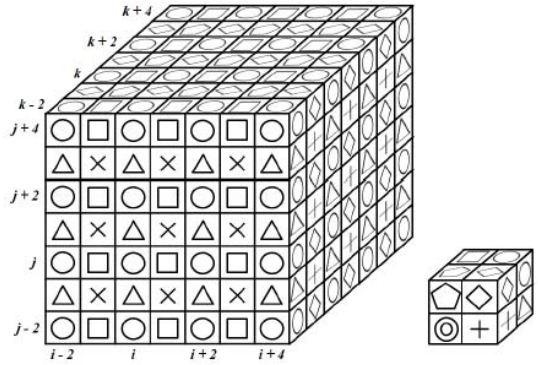

Figure 2: Three-dimensional dyadic gridset

Here, values at ○ cells are saved in the coarser level gridset, and 4th order of interpolating polynomial is employed at the other cells (□, △, ◇, ×, +, ⬠, ◎) for maintaining the 2nd order accuracy of a conventional solver. The 4th order interpolation is as

$$\square: \tilde{Q}^n_{i+1,j,k} = \frac{1}{16}(-Q^n_{i-2,j,k} + 9Q^n_{i,j,k} + 9Q^n_{i+2,j,k} - Q^n_{i+4,j,k}),$$

$$\triangle: \tilde{Q}^n_{i,j+1,k} = \frac{1}{16}(-Q^n_{i,j-2,k} + 9Q^n_{i,j,k} + 9Q^n_{i,j+2,k} - Q^n_{i,j+4,k}),$$

$$\diamond: \tilde{Q}^n_{i,j,k+1} = \frac{1}{16}(-Q^n_{i,j,k-2} + 9Q^n_{i,j,k} + 9Q^n_{i,j,k+2} - Q^n_{i,j,k+4}),$$

$$\times: \tilde{Q}^n_{i+1,j+1,k} = \frac{1}{32}(-Q^n_{i-2,j-2,k} + 9Q^n_{i,j,k} + 9Q^n_{i+2,j+2,k} - Q^n_{i+4,j+4,k} - Q^n_{i-2,j+4,k} + 9Q^n_{i,j+2,k} + 9Q^n_{i+2,j,k} - Q^n_{i+4,j-2,k}),$$

$$+: \tilde{Q}^n_{i,j+1,k+1} = \frac{1}{32}(-Q^n_{i,j-2,k-2} + 9Q^n_{i,j,k} + 9Q^n_{i,j+2,k+2} - Q^n_{i,j+4,k+4} - Q^n_{i,j-2,k+4} + 9Q^n_{i,j,k+2} + 9Q^n_{i,j+2,k} - Q^n_{i,j+4,k-2}),$$

$$\pentagon: \tilde{Q}^n_{i+1,j,k+1} = \frac{1}{32}(-Q^n_{i-2,j,k-2} + 9Q^n_{i,j,k} + 9Q^n_{i+2,j,k+2} - Q^n_{i+4,j,k+4} - Q^n_{i-2,j,k+4} + 9Q^n_{i,j,k+2} + 9Q^n_{i+2,j,k} - Q^n_{i+4,j,k-2}),$$

$$\text{◎}: \tilde{Q}^n_{i+1,j+1,k+1} = \frac{1}{64}(-Q^n_{i-2,j-2,k-2} + 9Q^n_{i,j,k} + 9Q^n_{i+2,j+2,k+2} - Q^n_{i+4,j+4,k+4} - Q^n_{i-2,j-2,k+4} + 9Q^n_{i,j,k+2} + 9Q^n_{i+2,j+2,k} - Q^n_{i+4,j+4,k-2} - Q^n_{i-2,j+4,k-2} + 9Q^n_{i,j+2,k} + 9Q^n_{i+2,j,k+2} - Q^n_{i+4,j-2,k+4} - Q^n_{i+4,j-2,k-2} + 9Q^n_{i+2,j,k} + 9Q^n_{i,j+2,k+2} - Q^n_{i-2,j+4,k+4}).$$

After the interpolation of each cell, the wavelet coefficients are computed as

$$\square: d^n_{i+1,j,k} = Q^n_{i+1,j,k} - \widetilde{Q}^n_{i+1,j,k},$$

$$\triangle: d^n_{i,j+1,k} = Q^n_{i,j+1,k} - \widetilde{Q}^n_{i,j+1,k},$$

$$\diamond: d^n_{i,j,k+1} = Q^n_{i,j,k+1} - \widetilde{Q}^n_{i,j,k+1},$$

$$\times: d^n_{i+1,j+1,k} = Q^n_{i+1,j+1,k} - \widetilde{Q}^n_{i+1,j+1,k},$$

$$+: d^n_{i,j+1,k+1} = Q^n_{i,j+1,k+1} - \widetilde{Q}^n_{i,j+1,k+1},$$

$$\pentagon: d^n_{i+1,j,k+1} = Q^n_{i+1,j,k+1} - \widetilde{Q}^n_{i+1,j,k+1},$$

$$\text{◎}: d^n_{i+1,j+1,k+1} = Q^n_{i+1,j+1,k+1} - \widetilde{Q}^n_{i+1,j+1,k+1}.$$

Then the wavelet coefficients are compared with the threshold value; if the wavelet coefficients are larger than the threshold value, the points are remained in an adaptive dataset so as to follow the local feature of a CFD solution. If a wavelet coefficient is smaller than ε', the cell doesn't belong to the adaptive dataset. Here, in order to prevent additional $O(\varepsilon)$ due to the data loss below $O(\varepsilon)$, the thresholding method is modified by considering the order of truncation errors as

$$\varepsilon' = min(\varepsilon, \Delta x^2).$$

Therefore the adaptive dataset is constructed with 2nd order of accuracy and order of accuracy of a conventional CFD solver is guaranteed. In this study, ε is set to 1×10^{-5}, so $\varepsilon'=\min(1\times10^{-5}, \Delta x^2)$. More detail about modified thresholding value is in reference 4 and 5.

2.2 Flux Evaluation

After the wavelet transformation, flux values are only calculated at the included cells in the adaptive dataset. This research uses the Finite Volume Method (FVM) to calculate the numerical fluxes; flux values are then computed on all sides of the cell with 2nd order accuracy. Using these cell interface values, spatial discretization is performed with Roe's FDS method.

2.3 Residual Interpolation & Time Integration

At unimportant cells which doesn't belong to the adaptive dataset, residual values are interpolated by 4th order of interpolating polynomial as shown in below equations.

$$\square: \widetilde{R}^n_{i+1,j,k} = \frac{1}{16}(-R^n_{i-2,j,k} + 9R^n_{i,j,k} + 9R^n_{i+2,j,k} - R^n_{i+4,j,k}),$$

$$\triangle: \widetilde{R}^n_{i,j+1,k} = \frac{1}{16}(-R^n_{i,j-2,k} + 9R^n_{i,j,k} + 9R^n_{i,j+2,k} - R^n_{i,j+4,k}),$$

$$\diamond: \widetilde{R}^n_{i,j,k+1} = \frac{1}{16}(-R^n_{i,j,k-2} + 9R^n_{i,j,k} + 9R^n_{i,j,k+2} - R^n_{i,j,k+4}),$$

$$\times: \widetilde{R}^n_{i+1,j+1,k} = \frac{1}{32}(-R^n_{i-2,j-2,k} + 9R^n_{i,j,k} + 9R^n_{i+2,j+2,k} - R^n_{i+4,j+4,k} - R^n_{i-2,j+4,k} + 9R^n_{i,j+2,k} + 9R^n_{i+2,j,k} - R^n_{i+4,j-2,k}),$$

$$+: \widetilde{R}^n_{i,j+1,k+1} = \frac{1}{32}(-R^n_{i,j-2,k-2} + 9R^n_{i,j,k} + 9R^n_{i,j+2,k+2} - R^n_{i,j+4,k+4} - R^n_{i,j-2,k+4} + 9R^n_{i,j,k+2} + 9R^n_{i,j+2,k} - R^n_{i,j+4,k-2}),$$

$$\pentagon: \widetilde{R}^n_{i+1,j,k+1} = \frac{1}{32}(-R^n_{i-2,j,k-2} + 9R^n_{i,j,k} + 9R^n_{i+2,j,k+2} - R^n_{i+4,j,k+4} - R^n_{i-2,j,k+4} + 9R^n_{i,j,k+2} + 9R^n_{i+2,j,k} - R^n_{i+4,j,k-2}),$$

$$\widetilde{R}^n_{i+1,j+1,k+1} = \frac{1}{64}\left(-R^n_{i-2,j-2,k-2} + 9R^n_{i,j,k} + 9R^n_{i+2,j+2,k+2} - R^n_{i+4,j+4,k+4}\right.$$

◎: $$- R^n_{i-2,j-2,k+4} + 9R^n_{i,j,k+2} + 9R^n_{i+2,j+2,k} - R^n_{i+4,j+4,k-2}$$

$$- R^n_{i-2,j+4,k-2} + 9R^n_{i,j+2,k} + 9R^n_{i+2,j,k+2} - R^n_{i+4,j-2,k+4}$$

$$\left. - R^n_{i+4,j-2,k-2} + 9R^n_{i+2,j,k} + 9R^n_{i,j+2,k+2} - R^n_{i-2,j+4,k+4}\right)$$

Through the 4th order of interpolating polynomial, the error caused by interpolation becomes smaller than the truncation errors of the numerical schemes. After residual interpolation, time integration (LU-SGS) is performed in the whole computation domain.

3 Numerical Tests and Discussion

For the assessment of the computational efficiency and numerical accuracy of the three-dimensional multi-resolution algorithm, it is applied to the simulation of flow field around the ONERA-M6 wing with Mach number of 0.8395 and angle of attack of 3.06° [9]. After the computations, the adaptive dataset of all level resolutions are shown in Figure 3. This figure shows that the dataset follows the local features of the solution; many cells remain near the wing and downstream. In other smooth regions, the remaining cells are sparsely distributed, because the changes in the flow properties are negligible.

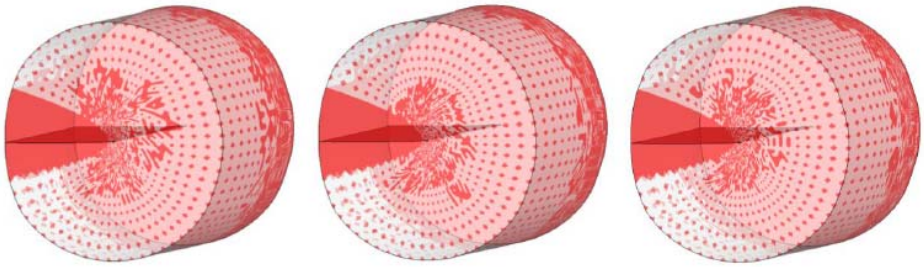

(a) Level 1 (b) Level 2 (c) Level 3

Figure 3: Adaptive dataset of three-dimensional gridset.

The overall efficiency improvement and the L_2 error according to the wavelet resolution level are summarized in Table 1. Here, the computation speed of adaptive wavelet method becomes about 3 times faster than the reference CFD method, and in this problem 1 level resolution of wavelet is the fastest. The L_2 errors between the results of reference method and adaptive wavelet methods are only about $O(10^{-7})$.

Table 1. Results of efficiency improvements and L_2 error

		Iteration	SPR Pt.	CPU Time	Time Ratio	L_2 Error
Reference Solver		10764	·	29329.3	·	·
Multi-Resolution Analysis	1 Level	3206	64.61%	9192.5	3.19	2.51×10^{-7}
	2 Level	3267	64.57%	9438.4	3.11	3.14×10^{-7}
	3 Level	3205	64.74%	9351.8	3.14	3.49×10^{-7}

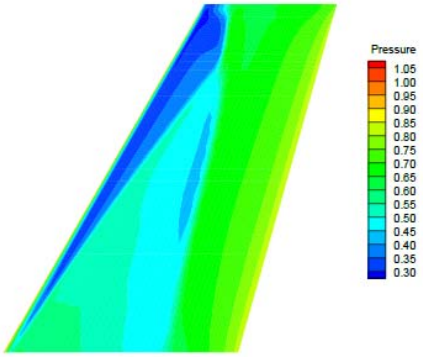

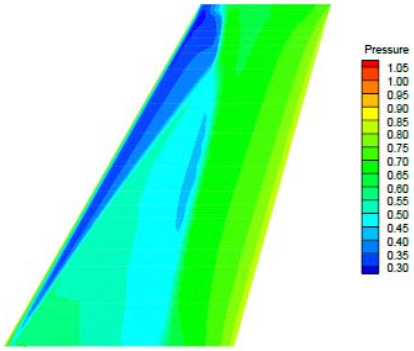

(a) Reference solver (b) Multi-resolution analysis – 2 level of resolution

Figure 4: Pressure contour on the upper surface of the wing.

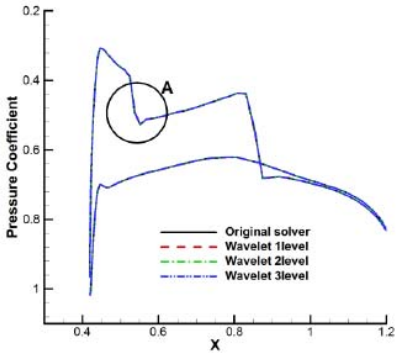

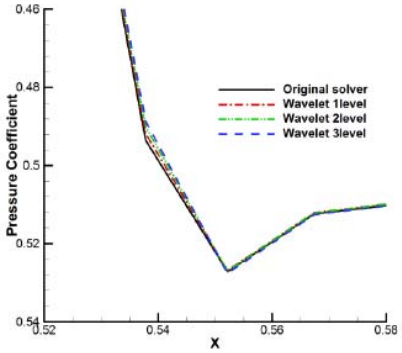

(a) Pressure distribution at 0.5 of span (b) Detailed pressure distribution at A region

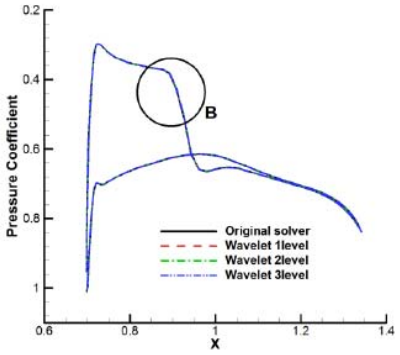

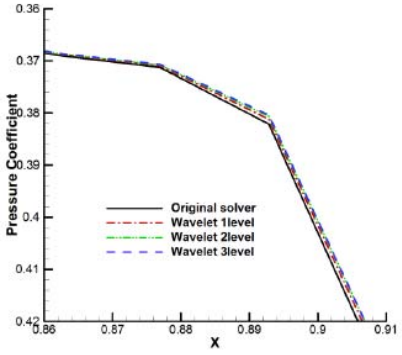

(a) Pressure distribution at 0.8 of span (b) Detailed pressure distribution at B region

Figure 5: Pressure distribution on the surface of the wing.

Figure 4 shows the pressure contours on the upper surfaces of ONERA-M6 wings computed by the reference CFD solver and the multi-resolution analysis. In both contours, the patterns of lambda shock which is the crucial feature of ONERA-M6 wing are very similar. For more detailed comparison of the results, pressure distributions of the two solvers at the positions of 50% and 80% of wing span are presented at Figure 5. In the figures, it is shown that the positions of shock, shock strength and pressure distributions are almost same. Through the application, it is substantiated that

the three-dimensional multi-resolution analysis can present much better efficiency while numerical accuracy of the reference CFD solver is preserved.

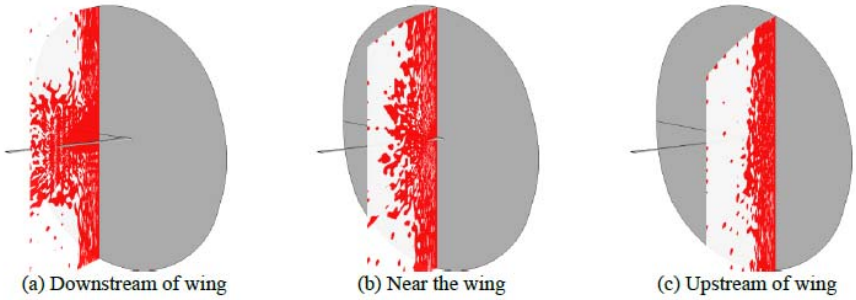

(a) Downstream of wing (b) Near the wing (c) Upstream of wing

Figure 6: Adaptive dataset of 2 level resolution at specific flow field.

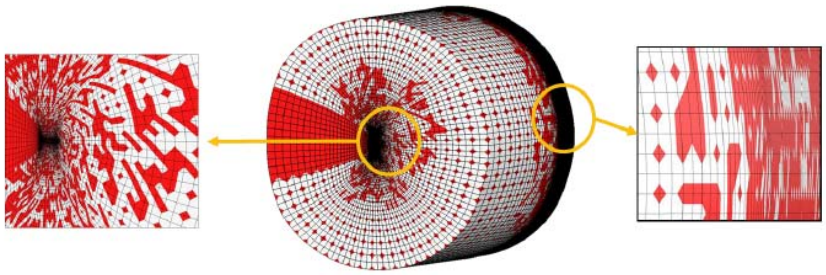

Figure 7: Adaptive dataset at specific flow field.

However many data points in the upstream and far regions from the wing are still remained as shown in Figure 6 and 7. Because the interpolating coefficients of this study are derived from the uniform gridset, the approximation of original value may be insurfficient where grid points are clustered or distorted. In order to solve this problem new concepts of interpolation or thresholding strategies are necessary such as the reconsturction of the supporting points for interpolation, the combination of various order of polynomials, regional variable threshold values, and etc. based on cell aspect ratio and skewness. However, they should originate more computational cost and memory. Thus our on-going researches are the combination of various order control of polynomial and regional variable threshold values for the more enhancement of computational efficiency.

4 Conclusion and Future Work

In this study, the three dimensional multi-resolution algorithm is developed to enhance computational efficiency of three-dimensional flow field simulation. The developed three dimensional multi-resolution algorithm is applied to ONERA-M6 wing in transonic regime. For the application, adaptive wavelet dataset are constructed so as to capture local features of solution automatically. However many data points, including in the upstream region of the wing, are not discarded since the current wavelet procedure does not reflect the grid skewness and aspect ratio. Nevertheless, the proposed multi-resolution analysis significantly enhances the computational efficiency about 3 times faster than reference solver even with preservation of the accuracy of numerical solution. If new ideas such as combination of interpolation order control method and regional variable threshoing techniequ are implemented based on grid skewness, it is expected that computational efficiency is much more enhanced.

Acknowledgments

We appreciate the support of the Ministry of Education, Science and Technology, subjected to the project EDISON (EDucation-research Integration through Simulation On the Net, Grant No.: 2011-0020562) , the Asian Office of Aerospace R&D (AOARD) project (Award No:FA2386-10-1-4001), and the second stage of the Brain Korea 21 Project in 2012.

References

[1] Harten A., Adaptive multiresolution schemes for shock computation, Journal of Computational Physics, 115:319-338, 1994.
[2] Holmström M., Solving hyperbolic PDEs using interpolation wavelets, SIAM Journal on Scientific Computing, 21:405-420, 1999.
[3] Sjögreen B., Numerical experiments with the multi-resolution scheme for the compressible Euler equations, Journal of Computational Physics, 117: 251-261, 1995.
[4] D. Lee, Multidimensional supercompact wavelets for fluid dynamics, Numerical Heat Transfer Part B: Fundamentals, 43, 4:307-329, 2003.
[5] H. Kang, K. Kim, D. Lee and D. Lee, Improvement in computational efficiency of Euler equations via a modified Sparse Point Representation method, Compu. and Fluids, 37:265-280, 2008.
[6] H. Kang, K. Kim, D. Lee and D. Lee, Improved computational efficiency of unsteady flow problems via the modified wavelet method, AIAA Journal, 46:1191-1203, 2008.
[7] H. Kang, D. Lee, D. Lee, D. Kwak and J. Seo, Efficiency Enhancement in High Order Accurate Euler Computation Via AWM, International Conference of Computational Fluid Dynamics 2010, 495-500, 2010.
[8] D. Wirasaet and S. Paolucci, Three-dimensional Flow in the Differentially Heated Cavity Using an Adaptive Wavelet Method, 9th AIAA/ASME Joint Thermophysics and Heat Transfer Conference, AIAA-2006-3924, 2006.
[9] V. Schmitt and F. Charpin, Pressure Distributions on the ONERA-M6-Wing at Transonic Mach Numbers, Experimental Data Base for Computer Program Assessment. Report of the Fluid Dynamics Panel Working Group 04, AGARD AR 138, 1979.